HOLTEC INTERNATIONAL

HI-STAR 100 CERTIFICATE OF COMPLIANCE 71-9261

LICENSE AMENDMENT REQUEST 9261-2

REVISION 0

VOLUME 2 OF 2

MAY, 2002

(NON-PROPRIETARY VERSION)

HOLTEC INTERNATIONAL

LAR 9261-2

VOLUME 2 OF 2

CHAPTER 3: THERMAL EVALUATION

3.0 INTRODUCTION

In this chapter, compliance of the HI-STAR System thermal performance to 10CFR71 requirements is established for normal transport and hypothetical accident conditions of transport. The analysis considers passive rejection of decay heat from the spent nuclear fuel (SNF) to an environment under the most severe 10CFR71 mandated design basis ambient conditions.

10CFR71 defines the requirements and acceptance criteria that must be fulfilled by the cask thermal design. The requirements and acceptance criteria applicable to the thermal analysis presented in this chapter are summarized here as follows:

1. The applicant must include a description of the proposed package in sufficient detail to identify the package accurately and provide a sufficient basis for the evaluation of the package. [71.33].

   The description must include, with respect to the packaging, specific materials of construction, weights, dimensions, and fabrication methods of materials specifically used as nonfissile neutron absorbers or moderators [71.33(a)(5)(ii)]; and structural and mechanical means for the transfer and dissipation of heat [71.33(a)(5)(v)].

   The description must include, with respect to the contents of the package, chemical and physical form [71.33(b)(3)]; maximum normal operating pressure [71.33(b)(5)]; maximum amount of decay heat [71.33(b)(7)]; and identification and volumes of any coolants [71.33(b)(8)].

2. A package must be designed, constructed, and prepared for shipment so that under normal conditions of transport there would be no substantial reduction in the effectiveness of the packaging [71.43(f) and 71.51(a)(1)].

3. A package must be designed, constructed, and prepared for shipment so that in still air at 100°F and in the shade, no accessible surface of the package would have a temperature exceeding 185°F in an exclusive use shipment [71.43(g)].

4. Compliance with the permitted activity release limits for a Type B package may not depend on filters or on a mechanical cooling system [71.51(c)].

5. With respect to the initial conditions for the events of normal conditions of transport and hypothetical accident conditions, the demonstration of

compliance with the requirements of 10CFR71 must be based on the ambient temperature preceding and following the event remaining constant at that value between -20°F and 100°F which is most unfavorable for the feature under consideration. The initial internal pressure within the containment system must be considered to be the maximum normal operating pressure, unless a lower internal pressure consistent with the ambient temperature considered to precede and follow the event is more unfavorable [71.71(b) and 71.73(b)].

6. For normal conditions of transport, a heat event consisting of an ambient temperature of 100°F in still air and prescribed insolation must be evaluated [71.71(c)(1)].

7. For normal conditions of transport, a cold event consisting of an ambient temperature of -40°F in still air and shade must be evaluated [71.71(c)(2)].

8. Evaluation for hypothetical accident conditions is to be based on sequential application of the specified events, in the prescribed order, to determine their cumulative effect on a package [71.73(a)].

9. For hypothetical accident conditions, a thermal event consisting of a fully engulfing hydrocarbon fuel/air fire with an average emissivity coefficient of at least 0.9, with an average flame temperature of at least 1475°F for a period of 30 minutes [71.73(c)(4)].

As demonstrated in this chapter, the HI-STAR System design and thermal analyses comply with *all* nine requirements and acceptance criteria listed above. Subsection 3.2 lists the material properties data required to perform the thermal analyses and Subsection 3.3 provides the applicable temperature limits criteria required to demonstrate the adequacy of the HI-STAR System design under all conditions. All thermal analyses to evaluate the normal conditions of transport performance of a HI-STAR System are described in Subsection 3.4. All thermal analyses for hypothetical accident conditions are described in Subsection 3.5. A summary discussion of regulatory compliance is included in Subsection 3.6.

This revision to the HI-STAR transport Safety Analysis Report incorporates certain conforming changes to the multi purpose canisters (MPCs) that are engineered to be transported in the HI-STAR overpack. The principal changes are:

- *The Aluminum Heat Conduction Elements (AHCE) in the MPC, required under CoCs 9261-1 and 9261-2, are rendered optional hardware. (A similar change has been made in the HI-STORM Docket 72-1014 for all MPCs under CoC 1014-1).*

- *Include a higher capacity PWR basket configuration (MPC-32).*
- *Include an enhanced 24-cell PWR basket layout (MPC-24E), an enlarged cell opening option for the MPC-24 and a shortened-height MPC-24E canister for Trojan fuel.*
- *Raise the nominal helium fill pressure limit to 42.8 psig.*
- *Relax certain elements of excessive conservatism in the mathematical models to retain a moderate level of conservatism.*

Aside from the above-mentioned changes, this revision of this chapter is essentially identical to its predecessor.

3.1 DISCUSSION

Sectional views of the HI-STAR System have been presented earlier (see Figures 1.1.3 and 1.1.4). The system essentially consists of a loaded MPC situated inside an overpack equipped with a bolted closure. The fuel assemblies reside inside the MPC that has two redundant welded closures. The MPC contains a stainless steel honeycomb fuel basket that provides square-shaped fuel compartments of appropriate dimensions to facilitate insertion of fuel assemblies prior to welding of the MPC lid. Each fuel cell wall (except outer periphery MPC-68 cell walls) is provided with Boral (thermal neutron absorber) sandwiched between a stainless steel sheathing plate and the cell wall along the entire length of the active fuel region. Prior to sealing the MPC lid, the MPC is backfilled with helium to the levels specified in Table 1.2.3. This provides a stable and inert environment for the transport of the SNF. Additionally, the annular gap between the MPC and the overpack is backfilled with helium before the overpack vent and drain port plug plugs are installed. Heat is transferred from the SNF in the HI-STAR to the environment by passive heat transport mechanisms only.

The helium backfill gas is an integral part of the MPC and overpack thermal designs. The helium fills all the spaces between solid components and provides an improved conduction medium (compared to air) for dissipating decay heat in the MPC. Additionally, helium in the spaces between the fuel basket and the MPC shell is heated differentially and, therefore, subject to the "Rayleigh" effect which is discussed in detail later (Subsection 3.4.1.1.5). To ensure that the helium gas is retained and is not diluted by lower conductivity air, the MPC helium retention boundary is designed to comply with the provisions of the ASME B&PV Code Section III, Subsection NB, as an all-seal-welded pressure vessel with redundant closures. Similarly, the overpack containment boundary is designed as an ASME B&PV Code Section III, Subsection NB pressure vessel. Both the MPC helium retention boundary and the overpack containment boundary are required to meet maximum leakage rate requirements included in Section 7.4 of this SAR. These leakage rate criteria ensure the presence of helium during transport. The helium gas is therefore retained and undiluted, and may be credited in the thermal analyses.

An important thermal design criterion imposed on the HI-STAR System is to limit the maximum fuel cladding temperature during normal transport to below design basis limits (Table 1.2.3). An equally important design criterion is to reduce temperature gradients within the MPC to minimize thermal stresses. In order to meet these design objectives, the HI-STAR MPC basket is designed to possess certain distinctive characteristics, which are summarized in the following.

The MPC design minimizes resistance to heat transfer within the basket and basket periphery regions. This is ensured by a high structural integrity all-welded honeycomb structure. The MPC design incorporates top and bottom plenums with interconnected downcomer paths. The top plenum is formed between the MPC lid and the top of the honeycomb fuel basket with additional semicircular holes in the top of each fuel cell wall. The bottom plenum is formed by large elongated semicircular holes at the base of all cell walls. The MPC basket is designed to eliminate structural discontinuities (i.e., gaps) which introduce large thermal resistances to heat flow. Consequently, temperature gradients are minimized in this design, which results in lower thermal stresses within the basket. Low

thermal stresses are also ensured by an MPC design that permits unrestrained axial and radial growth of the basket to eliminate the possibility of thermally induced stresses due to restraint of free-end expansion. ~~The basket is thermally connected to the MPC shell by full length heat conduction elements made of aluminum. The aluminum heat conduction elements are specially fabricated to conform to the geometry of the large basket to MPC shell peripheral regions. The aluminum heat conduction elements and the MPC fuel basket or MPC shell walls facing each other are pressed together to ensure conformal interfacial contact. The aluminum heat conduction elements are provided with elongated semicircular holes to match up with the holes in the fuel basket periphery walls. HI-STAR System MPC Drawings 1395, and 1401 illustrate the geometry of the thermal conduction elements.~~

The HI-STAR System is designed for transport of PWR and BWR spent fuel assemblies and features two distinct MPC fuel basket geometries. For intact PWR fuel, a 24-assembly design ~~is~~ (depicted in Figure 1.2.5) *and a higher capacity canister (MPC-32) are available.* A 68-assembly design for the transport of intact or specified damaged BWR fuel is shown in Figure 1.2.3. Damaged BWR fuel must be placed in a damaged fuel container and must comply with the design basis characteristics specified in Table 1.2.14 to enable transport in the MPC-68. Extensively damaged BWR fuel assemblies (e.g. severed rods) classified as fuel debris shall be transported in the MPC-68F. The MPC-68F is identical to the MPC-68, except for the ^{10}B loading of the Boral panels for criticality control. Each basket design must comply with the required temperature limits under the imposed heat generation loads from the fuel assembly contents. For normal transport conditions, the maximum decay heat loads for the ~~24 (PWR basket)~~ *PWR* and ~~68 (BWR basket) assembly~~ *BWR* MPC*s* ~~designs~~ are summarized in Table 1.2.3. Table 1.2.14 lists the design basis thermal requirements for damaged fuel. The complete HI-STAR System consisting of the overpack and MPC under transport conditions is conservatively analyzed for the imposed design heat loads.

Thermal analysis of the HI-STAR System is based on including all three fundamental modes of heat transfer: conduction, natural convection and thermal radiation. Different combinations of these modes are active in different parts of the system. These modes are properly identified and conservatively analyzed within each region of the MPC and overpack, to enable bounding calculations of the temperature distribution within the HI-STAR System for both *PWR and BWR* MPC basket designs.

On the outside surface of the overpack, heat is dissipated to the environment by buoyancy induced convective air flow (natural convection) and thermal radiation. In the overpack internal metal structure, only conductive heat transport is possible. Between metal surfaces (e.g., between neighboring fuel rod surfaces) heat transport is due to a combination of conduction through a gaseous medium (helium) and thermal radiation. Finally, buoyancy-induced convective heat transport occurs within the open spaces of the MPC, aided by the MPC design which provides low pressure drop helium flow recirculation loops formed by the fuel cells, top plenum, downcomers, and bottom plenum. However, in the interest of conservatism, no credit for buoyancy-induced heat transport in the HI-STAR MPC basket is taken to satisfy either temperature or stress intensity limits. Heat transfer between the fuel basket external surface and MPC enclosure shell inside wall is further

influenced by the so-called "Rayleigh" effect in differentially heated vertical cavities and "Rayleigh-Benard" effect in horizontal channels heated from below. A discussion on these effects is provided in Subsection 3.4.1.1.5.

The total heat generation in each assembly is non-uniformly distributed over the active fuel to account for design basis-fuel burnup distribution listed in Chapter 1 (Table 1.2.15 and Figures 1.2.13 and 1.2.14). As discussed later in this chapter (Subsection 3.4.6), an array of conservative assumptions bias the results of the thermal analysis towards much reduced computed margins than would be obtained by a rigorous analysis of the problem.

The complete thermal analysis is performed using the industry standard ANSYS finite element modeling package [3.1.1] and the finite volume Computational Fluid Dynamics (CFD) code FLUENT [3.1.2]. ANSYS has been previously used and accepted by the NRC on numerous dockets. The FLUENT CFD program is independently benchmarked and validated with a wide class of theoretical and experimental studies reported in the technical journals. Additionally, Holtec has confirmed the code's capability to reliably predict temperature fields in dry storage applications using independent full-scale test data from a loaded cask [3.1.3]. This study concluded that FLUENT can be used to model all modes of heat transfer, namely, conduction, convection, and radiation in dry cask systems.

3.2 SUMMARY OF THERMAL PROPERTIES OF MATERIALS

Materials present in the HI-STAR System include stainless steels, carbon steels, aluminum, neutron shield, Boral neutron absorber and helium. In Table 3.2.1, a summary of references used to obtain cask material properties for performing all thermal analyses is presented.

Tables 3.2.2, 3.2.3 and 3.2.9 provide numerical thermal conductivity data for all materials at several representative temperatures. Table 3.2.8 lists the thermal properties of Boral components (i.e., B_4C core and aluminum cladding materials).

Surface emissivity data for key materials of construction are provided in Table 3.2.4. The emissivity properties of painted surfaces are generally excellent. Kern [3.2.5] reports an emissivity range of 0.8 to 0.98 for a wide variety of paints. In the HI-STAR thermal analysis, an emissivity of 0.85[†] is applied to exterior painted surfaces. A conservative solar absorbtivity coefficient of 1.0 is applied to all exposed cask surfaces.

In Table 3.2.5, the heat capacity and density data of different cask materials is presented. These properties are used in performing transient (hypothetical fire accident condition, for example) analyses. MPC Rayleigh effect calculations use helium density, heat capacity, and gas viscosity properties data which are listed in Tables 3.2.5 and 3.2.6.

The HI-STAR System's outside surface heat transfer coefficient is calculated by accounting for both natural convection heat transfer and radiation. The natural convection coefficient of a heated horizontal cylinder depends upon the product of the Grashof (Gr) and Prandtl (Pr) numbers. Following the approach developed by Jakob and Hawkins [3.2.9], GrPr is expressed as $L^3\Delta T\ Z$, where L is the diameter of the cask, ΔT is the HI-STAR System overpack surface-to-ambient temperature differential and Z is a parameter which depends upon air properties, which are known functions of temperature, evaluated at the average film temperature. The temperature dependence of Z for air is provided in Table 3.2.7.

[†] This is conservative with respect to prior cask industry practice, which has historically accepted higher emissivities. For example, the emissivity for painted surfaces (ε=0.95) is used in the TN-32 cask TSAR (Docket 72-1021).

Table 3.2.1

SUMMARY OF HI-STAR SYSTEM MATERIALS
THERMAL PROPERTY REFERENCES

Material	Emissivity	Conductivity	Density	Heat Capacity
Helium	NA	Handbook [3.2.2]	Ideal Gas Law	Handbook [3.2.2]
Air	NA	Handbook [3.2.2]	Ideal Gas Law	Handbook [3.2.2]
Zircaloy Cladding	EPRI [3.2.3]	NUREG [3.2.6], [3.2.7]	Rust [3.2.4]	Rust [3.2.4]
UO_2	Not Used	NUREG [3.2.6], [3.2.7]	Rust [3.2.4]	Rust [3.2.4]
Stainless Steel	Kern [3.2.5]	ASME [3.2.8]	Marks [3.2.1]	Marks [3.2.1]
Carbon Steel	Kern [3.2.5]	ASME [3.2.8]	Marks [3.2.1]	Marks [3.2.1]
Aluminum Alloy 5052 (Impact Limiters)	Not Used	ASME [3.2.8]	ASME [3.2.8]	ASME [3.2.8]
Aluminum Alloy 1100 (Heat Conduction Elements)	Handbook [3.2.2]	ASME [3.2.8]	ASME [3.2.8]	ASME [3.2.8]
Boral†	~~Not Used~~ *Marks [3.2.1]*	Test Data	Test Data	Test Data
Holtite-A††	Not Used	Test Data	Test Data	Test Data

† AAR Structures' Boral thermophysical test data.

†† From ~~neutron shield manufacturer's~~*Holtite-A test* data (Appendix 1.B).

Table 3.2.2

SUMMARY OF HI-STAR SYSTEM MATERIALS
THERMAL CONDUCTIVITY DATA

Material	**@ 200°F (Btu/ft-hr-°F)**	**@ 450°F (Btu/ft-hr-°F)**	**@ 700°F (Btu/ft-hr-°F)**
Helium	0.0976	0.1289	0.1575
Air	0.0173	0.0225	0.0272
Alloy X	8.4	9.8	11.0
Carbon Steel Radial Connectors	29.2	27.1	24.6
Carbon Steel Gamma Shield Layers	24.4	23.9	22.4
Impact Limiter Aluminum Alloy 5052	84.4	90.9	97.4
Holtite-A	~~0.373~~*See Footnote*[†]	~~0.373~~	~~0.373~~
Cryogenic Steel	23.8	23.7	22.3

[†] No credit taken for conduction through radial Holtite for the steady-state analysis, and before and after fire conditions for fire accident analysis. A conductivity of 1.0 Btu/ft-hr-°F is applied during the fire condition to the radial neutron shield (between intermediate shells and overpack enclosure shell).

Table 3.2.3

SUMMARY OF FUEL ELEMENT COMPONENTS
THERMAL CONDUCTIVITY DATA

Fuel Cladding		Fuel (UO_2)	
Temperature (°F)	**Conductivity (Btu/ft-hr-°F)**	**Temperature (°F)**	**Conductivity (Btu/ft-hr-°F)**
392	8.28†	100	3.48
572	8.76	448	3.48
752	9.60	570	3.24
932	10.44	793	2.28†

† Lowest value of conductivity is used in the thermal analysis for conservatism.

Table 3.2.4

SUMMARY OF MATERIALS SURFACE EMISSIVITY DATA

Material	**Emissivity**
Fuel cladding	0.80
Painted exterior surface	0.85
Rolled carbon steel	0.66
Stainless steel	0.36
Sandblasted aluminum	0.40
Boral	*0.26**

* *From Marks' Handbook (Oxidized Aluminum Surface)*

Table 3.2.5

MATERIALS DENSITY AND HEAT CAPACITY PROPERTIES SUMMARY

Materials	**Density (lbm/ft^3)**	**Heat Capacity (Btu/lbm-°F)**
Helium	(Ideal Gas Law)	1.24
Zircaloy Cladding	409	0.0728
Fuel (UO_2)	684	0.056
Carbon Steel	489	0.1
Stainless Steel	501	0.12
Boral	154.7	0.13
Impact Limiter Alloy 5052	167.6	0.23
Aluminum Alloy 1100	169.3	0.23
Holtite-A*	105.0	0.39

* *Conservatively postulated to un derestimate thermal inertia for fire accident analysis.*

Table 3.2.6

HELIUM GAS VISCOSITY[†] VARIATION WITH TEMPERATURE

Temperature (°F)	Viscosity (Micropoise)
167.4	220.5
200.3	228.2
297.4	250.6
346.9	261.8
463.0	288.7
537.8	299.8
737.6	338.8

[†] Obtained from Rohsenow and Hartnett [3.2.2].

Table 3.2.7

VARIATION OF NATURAL CONVECTION PROPERTIES
PARAMETER "Z" FOR AIR WITH TEMPERATURE

Temperature (°F)	**Z (ft^{-3} $°F^{-1}$)†**
40	2.1×10^{6}
140	9.0×10^{5}
240	4.6×10^{5}
340	2.6×10^{5}
440	1.5×10^{5}

† Obtained from Jakob and Hawkins [3.2.9].

Table 3.2.8

BORAL COMPONENT MATERIALS[†]
THERMAL CONDUCTIVITY DATA

Temperature (°F)	B_4C Core Conductivity (Btu/ft-hr-°F)	Aluminum Cladding Conductivity (Btu/ft-hr-°F)
212	48.09	100.00
392	48.03	104.51
572	47.28	108.04
752	46.35	109.43

[†] Both B_4C and aluminum cladding conductivity values are obtained from AAR Structures Boral thermophysical test data.

Table 3.2.9

HEAT CONDUCTION ELEMENTS (ALUMINUM ALLOY 1100)
THERMAL CONDUCTIVITY DATA

Temperature (°F)	**Conductivity (Btu/ft×hr×°F)**
100	131.8
200	128.5
300	126.2
400	124.5

3.3 TECHNICAL SPECIFICATIONS FOR COMPONENTS

HI-STAR System materials and components which are required to be maintained within their safe operating temperature ranges to ensure their intended function are summarized in Table 3.3.1. Long-term stability and continued neutron shielding ability of the Holtite-A neutron shield material under normal transport conditions are ensured when material exposure temperatures are maintained below the maximum allowable limit. The overpack metallic seals will continue to ensure leak tightness of the closure plate, and drain and vent ports if the manufacturer's recommended design temperature limits are not exceeded. Integrity of SNF during transport requires demonstration of HI-STAR System thermal performance to maintain fuel cladding temperatures below design basis limits. Boral used in MPC baskets for criticality control (a composite material composed of B_4C and aluminum) is stable up to 1000°F for short-term and 850°F for long term dry storage[†]. However, for conservatism, a lower maximum temperature limit is imposed.

Compliance to 10CFR71 requires evaluation of hypothetical accident conditions. The inherent mechanical stability characteristics of the HI-STAR System materials and components ensure that no significant functional degradation is possible due to exposure to short-term temperature excursions outside the normal long-term temperature limits. For evaluation of the HI-STAR System's thermal performance under hypothetical accident conditions, material temperature limits for short-duration events are also provided in Table 3.3.1.

3.3.1 Evaluation of Zircaloy Clad Fuel

The PNL study [3.3.2] proposes a 1058°F fuel cladding temperature limit for zircaloy clad fuel for periods of time which are relatively short compared to typical long-term dry storage durations. Many transport only cask systems[††] have stipulated this short-term cladding temperature limit as the design limit during transport. The HI-STAR System, however, is a dual-use (transport and storage) system. Therefore, unlike transport only cask systems, the HI-STAR can be placed in long-term storage following transport. Recognizing that the rate of cladding degradation increases at an accelerating pace with elevated temperatures, the design fuel cladding temperature limits for normal transport in the HI-STAR are specified to be the *long-term storage* temperature limits determined using the generic CSFM IDS temperature limit curves. These long-term temperature limits are a function of the fuel age at initial loading into the HI-STAR (see Table 3.3.7). This will serve to ensure that the cumulative cladding damage during transport does not substantially increase the probability of cladding failure during subsequent long-term storage conditions.

[†] AAR Structures Boral thermophysical test data.

[††] Nuclear Assurance Corporation (NAC) UMS, Docket 71-9270.
Vectra NUHOMS MP187, Docket 71-9255.
Sierra Nuclear Corp. (SNC) TRANSTOR, Docket 71-9268.

Pacific Northwest Laboratory (PNL) has established a Commercial Spent Fuel Management (CSFM) model based on creep rupture data for zircaloy [3.3.2]. The CSFM model enables a cask designer to determine fuel-specific maximum initial peak cladding temperature limits. The CSFM Inerted Dry Storage (IDS) temperature limit curves [3.3.2] define the maximum allowable initial storage temperature at initial cladding stresses as a function of fuel age. Therefore, for SNF of a given age (decay time), the permissible peak cladding temperature is a direct function of the cladding hoop stress, which in turn depends on the radius-to-thickness ratio of the fuel rod and its internal pressure. The rod internal pressure (P_i) is calculated based upon the maximum initial fill pressures (Tables 3.3.2 and 3.3.5) with fission gas release at a conservatively bounding maximum burnup under HI-STAR System transport conditions (40,000 MWD/MTU for BWR fuel and 42,500 MWD/MTU for PWR fuel).

The free rod volumes in the third column of Tables 3.3.2 and 3.3.5 are defined as free volumes available for pressurization with rod fill gas *in each rod.* Physically, the free rod volume is the cumulative sum of the open top plenum space, the pellet-to-cladding annular space and the inter-pellet junction space. As a lower bound value of the free rod volume will lead to a conservative estimate of the cladding stress at operating temperatures, the nominal plenum space is included in the free rod volume. The plenum length for miscellaneous BWR fuel assemblies is set to 12 inches. The fission gas release fraction data is based on Regulatory Guide 1.25 (Table 3.3.4). The radius-to-thickness ratio (r^*) is determined based on rod nominal dimension values (Table 3.3.3 and 3.3.6) including the maximum cladding thickness loss due to in-reactor oxidation, as reported in another PNL study [3.3.5].

By utilizing P_i and r^*, the cladding stress for various PWR fuel types is calculated from Lame's formula and summarized in Table 3.3.3. It can be seen from Figure 3.4.19 that the average temperature of the gas in the fuel rods, a great bulk of which is located in the top region of the SNF, is well below 300°C for the PWR fuel array types. Therefore, to compute the cladding hoop stress in a conservative manner, the ideal gas law is used to obtain the value of the in-rod gas pressure at 300°C. An inspection of cladding stress data summarized in Table 3.3.3 indicates 96.7 MPa as the bounding value of cladding stress (σ_{max}) for the PWR SNF. Corresponding fill gas data and calculations of cladding stress for the various BWR SNF types are summarized in Tables 3.3.5 and 3.3.6, respectively. It can be seen from Figure 3.4.20 that the average temperature of the gas in the fuel rods, a great bulk of which is located in the top region of the SNF, is well below 300°C for all BWR fuel array types considered in this topical report. Therefore, to compute the cladding hoop stress in a conservative manner, the ideal gas law is used to obtain the value of the in-rod gas pressure at 300°C. An inspection of the cladding stress data in Table 3.3.6 indicates that the bounding value of the cladding hoop stress for all BWR SNF types is 54.7 MPa (except for 8×8 and *6x6* GE Dresden-1, *Quad*$^+$, and 6×6 GE Humboldt Bay fuel types).

The bounding values of σ_{max} for the array of PWR and BWR SNF types are thus 96.7 MPa and 54.7 MPa, respectively (except for the 8×8 *and 6x6* GE Dresden-1, *Quad*$^+$ and 6×6 GE Humboldt Bay fuel types for which the bounding value of σ_{max} is *72.5* MPa).

Several implicit assumptions in the calculation of σ_{max}, such as neglect of the rod cavity growth due to thermal expansion, internal fill pressure, and in-core irradiation, ensure that the hoop stress value (which is the sole determinant in the establishment of permissible cladding temperature for a given cooling time) is indeed a bounding number.

The generic CSFM IDS temperature limit curves developed in the PNL study [3.3.2] are used to determine zircaloy cladding temperature limits at the conservative 300°C average rod temperature. The fuel cladding temperature limits obtained from these PNL curves ensure a low fuel rod failure probability. The calculated limits are presented, as a function of the fuel age, in Table 3.3.7.

3.3.2 Evaluation of Stainless Steel Clad Fuel

Approximately 2,200 PWR and BWR fuel assemblies stored in the United States employ stainless steel cladding. All stainless steel cladding materials are of the austenitic genre with the ASTM alloy compositions being principally type 304 and 348H. The long-term storage condition peak allowable temperature applicable for stainless steel fuel is significantly higher than that applicable to zircaloy clad fuel. A recent EPRI/PNL study [3.3.6] recommends a 430°C (806°F) peak stainless steel cladding temperature limit versus a typical 380°C (716°F) peak zircaloy cladding temperature limit. Since the peak cladding temperature limits applied to the thermal analysis are based on the zircaloy clad limit, it is readily apparent that this criterion is overly restrictive for stainless steel clad fuel. The peak clad temperature limits applied to both zircaloy and stainless steel clad fuel assemblies are provided in Table 3.3.7.

It is recognized that the peak cladding temperature of stainless fuel will differ from zircaloy clad fuel principally due to the following differences:

i. Differences in decay heat levels
ii. Differences in cladding emissivity
iii. Differences in cladding conductivity
iv. Differences in rod array dimensions

The net planar thermal resistance of the equivalent homogenized axisymmetric MPC basket containing stainless steel clad fuel is greater than the case with zircaloy clad fuel. The higher resistance arises principally from the significantly lower emissivity of stainless steel cladding. This factor is, however, offset by significantly lower design basis heat loads considered for stainless steel clad fuel. As demonstrated by examining Tables 3.4.6, 1.2.13 and 1.2.19, the percentage reduction in design basis heat duty for stainless steel fuel (at least 70% lower than zircaloy clad BWR fuel and 41% lower than zircaloy clad PWR fuel *for MPC-24, MPC-24E and 28% lower than zircaloy clad PWR for MPC-32*) is more pronounced than the nominal percentage decrease in MPC basket effective thermal conductivity[†] (stainless steel fueled baskets are between 9% to ~~13~~ *25%* less

[†] The term "effective conductivity" of the fuel basket is defined in Section 3.4.1.

conducting). Therefore, it is concluded that the peak cladding temperature for stainless steel clad fuel will be bounded by the zircaloy clad fuel results. Consequently, in view of significantly higher peak stainless steel cladding temperature levels recommended by the EPRI study, a separate thermal analysis to demonstrate the adequacy of stainless steel clad integrity for transport in the HI-STAR System is not necessary.

3.3.3 Accident Condition Cladding Temperature Limit

For short-term duration events (hypothetical fire accident, for example), relatively high fuel cladding temperature limits have been historically accepted by the USNRC. For example, the Safety Analysis Report of the STC transport cask (Docket No. 71-9235), recently certified by the USNRC, permits 1200°F (approximately 649°C) as the maximum value of the peak cladding temperature (T_{max}) for transport of SNF with up to 45,000 MWD/MTU burnup. PNL test data [3.3.5], limiting itself to medium burnup levels (28,800 MWD/MTU), endorses a somewhat lower T_{max} value (T_{max} = 570°C or 1058°F). Based on the published industry test data, guidance in the literature, and analytical reasoning, we herein prescribe 570°C as the admissible short-term value of T_{max} for the SNF for the relatively lower burnup levels in the HI-STAR System for transport[††].

A Brookhaven report written for EPRI [3.3.7] asserts that fuel cladding rupture becomes "virtually absent at stresses below about 200 MPa". It can be readily deduced that the peak cladding stress for the limiting condition of 570°C cladding temperature will be below 200 MPa for the SNF burnup levels considered in this SAR. Recalling σ_{max} at 96.7 MPa (Table 3.3.3) at 300°C gas temperature, the cladding circumferential stress (σ_{peak}) at 570°C is obtained by direct proportionality in absolute gas temperature:

$$\sigma_{peak} = \sigma_{max} (570 + 273)/(300 + 273) = 142.3 \text{ MPa (approximately 20,600 psi)}$$

Therefore, short-term temperature values (T_{max}) of 570°C for zircaloy cladding are considered safe to preclude fuel cladding failure.

The EPRI report cites experiments on fourteen irradiated Turkey Point Unit 3 rods carried out by Einziger et al.[†] in 1982 which showed no breach in cladding even after as much as 7% strain was

---

[††] 40,000 MWD/MTU for BWR fuel and 45,000 MWD/MTU for PWR fuel bounds permissible maximum burnups.

[†] "High Temperature Post Irradiation Materials Performance of Spent Pressurized Water Reactor Fuel Rods under Dry Storage Conditions," by R.E. Einziger, S.D. Atkin, D.E. Stallrecht, and V.S. Pasupathi, Nuclear Technology, 57:65-80 (1982).

accumulated at elevated temperatures lasting for 740-1,000 hours. Einziger's test data corroborates our selection of T_{max} = 570°C as the short duration limiting temperature.

For stainless steel clad fuel, the appropriate short-term temperature limits are based on high temperature creep rupture data presented in another EPRI report by Cunningham et. al. [3.3.6, Table 5-2, page 5-2]. In this report, stainless steel cladding stress limits for 10,000 hour exposure time (in excess of one year) at elevated temperature (1000°F) is provided. This is summarized in Table 3.3.8. From this table, it is apparent that the cladding rupture stresses are significantly higher than the σ_{peak} computed above. Consequently, there is reasonable assurance that stainless steel cladding integrity is maintained by exposure at 540°C temperature for short-term conditions.

Table 3.3.1

HI-STAR SYSTEM MATERIAL TEMPERATURE LIMITS

Material	Normal Condition Temperature Limits	Accident Condition Temperature Limits
Fuel Cladding (Zircaloy and Stainless Steel)	720°F (PWR Fuel) 749°F (BWR Fuel)	1058°F (zircaloy) 1000°F (stainless steel)
Boral†	800°F	950°F
Overpack Closure Plate Mechanical Seals	See Table 4.1.1	See Table 4.1.1
Overpack Vent and Drain Port Plug Seals	See Table 4.1.1	See Table 4.1.1
Aluminum Alloy 5052	176°F††	1105°F†††
Holtite-A	300°F††††	N/A†††††
Aluminum Heat Conduction Elements (Alloy 1100)	725°F	950°F

† Based on AAR Structures Boral thermophysical test data.

†† AL-STAR impact limiter aluminum honeycomb test data.

††† Melting range of alloy is 1105°F-1200°F [3.3.1].

†††† Neutron shield manufacturer's test data (Appendix 1.B).

††††† For shielding analysis (Chapter 5), Holtite-A is conservatively assumed to be lost during the fire accident.

Table 3.3.2

SUMMARY OF PWR ASSEMBLY RODS INITIAL FILL GAS DATA

Assembly Type	Rods Per Assembly	Free Rod Volume (inch^3)	Fill Pressure (psig)	Maximum Fill Volume (Liters at STP†)	
				Per Rod	Per Assembly
W 14×14 Std.	179	1.72	0-460	0.845	151.2
W 15×15 Std.	204	1.25	0-475	0.633	129.1
W 17×17 Std.	264	1.05-1.25	275-500	0.666	175.8
B&W 15×15 Mark B	208	1.308	415	0.582	121.1
B&W 17×17 Mark C	264	0.819	435	0.381	100.6
CE 14×14 Std.	164	1.693	300-450	0.814	133.5
CE 16×16 Sys 80	220	1.411	300-450	0.678	149.2
B&W-15x15 Mark B-11	208	1.260	415	0.524	109.0
CE-14x14 (MP2)	176	1.728	300-450	0.777	136.8

† STP stands for standard temperature and pressure.

Table 3.3.3

BOUNDING VALUES OF FUEL CLADDING STRESS FOR PWR SNF

	W 14×14 Std.	**W 15×15 Std.**	**W 17×17 Std.**	**B&W 15×15 Mark B**	**B&W 17×17 Mark C**	**CE 14×14 Std.**	**CE 16×16 Sys 80**	B&W 15x15 Mark B-11	CE 14x14 (MP2)
Fresh Fuel Rods O.D. (inch)	0.4220	0.422	0.374	0.430	0.379	0.440	0.382	0.414	0.440
End of Life Oxidation Thickness (inch)†	0.0027	0.0027	0.0027	0.0027	0.0027	0.0027	0.0027	0.0027	0.0027
End of Life Rods O.D. (inch)	0.4166	0.4166	0.3686	0.4246	0.3736	0.4346	0.3766	0.4086	0.4346
Rods I.D. (inch)	0.3734	0.373	0.329	0.377	0.331	0.384	0.332	0.370	0.385
Average tube Diameter (inch)	0.3950	0.3948	0.3488	0.4008	0.3523	0.4093	0.3493	0.3893	0.4113
Wall Thickness (inch)	0.0216	0.0218	0.0198	0.0238	0.0213	0.0253	0.0223	0.0193	0.0233
Hot Volume Pressure at 300°C (MPa)††	9.77	10.67	10.08	9.62	10.87	10.01	9.61	9.40	9.23
Cladding Stress (MPa)	89.3	96.7	88.8	81.0	90.0	81.0	75.2	94.8	81.4

† PNL-4835 [3.3.5] reported maximum cladding thickness loss due to in-reactor oxidation.

†† This average rod gas temperature conservatively bounds the plenum gas temperature.

Table 3.3.4

SUMMARY OF FISSION GASES RELEASE PER ASSEMBLY†

Component	Release Fraction††	Release Amount (g-moles/ PWR assembly)	Release Amount (g-moles/ BWR assembly)
Tritium	0.3	0.004	0.003
^{85}Kr	0.3	0.805	0.297
^{129}I	0.12	0.137	0.050
^{131}Xe	0.10	2.664	0.985

† Bounding for 42,500 MWD/MTU burnup PWR assemblies and 40,000 MWD/MTU burnup BWR assemblies.

†† From Regulatory Guide 1.25.

Table 3.3.5

SUMMARY OF BWR ASSEMBLY RODS INITIAL GAS FILL DATA

Assembly Type	Rods Per Assembly	Free Rod Volume (inch^3)	Fill Pressure (psig)	Max. Fill Volume (Liters at STP)	
				Per Rod	Per Assy
GE 7×7 (1966)	49	2.073	0-44.1†	0.126	6.17
GE 7×7 (1968)	49	2.073	0-44.1	0.126	6.17
GE 7×7R	49	1.991	0-44.1	0.121	5.93
GE 8×8	60	1.504	0-44.1	0.0915	5.49
GE 8×8R	~~60~~ *62*	1.433	0-147††	0.240	~~14.4~~ *14.88*
Exxon 9×9	79	1.323	58.8-88.2†††	0.141	11.1
6×6 GE Dresden-1	36	2.304	58.8-88.2	0.245	8.82
6×6 GE Dresden-1 MOX	36	2.286	58.8-88.2	0.243	8.75
6×6 GE Humboldt Bay	36	2.346	58.8-88.2	0.250	9.0
7×7 GE Humboldt Bay	49	*1.666*	58.8-88.2	0.177	8.67
8×8 GE Dresden-1	64	1.235	58.8-88.2	0.131	8.38
8×8 SPC	63	1.615	58.8-88.2	0.172	10.8
9×9 SPC w/2 water rods	79	1.248	58.8-88.2	0.133	10.5
9×9 SPC w/1 water rod	80	1.248	58.8-88.2	0.133	10.6
9×9 GE11/GE13	74	1.389	58.8-88.2	0.150	11.1
9×9 Atrium 9B SPC	72	1.366	58.8-88.2	0.145	10.4
10×10 SVEA-96	96	1.022	58.8-88.2	0.109	10.5
10×10 GE12/GE14	92	1.167	58.8-88.2	0.124	11.4
6x6 Dresden Thin Clad	36	2.455	58.8-88.2	0.261	9.4
7x7 Oyster Creek	49	2.346	58.8-88.2	0.234	11.5

† Conservatively bounding for GE-7x7 (1966), GE-7x7 (1968), GE-7x7R and GE-8x8 (ORNL/TM-9591/V1-R1).

†† Conservatively bounding for GE-8x8R (ORNL/TM-9591/V1-R1 reports 3 atm).

††† BWR fuel rods internal pressurization between 4 and 6 atm (PNL-4835).

Table 3.3.5 (continued)

SUMMARY OF BWR ASSEMBLY RODS INITIAL GAS FILL DATA

Assembly Type	Rods Per Assembly	Free Rod Volume ($inch^3$)	Fill Pressure (psig)	Max. Fill Volume (Liters at STP)	
				Per Rod	Per Assy
8x8 Oyster Creek	64	1.739	58.8-88.2	0.173	11.1
8x8 Quad[†]	64	1.201	58.8-88.2	0.120	7.68
8x8 TVA Browns Ferry	61	1.686	58.8-88.2	0.168	10.2
9x9 SPC-5	76	1.249	58.8-88.2	0.124	9.4

Table 3.3.6

BOUNDING VALUES OF FUEL CLADDING STRESS FOR BWR SNF

Fuel Type	Fresh Fuel Rod O.D. (in.)	End of Life Rod O.D.† (in.)	Rod I.D. (in.)	Avg. Tube Diameter (in.)	Wall Thickness (in.)	Hot Vol. Pressure at 300°C (MPa)	Cladding Stress (MPa)
GE 7×7 (1966)	0.563	0.5536	0.499	0.5263	0.0273	4.61	44.4
GE 7×7 (1968)	0.570	0.5606	0.499	0.5298	0.0308	4.61	39.6
GE 7×7R	0.563	0.5536	0.489	0.5213	0.0323	4.76	38.4
GE 8×8	0.493	0.4836	0.425	0.4543	0.0293	5.08	39.4
GE 8×8R	0.483	0.4736	0.419	0.4463	0.0273	~~6.68~~ *6.52*	~~54.7~~ *53.3*
Exxon 9×9	0.42	0.4106	0.36	0.3853	0.0253	5.08	38.7
6×6 GE Dresden-1	0.5645	0.5551	0.4945	0.5248	0.0303	6.1	52.8
6×6 MOX Dresden-1	0.5625	0.5531	0.4925	0.5228	0.0303	6.1	52.8
Humboldt Bay 6×6	0.563	0.5536	0.499	0.5263	0.0273	5.98	57.6††
Humboldt Bay 7×7	0.486	0.4766	0.42	0.4483	0.0283	6.15	48.7
8×8 GE Dresden-1	0.412	0.4026	0.362	0.3813	0.0203	6.29	59.1††

† Excludes 0.0047 inch end of life oxidation thickness.

†† These fuel types are separately evaluated for peak fuel cladding temperature limits.

Table 3.3.6 (continued)

BOUNDING VALUES OF FUEL CLADDING STRESS FOR BWR SNF

Fuel Type	Fresh Fuel Rod O.D. (in.)	End of Life Rod O.D. (in.)	Rod I.D. (in.)	Avg. Tube Diameter (in.)	Wall Thickness (in.)	Hot Vol. Pressure at 300°C (MPa)	Cladding Stress (MPa)
8×8 SPC	0.484	0.4746	0.414	0.4443	0.0303	5.19	38.0
9×9 SPC w/ 2 water rods	0.424	0.4146	0.364	0.3893	0.0253	5.32	40.9
9×9 SPC w/ 1 water rod	0.423	0.4136	0.364	0.3888	0.0248	5.25	41.1
9×9 GE-11/13	0.44	0.4306	0.384	0.4073	0.0233	5.17	45.2
9×9 Atrium 9B SPC	0.433	0.4236	0.3808	0.4022	0.0214	5.32	50.0
10×10 SVEA-96	0.379	0.3696	0.3294	0.3495	0.0201	4.38	38.1
10×10 GE-12/14	0.404	0.3946	0.352	0.3733	0.0213	4.99	43.7
6x6 Dresden Thin Clad	0.5625	0.5531	0.5105	0.5318	0.0213	5.77	72.5[†]
7x7 Oyster Creek	0.5700	0.5606	0.499	0.5298	0.0308	4.68	40.2
8x8 Oyster Creek	0.5015	0.4921	0.4295	0.4608	0.0313	4.78	35.2
8x8 Quad[+] Westinghouse	0.4576	0.4482	0.3996	0.4239	0.0243	6.33	55.2[†]
8x8 TVA Browns Ferry	0.483	0.4736	0.423	0.4483	0.0253	5.05	44.7
9x9 SPC-5	0.417	0.4076	0.364	0.3858	0.0218	5.38	47.6

Table 3.3.7

INITIAL PEAK CLADDING[†] TEMPERATURE LIMITS FOR TRANSPORT

Fuel Age (years)	Temperature Limits for PWR SNF (°C) [°F]	Temperature Limits for BWR[††] SNF (°C) [°F]	Temperature Limits for 8x8 and 6x6 Dresden-1, Quad[+], and 6x6 Humboldt Bay SNF[†††] (°C) [°F]
5	382.3 [720]	398.2 [749]	391.2 [736]
6	370.2 [698]	382.3 [720]	376.2 [709]
7	347.0 [657]	357.9 [676]	352.2 [666]
10	341.6 [647]	351.4 [665]	346.6 [656]
15	334.1 [633]	344.9 [653]	339.5 [643]

[†] These limits are conservatively applied to stainless steel clad fuel assemblies, which actually have substantially higher limits.

[††] 8x8 and 6x6 GE Dresden-1, Quad[+], and 6x6 GE Humboldt Bay SNF, for which cladding temperature limits are evaluated separately, are excluded from this group.

[†††] The 8x8 and 6x6 GE Dresden-1, Quad[+], and 6x6 GE Humboldt Bay fuel types are low heat emitting assemblies. The heat load for these assembly types is limited to 115 watts per assembly (160 watts Quad[+]) (approximately 58% lower (41% Quad[+]) than the design basis maximum load for BWR fuel). Consequently, these two assembly types are not deemed to be limiting.

Table 3.3.8

HIGH-TEMPERATURE CREEP RUPTURE DATA
FOR STAINLESS STEEL ALLOYS

Alloy	**10,000 hour Rupture Stress at 1000°F (MPa)**
304	170
348	275
316	210

3.4 THERMAL EVALUATION FOR NORMAL CONDITIONS OF TRANSPORT

3.4.1 Thermal Model

The HI-STAR MPC basket designs consist of ~~two~~ *four* distinct geometries engineered to hold 24 *and 32* PWR *(MPC-24, MPC-24E and MPC-32)* or 68 BWR *(MPC-68)* fuel assemblies. The fuel basket forms a honeycomb matrix of square-shaped fuel compartments to retain the fuel assemblies during transport (refer to Figures 1.2.3 and 1.2.5 *for an illustration of PWR and BWR baskets*). The basket is formed by an interlocking honeycomb structure of steel plates and full-length edge welding of the cell corners to form an integral basket configuration. Individual cell walls (except outer periphery MPC-68 *and MPC-32* cell walls) are provided with Boral neutron absorber panels, which consists of a Boral plate sandwiched between the cell wall and a stainless steel sheathing plate, for the full length of the active fuel region.

The design basis decay heat generation per PWR or BWR assembly for normal transport for each MPC type is specified in Table 1.2.13. The decay heat is considered to be nonuniformly distributed over the active fuel length based on the design basis axial burnup distribution specified in Chapter 1 (see Table 1.2.15 and Figures 1.2.13 and 1.2.14).

Transport of heat from the MPC basket interior to the basket periphery is accomplished by conduction through the MPC basket metal grid structure and the narrow helium gaps between the fuel assemblies and fuel cell walls. Heat dissipation in the MPC basket periphery-to-MPC shell gap is by a combination of helium conduction, natural convection (by means of the "Rayleigh" effect), radiation across the gap, and conduction through the aluminum alloy 110 0 heat conduction elements. Between the MPC shell and the overpack inner shell is a small clearance region which is evacuated and backfilled with helium. Helium, besides being inert, is a better conductor of heat than air. Thus, heat conduction through the helium gap between the MPC and the overpack will minimize temperature differentials across this region.

The overpack, under normal transport conditions, passively rejects heat to the environment. Cooling of the exterior system surfaces is by natural convection and radiation. During transport, the HI-STAR System is placed in a horizontal position with stainless steel encased aluminum honeycomb impact limiters installed at both ends of the overpack. To conservatively maximize the calculated internal temperatures, the thermal conductivity of the impact limiters is set essentially equal to zero. Under normal transport conditions, the MPC shell rests on the overpack internal cavity surface forming an eccentric gap. Direct contact between the MPC and overpack surfaces is expected to minimize heat transfer resistance in this region of intimate contact. Significantly improved conductive heat transport due to reduction in the helium gap near the contact region is accounted for in the thermal analysis of the HI-STAR System. The HI-STAR System is conservatively analyzed assuming a minimum 0.02-inch gap at the line of metal-to-metal contact. Analytical modeling details of the various thermal transport mechanisms are provided in the following.

3.4.1.1 Analytical Model - General Remarks

Transport of heat from the heat generation region (fuel assemblies) to the outside environment is analyzed broadly in terms of three interdependent thermal models.

i. The first model considers transport of heat from the fuel assembly to the basket cell walls. This model recognizes the combined effects of conduction (through helium) and radiation, and is essentially a finite element technology-based update of the classical Wooton & Epstein [3.4.1] formulation (which considers radiative heat exchange between fuel rod surfaces).

ii. The second model considers heat transport within an MPC cross section by conduction and radiation. The effective cross sectional thermal conductivity of the basket region obtained from the combined fuel assembly/basket heat conduction radiation model is applied to an axisymmetric thermal model of the HI-STAR System on the FLUENT [3.1.2] code.

iii. The third model deals with the transmission of heat from the MPC exterior surface to the external environment (heat sink). From the MPC shell to the cask exterior surface, heat is conducted through an array of concentric shells representing the MPC -to-overpack helium gap, the overpack inner shell, the intermediate shells, the Holtite-A neutron shielding and finally the overpack outer shell. Heat rejection from the outside cask surfaces to ambient air is considered by accounting for natural convection and thermal radiation heat transfer mechanisms from the exposed cask surfaces. Insolation on exposed cask surfaces is based on 12-hour levels prescribed in 10CFR71, averaged over a 24-hour period.

The following subsections contain a systematic description of the mathematical models devised to articulate the temperature field in the HI-STAR System. Table 3.4.2 shows the relationship between the mathematical models and the corresponding regions (i.e., fuel, MPC, overpack, etc.) of the HI - STAR System. The description begins with the method to characterize the heat transfer behavior of the prismatic (square) opening referred to as the "fuel space" containing a heat emitting fuel assembly. The methodology utilizes a finite-volume procedure to replace the heterogeneous SNF/fuel space region with an equivalent solid body having a well-defined temperature-dependent conductivity. In the following subsection, the method to replace the composite walls of the fuel basket cells with equivalent "solid" walls is presented. Having created the mathematical equivalents for the SNF/fuel spaces and the fuel basket walls, the method to represent the MPC cylinder containing the fuel basket by an equivalent cylinder whose thermal conductivity is a function of the spatial location and coincident temperature is presented.

Following the approach of presenting descriptions starting from the inside and moving to the outer region of a cask, the next subsections present the mathematical model to simulate the overpack. Subsection 3.4.1.1.12 concludes the presentation with a description of how the different models for the specific regions within the HI-STAR System are assembled into the final finite element model.

3.4.1.1.1 Overview of the Thermal Model

Thermal analysis of the HI-STAR System is performed by assuming that the system is subject to its maximum heat duty with each storage location occupied and with the heat generation rate in each stored fuel assembly equal to the design basis maximum value. While the assumption of equal heat generation imputes a certain symmetry to the cask thermal problem, the thermal model must incorporate three attributes of the physical problem to perform a rigorous analysis:

i. While the rate of heat conduction through metals is a relatively weak function of temperature, radiation heat exchange is a nonlinear function of surface temperatures.

ii. Heat generation in the MPC is axially non-uniform due to a non-uniform axial burnup profile in the fuel assemblies.

iii. Inasmuch as the transfer of heat occurs from the inside of the basket region to the outside, the temperature field in the MPC is spatially distributed with the maximum values reached in the central region.

It is clearly impractical to explicitly model every fuel rod in every stored fuel assembly explicitly. Instead, the cross section bounded by the inside of the storage cell, which surrounds the assemblage of fuel rods and the interstitial helium gas, is replaced with an "equivalent" square (solid) section characterized by an effective thermal conductivity. Figure 3.4.1 pictorially illustrates the homogenization concept. Further details on this process for determining the effective conductivity is presented in Subsection 3.4.1.1.2. It suffices to state here that the effective conductivity of the cell space will be a function of temperature, because radiation heat transfer (a major component of the heat transport mechanism between the fuel rods to the basket metal square) is a strong function of the absolute temperatures of the participating bodies. Therefore, in effect, every storage cell location will have a different value of effective conductivity in the homogenized model. The process of determining the temperature-dependent effective conductivity is carried out using a finite volume procedure.

In the next step of homogenization, a planar section of MPC is considered. With each storage cell inside space replaced with an equivalent solid square, the MPC cross section consists of a metallic gridwork (basket cell walls with each cell space containing a solid fuel square with an effective thermal conductivity) circumscribed by a circular ring (MPC shell). There are five distinct materials in this section, namely the homogenized fuel cell squares, the Alloy X MPC structural materials in the MPC (including Boral sheathing material), Boral, aluminum heat conduction elements, and helium gas. Each of the five constituent materials in this section has a different conductivity. As discussed earlier, the conductivity of the homogenized fuel cell is a strong function of temperature.

In order to replace this thermally heterogeneous MPC section with an equivalent conduction-only lamina, resort to the finite-element procedure is necessary. Because the rate of transport of heat within the MPC is influenced by radiation, which is a temperature-dependent effect, the equivalent conductivity of the MPC lamina must be computed as a function of temperature. Finally, it is

recognized that the MPC section consists of two discrete regions, namely, the basket region and the periphery region. The periphery region is the space between the peripheral storage cells and the MPC enclosure shell. This space is essentially full of helium gas surrounded by Alloy X plates and *optionally* aluminum heat conduction elements. Accordingly, as illustrate d in Figure 3.4.2 for MPC-68, the MPC cross section is replaced with two homogenized regions with temperature -dependent conductivities. In particular, the effective conductivity of the fuel cells is subsumed into the equivalent conductivity of the basket c ross section using a finite element procedure. The ANSYS finite -element code is the vehicle for all modeling efforts described in the foregoing.

In summary, appropriate finite element models are used to replace the MPC cross section with an equivalent two-region homogeneous conduction lamina whose local conductivity is a known function of coincident absolute temperature. Thus, the MPC cylinder containing discrete fuel assemblies, helium, Boral, aluminum, and Alloy X is replaced with a right circular cylinder whose material conductivity will vary with radial and axial position as a function of the coincident temperature.

The MPC-to-overpack gap is simply an annular space that is readily modeled with an equivalent conductivity that reflects the conduction an d radiation modes of heat transfer. The overpack is a radially symmetric structure except for the neutron absorber region which is built from radial connectors and Holtite. Using the classical equivalence procedure as described in Section 3.4.1.1.9, this region is replaced with an equivalent radially symmetric annular cylinder.

The thermal analysis procedure described above makes frequent use of equivalent thermal properties to ease the geometric modeling of the cask components. These equivalent properties are rigorously calculated values based on detailed evaluations of actual cask system geometries. All these calculations are performed conservatively to ensure a bounding representation of the cask system. This process, commonly referred to as submodeling, yields accurate (not approximate) results. Given the detailed nature of the submodeling process, experimental validation of the individual submodels is not necessary.

In this manner, a HI-STAR System overpack containing a loaded MPC is replaced with a ri ght circular cylinder with spatially varying temperature-dependent conductivity. Heat is generated within the basket space in this cylinder in the manner of the prescribed axial distribution. In addition, heat is deposited from insolation on its external surface. Natural convection and thermal radiation to ambient air dissipate heat. Details of the elements of mathematical modeling are provided in the following sections.

3.4.1.1.2 Fuel Region Effective Thermal Conductivity Calculation

Thermal properties of a large number of PWR and BWR fuel assembly configurations manufactured by the major fuel suppliers (i.e., Westinghouse, CE, B&W, and GE) have been evaluated for inclusion in the HI-STAR System thermal analysis. Bounding PWR and BWR fuel assembly configurations are determined using the simplified procedure described below. This is followed by the determination of temperature-dependent properties of the bounding PWR and BWR fuel as sembly configurations to be used for cask thermal analysis using a finite-volume (FLUENT) approach.

To determine which of the numerous PWR assembly types listed in Table 3.4.4 should be used in the thermal model for the ~~MPC-24~~ *PWR* fuel baskets, we must establish which assembly has the maximum thermal resistance. The same determination must be made for the MPC-68, out of the menu of SNF types listed in Table 3.4.5. For this purpose, we utilize a simplified procedure that we describe below.

Each fuel assembly consists of a large array of fuel rods typically arranged on a square layout. Every fuel rod in this array is generating heat due to radioactive decay in the enclosed fuel pellets. There is a finite temperature difference required to transport heat from the innermost fuel rods to the storage cell walls. Heat transport within the fuel assembly is based on principles of conduction heat transfer combined with the highly conservative analytical model proposed by Wooton and Epstein [3.4.1]. The Wooton-Epstein model considers radiative heat exchange between individual fuel rod surfaces as a means to bound the hottest fuel rod cladding temperature.

Transport of heat energy within any cross section of a fuel assembly is due to a combination of radiative energy exchange and conduction through the helium gas that fills the interstices between the fuel rods in the array. With the assumption of uniform heat generation within any given horizontal cross section of a fuel assembly, the combined radiation and conduction heat transport effects result in the following heat flow equation:

$$Q = \sigma\, C_o\, F_\varepsilon\, A[T_C^4 - T_B^4] + 13.5740\, L\, K_{cs}[T_C - T_B]$$

where,

$$F_\varepsilon = \textit{Emissivity Factor} = \frac{1}{\left(\frac{1}{\varepsilon_C} + \frac{1}{\varepsilon_B} - 1\right)}$$

ε_C, ε_B = emissivities of fuel cladding, fuel basket (see Table 3.2.4)

C_o = *Assembly Geometry Factor*

$$= \frac{4N}{(N+1)^2} \textit{ (when N is odd)}$$

$$= \frac{4}{N+2} \textit{ (when N is even)}$$

N = Number of rows or columns of rods ar ranged in a square array

A = fuel assembly "box" heat transfer area
= 4 × width × length (ft^2)

L = fuel assembly length (ft)

K_{cs} = fuel assembly constituent materials volume fraction weighted mixture conductivity (Btu/ft-hr-°F)

T_C = hottest fuel cladding temperature (°R)

T_B = box temperature (°R)

Q = net radial heat transport from the assembly interior (Btu/hr)

σ = Stefan-Boltzman Constant (0.1714×10^{-8} Btu/ft^2-hr-°R^4)

In the above heat flow equation, the first term is the Wooten -Epstein radiative heat flow contribution while the second term is the conduction heat transport contribution based on the classical solution to the temperature distribution problem inside a square shaped block with uniform heat generation [3.4.3]. The 13.574 factor in the conduction term of the equation is the shape factor for two - dimensional heat transfer in a square section. Planar fuel assembly heat transport by conduction occurs through a series of resistances formed by the interstitial helium fill gas, fuel cladding and enclosed fuel. An effective planar mixture conductivity is determined by a volume fraction weighted sum of the individual constituent materials resistances. For BWR assemblies, this formulation is applied to the region inside the fuel channel. A seco nd conduction and radiation model is applied between the channel and the fuel basket gap. These two models are combined, in series, to yield a total effective conductivity.

The effective thermal conductivities of several representative intact PWR and BWR assemblies are presented in Tables 3.4.4 and 3.4.5. At higher temperatures (greater than 450 °F), the zircaloy clad fuel assemblies with the lowest effective thermal conductivities are the Westinghouse 17×17 OFA (PWR) and the General Electric GE-11 9×9 (BWR). A discussion of fuel assembly conductivities for some of the newer 10×10 array *and plant specific* BWR fuel designs is presented near the end of this

subsection. Based on this *simplified* analysis, the Westinghouse 17×17 OFA PWR and GE-11 9×9 BWR fuel assemblies are determined to be the bounding configurations for analysis at design basis maximum heat loads. As discussed in Section 3.3.2, stainless clad fuel assemblies with significantly lower decay heat emission characteristics are not deemed to be boundi ng.

Several of the assemblies listed in Tables 3.4.5 were excluded from consideration when determining the bounding assembly because of their extremely low decay heat loads. The excluded assemblies, which were each used at a single reactor only, are physi cally small and have extremely low burnups and long cooling times. These factors combine to result in decay heat loads that are much lower than the design basis maximum. The excluded assemblies are:

Dresden Unit 1 8×8
Dresden Unit 1 6×6
Allis-Chalmers 10×10 Stainless
Exxon Nuclear 10×10 Stainless
Humboldt Bay 7x7
Quad$^+$ 8x8

The Allis-Chalmers and Exxon assemblies are used only in the LaCrosse reactor of the Dairyland Power Cooperative. The design basis assembly decay heat loads for Dresden Unit 1 and LaC rosse SNF (Tables 1.2.14 and 1.2.19) are approximately 58% lower and 69% lower, respectively, than the MPC-68 design basis assembly maximum heat load (Table 1.2.13). Examining Table 3.4.5, the effective thermal conductivity of damaged Dresden Unit 1 fuel a ssemblies inside DFCs (the lowest of any Dresden Unit 1 assembly) and LaCrosse fuel assemblies are approximately 40% lower and 30% lower, respectively, than that of the bounding (GE -11 9×9) fuel assembly. Consequently, the fuel cladding temperatures in the HI-STAR System with Dresden Unit 1 and LaCrosse fuel assemblies (intact or damaged) will be bounded by design basis fuel cladding temperatures.

To accommodate Trojan Nuclear Plant (TNP) SNF in a HI-STAR System's MPC-24E canister, the discharged fuel characteristics at this permanently shutdown site are evaluated herein. To permit TNP fuel in the HI-STAR System, it is necessary to confirm that certain key fuel parameters, viz. burnup (B) and cask decay heat (D) are bounded by the thermal design limits (42,500 MWD/MTU and 20 kW for PWR MPCs). The TNP SNF is a member of the 17x17 class of fuel types. The bulk of the fuel inventory is from Westinghouse and balance from B&W. The B&W SNF configuration and cladding dimensions are same as that of the Westinghouse 17x17 SNF. The fuel is more than nine years old and the burnups are in the range of 5073 MWD/MTU to 41889 MWD/MTU. The TNP SNF burnups are bounded by the design maximum for PWR class of fuel (i.e. B < 42500 MWD/MTU). Because the fuel decay heat is exponentially attenuating with time, it is conservative to evaluate decay heat on a date that precedes fuel loading. For this purpose, a reference date (RD) of 11/9/2001 is employed herein. The decay heat from the most emissive Trojan fuel is bounded by 725 W on RD. Postulating every cell location in an MPC-24E is occupied by this most heat emissive fuel*

* *The height of MPC-24E for Trojan SNF is shorter than the height of generic HI-STAR MPCs.*

assembly, a conservatively bounding D = 17.4 kW is computed. The Trojan MPC-24E heat loads are below the HI-STAR System design heat load (i.e. D < 20 kW) by a significant margin.*

A limited number of Trojan assemblies have poison inserts (RCCAs and BPRAs) and other non-fuel hardware (Thimble Plugs). The inclusion of PWR non-fuel hardware influences the MPC thermal response in two ways: (i) The presence of non-fuel hardware increases the effective basket conductivity, thus enhancing heat dissipation and lowering fuel temperatures and (ii) The volume displaced by the mass of non-fuel hardware lowers the available cavity free volume for accommodating gas released in hypothetical rod rupture scenarios. For a conservatively bounding evaluation, the thermal modeling ignores presence of non-fuel hardware and the MPC cavity volume is computed based on volume displacement by the heaviest fuel (bounding weight) with non-fuel hardware included.

Having established the governing (most resistive) PWR and BWR SNF types, a finite-volume code is used to determine the effective conductivities in a conservative manner. Detailed conduction -radiation finite-volume models of the bo unding PWR and BWR fuel assemblies are developed in the FLUENT code as shown in Figures 3.4.7 and 3.4.8, respectively. The PWR model was originally developed on the ANSYS code which enables individual rod -to-rod and rod -to-basket wall view factor calculations to be performed using that code's AUX12 processor. Limitations of radiation modeling techniques implemented in ANSYS make it difficult to take advantage of the symmetry of the fuel assembly geometry. Unacceptably long CPU time and large workspace requi rements necessary for performing gray body radiation calculations for a complete fuel assembly geometry on ANSYS prompted the development of an alternate simplified model on the FLUENT code. The FLUENT model was benchmarked with the ANSYS model results for a Westinghouse 17×17 OFA fuel assembly geometry for the case of black body radiation (emissivities = 1). The FLUENT model was found to yield conservative results in comparison to the ANSYS model for the "black" surface case. The FLUENT model benchmarked in this manner is used to solve the gray body radiation problem to provide the necessary results for determining the effective thermal conductivity of the governing PWR fuel assembly. The same modeling approach using FLUENT is then applied to the governing BWR fuel assembly and the effective conductivity of GE-11 9×9 fuel is determined.

An equivalent homogeneous material that fills the basket opening replaces the combined fuel rods - helium matrix by the following two-step procedure. In the first step, the FL UENT-based fuel assembly model is solved by applying equal heat generation per unit length to the individual fuel rods and a uniform boundary temperature along the basket cell opening inside periphery. The temperature difference between the peak cladding a nd boundary temperatures is used to determine an effective conductivity as described in the next step. For this purpose, we consider a two -dimensional cross section of a square shaped block of size equal to 2L and a uniform volumetric heat source (q_g) cooled at the periphery with a uniform boundary temperature. Under the assumption of constant material thermal conductivity (K), the temperature difference (ΔT) from the center of the cross section to the periphery is analytically given by [3.4.3]:

* *Projected MPC heat loads are much lower (in the range of 6 kw to 14.5 kW in circa 2003).*

$$\Delta T = 0.29468 \frac{q_g L^2}{K}$$

This analytical formula is applied to determine the effective material conductivity from a known quantity of heat generation applied in the FLUENT model (smeared as a uniform heat source, q_g), basket opening size and ΔT calculated in the first step.

As discussed earlier, the effective fuel space conductivity is a function of the temperature coordinate. The above two step analysis is carried out for a number of reference temperatures. In this manner, the effective conductivity as a function of temperature is established.

In Table 3.4.25, 10×10 array type BWR fuel assembly effective thermal conductivity results from a simplified analysis are presented to determine the most resistive fuel assembly in this class. Using the simplified analysis procedure discussed earlier, the Atrium-10 fuel type is determined to be the most resistive in this class of fuel assemblies. A detailed finite-element model of this assembly type was developed to rigorously quantify the heat dissipation characteristics. The results of this study are presented in Table 3.4.26 and compared to the bounding BWR fuel assembly effective thermal conductivity depicted in Figure 3.4.13. The results of this study demonstrate that the bounding BWR fuel assembly effective thermal conductivity is conservative with respect to the 10×10 class of BWR assemblies. Table 3.4.34 summarizes plant specific fuel types' effective conductivities. From these analytical results, the SPC-5 is determined to be the most resistive fuel assembly in this group of fuel types. A rigorous finite element model of SPC-5 fuel assembly was developed to confirm that its in-plane heat dissipation characteristics are bounded from below by the design basis BWR fuel conductivities used in the HI-STAR thermal analysis.

Temperature-dependent effective conductivities of PWR and BWR design basis fuel assemblies (most resistive SNF types) are shown in Figure 3.4.13. The finite-volume results are also compared to results reported from independent technical sources. From this comparison, it is readily apparent that FLUENT-based fuel assembly conductivities are conservative. The FLUENT computed values (not the published literature data) are used in the MPC thermal analysis presented in this document.

3.4.1.1.3 Effective Thermal Conductivity of Sheathing/Boral/Cell Wall Sandwich

Each MPC basket cell wall (except outer periphery MPC-68 cell walls) is manufactured with a Boral neutron absorbing plate for criticality control. Each Boral plate is sandwiched in a sheathing-to-basket wall pocket. A schematic of the "Box Wall-Boral-Sheathing" sandwich geometry of an MPC basket is illustrated in Figure 3.4.5. During fabrication, a uniformly applied normal pressure on each sheathing-Boral-cell wall sandwich prior to stitch welding of the sheathing periphery to the box wall ensures adequate surface-to-surface contact for elimination of any macroscopic ~~air~~ gaps. The mean coefficient of linear expansion of Boral is higher than the basket materials thermal expansion coefficients. Consequently, basket heat-up from the contained SNF will further ensure a tight fit of the Boral plate

in the sheathing-to-cell wall pocket. The presence of small microscopic gaps due t o less than perfect surface finish characteristics requires consideration of an interfacial contact resistance between the Boral and the box and sheathing surfaces. A conservative contact resistance resulting from a 2 mils Boral-to-pocket ~~air~~ gap is applied to the analysis. Note that this gap would actually be filled with helium~~, so this is very conservative~~. In other words, no credit is taken for the interfacial pressure between Boral and stainless plate/sheet stock produced by the fixturing and welding pr ocess. ~~Furthermore, no credit is taken for the presence of helium and radiative heat exchange across the Boral-to-sheathing or Boral-to-box wall gaps.~~

Heat conduction properties of a composite "Box Wall -Boral-Sheathing" sandwich in the two principal basket cross sectional directions as illustrated in Figure 3.4.5 (i.e., lateral "out -of-plane" and longitudinal "in-plane") are unequal. In the lateral direction, heat is transported across layers of sheathing, ~~air~~ *helium*-gap, Boral (B_4C and cladding layers) ~~air~~ *helium*-gap, and cell wall resistances that are in series (except for the small helium filled end regions shown in Figure 3.4.6). Heat conduction in the longitudinal direction, in contrast, is through an array of essentially parallel resistances comprised of these same layers. Resistance network models applicable to the two directions are illustrated in Figure 3.4.6. It is noted that in addition to the essentially series and parallel resistances of the composite wall layers for the "out -of-plane" and "in-plane" directions, respectively, the effect of small helium filled end regions is also included in the resistance network analogy. For the ANSYS based MPC basket thermal model, corresponding non -isotropic effective thermal conductivities in the two orthogo nal directions are determined and applied in the analysis.

3.4.1.1.4 ANSYS Modeling of Basket In-Plane Conductive Heat Transport

The heat rejection capability of each MPC design (i.e., MPC-24, *MPC-24E, MPC-32* and MPC-68) is evaluated by developing a thermal model of the combined fuel assemblies and composite basket walls geometry on the ANSYS finite element code. The ANSYS model includes a geometric layout of the basket structure in which the "Box Wall-Boral-Sheathing" sandwich is replaced by a "homogeneous wall" with an equivalent thermal conductivity. Since the thermal conductivity of the Alloy X material is a weakly varying function of temperature, the equivalent "homogeneous wall" must have a temperature-dependent effective conductivity. Similarly, as illustrated in Figure 3.4.6, the conductivities in the in-plane and through-thickness direction of the equivalent "homogeneous wall" are different. Finally, as discussed earlier, the fuel assemblies occupying the basket cell openings are modeled as homogeneous heat generating regions with effective temperature dependent in -plane conductivities. The methodology used to reduce the heterogeneous MPC basket - fuel assemblage to an equivalent homogeneous region with effective thermal properties is discussed in the following.

Consider a cylinder of height L and radius r_o with a uniform volumetric heat source term q_g, with insulated top and bottom faces and its cylindrical boundary maintained at a uniform temperature T_c. The maximum centerline temperature (T_h) to boundary temperature difference is readily obtained from classical one-dimensional conduction relationships (for the case of a conducting region with constant thermal conductiv ity K_s):

$$(T_h - T_c) = q_g r_o^2/(4 K_s)$$

Noting that the total heat generated in the cylinder (Q_t) is $\pi r_o^2 L q_g$, the above temperature rise formula can be reduced to the following simplified form in terms of the total heat generation per unit length (Q_t/L):

$$(T_h - T_c) = (Q_t / L)/ (4 \pi K_s)$$

This simple analytical approach is employed to determine an effective basket cross-sectional conductivity by applying an equivalence between the ANSYS finite element model of the basket and the analytical case. The equivalence principle employed in the HI-STAR System thermal analysis is depicted in Figure 3.4.2. The 2-dimensional ANSYS finite element model of the MPC basket is solved by applying a uniform heat generation per unit length in each basket cell region and a constant basket periphery boundary temperature, T_c'. Noting that the basket region with uniformly distributed heat sources and a constant boundary temperature is equivalent to the analytical case of a cylinder with uniform volumetric heat source discussed earlier, an effective MPC basket conductivity (K_{eff}) is readily derived from the analytical formula and the ANSYS solution leading to the following relationship:

$$K_{eff} = N (Q_f'/L) / (4 \pi [T_h' - T_c'])$$

where:

N = number of fuel assemblies

(Q_f'/L) = each fuel assembly heat generation per unit length applied in ANSYS model

T_h' = peak basket cross-section temperature from ANSYS model

Cross sectional views of ~~the~~ MPC basket ANSYS models are ~~depicted~~ *illustrated* in Figures 3.4.10 and 3.4.11 *for a PWR and BWR MPC*. Notice that many of the basket supports and all shims have been conservatively neglected in the models. This conservative geometry simplification, coupled with the conservative neglect of thermal expansion which would minimize the gaps, yields conservative gap thermal resistances. Temperature dependent equivalent thermal conductivities of the fuel region and composite basket walls, as determined from analysis procedures described earlier, are applied to the ANSYS model. The planar ANSYS conduction model is solved by applying a constant basket periphery temperature with uniform heat generation in the fuel region. Table 3.4.6 summarizes effective thermal conductivity results of each basket design obtained from the ANSYS models. ~~The effective calculated basket cross sectional conductivity and the effective axial direction effective conductivity are conservatively assumed to be equal in the comprehensive HI-STAR System thermal model (see Section 3.4.1.1.2).~~ It is recalled that the equivalent thermal conductivity values presented in Table 3.4.6 are lower bound values because, among other elements of conservatism, the effective conductivity of the most resistive SNF type (Tables 3.4.4 and 3.4.5) is used in the MPC finite-element simulations.

3.4.1.1.5 Heat Transfer in MPC Basket Peripheral Regions

Each of the MPC designs for storing PWR or BWR fuel are provided with relatively large helium filled regions formed between the relatively cooler MP C shell and hot basket peripheral panels. For a horizontally oriented cask under normal transport conditions, heat transfer in these helium -filled regions is similar to heat transfer in closed cavities under three cases listed below:

i. differentially heated short vertical cavity

ii. horizontal channel heated from below

iii. horizontal channel heated from above

In a closed cavity (case i scenario), an exchange of hot and cold fluids occurs near the top and bottom ends of the cavity, resulting in a net t ransport of heat across the gap.

The case (ii) scenario is similar to the classical Rayleigh-Benard instability of a layer of fluid heated from below [3.4.6]. If the condition for onset of fluid motion is satisfied, then a multi -cellular natural convection pattern is formed. The flow pattern results in upward motion of heated fluid and downward motion of relatively cooler fluid from the top plate, resulting in a net transport of heat across the heated fluid channel.

The case (iii) is a special form of case (ii) with an inverted (stably stratified) temperature profile. No fluid motion is possible in this circumstance and heat transfer is thus limited to fluid (helium) conduction only.

The three possible cases of closed cavity natural convection are illust rated in Figure 3.4.3 for an MPC-68 basket geometry. Peripheral spaces labeled B and B' illustrate the case (i) scenario, the space labeled D illustrates the case (ii) scenario, and the space labeled D' illustrates the case (iii) scenario. The basket is or iented to conservatively maximize the number of peripheral spaces having *no* fluid motion. A small alteration in the basket orientation will result in a non-zero gravity component in the x -direction which will induce case (i) type fluid motion in the D' spa ce. The rate of natural convection heat transfer is characterized by a Rayleigh number for the cavity defined as follows:

$$Ra_L = \frac{C_p \rho^2 g \beta \Delta T L^3}{\mu K}$$

where:

C_p = fluid heat capacity

ρ = average fluid density

g = acceleration due to gravity

β = coefficient of thermal expansion (equal to reciprocal of absolute temperature for gases)

ΔT = temperature difference between hot and cold surfaces

L = spacing between hot and cold surfaces

μ = fluid viscosity

K = fluid conductivity

Hewitt et al. [3.4.5] repo rt Nusselt number correlations for the closed cavity natural convection cases discussed earlier. A Nusselt number equal to unity implies heat transfer by fluid conduction only. A higher than unity Nusselt number is due to the so -called "Rayleigh" effect, which monotonically rises with increasing Rayleigh number. *Conservatively computed* Nusselt numbers applicable to- helium filled PWR and BWR ~~HI-STAR~~ MPCs in the peripheral voids are provided in Table 3.4.1. These numbers are *allowed to be* used to enhance h elium conductivity *only* in the basket peripheral spaces.

3.4.1.1.6 Effective Conductivity of Multi-Layered Intermediate Shell Region

Fabrication of the layered overpack intermediate shells is discussed in Section 1.2 of this SAR. In the thermal analysis, each intermediate shell metal-to-metal interface presents an additional resistance to heat transport. The contact resistance arises from microscopic pockets of air trapp ed between surface irregularities of the contacting surfaces. Since air is a relatively poor conductor of heat, this results in a reduction in the ability to transport heat across the interface compared to that of the base metal. Interfacial contact condu ctance depends upon three principal factors, namely: (i) base material conductivity, (ii) interfacial contact pressure, and (iii) surface finish.

Rohsenow and Hartnett [3.2.2] have reported results from experimental studies of contact conductance across a ir entrapped stainless steel surfaces with a typical 100 μ-inch surface finish. A minimum contact conductance of 350 Btu/ft -hr-°F is determined from extrapolation of results to zero contact pressure.

The thermal conductivity of carbon steel is about three times that of stainless steel. Thus the choice of carbon steel as the base material in a multi-layered construction significantly improves heat transport across interfaces. The fabrication process guarantees interfacial contact. Contact conductance values extrapolated to zero contact pressures are therefore conservative. The surface finish of hot -rolled carbon steel plate stock is generally in the range of 250 -1000 μ-inch [3.2.1]. The process of forming

hot-rolled flat plate stock to cylindrical shapes to form the intermediate shells by rolling will result in a smoother surface finish. This results from the large surface pressures exerted by the hardened roller faces that flatten out any surface irregularities.

In the HI-STAR thermal analysis, a conservatively bounding interfacial contact conductance value is determined based on the following assumptions:

1. No credit is taken for high base metal conductivity.
2. No credit is taken for interfacial contact pressure.
3. No credit is taken for a smooth surfac e finish resulting from rolling of hot-rolled plate stock to cylindrical shapes.
4. Contact conductance is based on a uniform 2000 μ-inch (1000 μ-inch for each surface condition) interfacial air gap at all interfaces.
5. No credit for radiation heat excha nge across this hypothetical inter-surface air gap.
6. Bounding low thermal conductivity at 200 °F.

These assumptions guarantee a conservative assessment of heat dissipation characteristics of the multi-layered intermediate shell region. The resistances of the five carbon steel layers along with the associated interfacial resistances are combined as resistances in series to determine an effective conductivity of this region leading to the following relationship:

$$K_{gs} = r_o \ell n\left[\frac{r_5}{r_o}\right]\left[\sum_{i=1}^{5} \frac{\delta}{K_{air}} \frac{r_o}{r_i} + \frac{r_o \ell n\left[\frac{r_5}{r_o}\right]}{K_{cst}}\right]^{-1}$$

where (in conventional U.S. units):

K_{gs} = effective intermediate shell region thermal conductivity
r_o = inside radius of inner gamma shield layer
r_i = outer radius of i^{th} intermediate shell layer
δ = interfacial air gap (2000 μ-inch)
K_{air} = air thermal conductivity
K_{cst} = carbon steel thermal conductivity

3.4.1.1.7 Heat Rejection from Overpack and Impact Limiter Outside Surfaces

Jakob and Hawkins [3.2.9] recommend the following correlations for natural convection heat transfer to air from heated vertical surfaces (flat impact limiter ends) and from single horizontal cylinders (overpack and impact limiter curved surfaces):

Turbulent range:

$$h = 0.19(\Delta T)^{1/3} \text{ (Vertical, } GrPr > 10^9)$$

$$h = 0.18(\Delta T)^{1/3} \text{ (Horizontal Cylinder, } GrPr > 10^9)$$

(in conventional U.S. units)

Laminar range:

$$h = 0.29\left(\frac{\Delta T}{L}\right)^{1/4} \text{ (Vertical, } GrPr < 10^9)$$

$$h = 0.27\left(\frac{\Delta T}{D}\right)^{1/4} \text{ (Horizontal Cylinder, } GrPr < 10^9)$$

(in conventional U.S. units)

where ΔT is the temperature differential between the system exterior surface and ambient air. During normal transport conditions, the surfaces to be cooled are the impact limiter and overpack cylindrical surfaces, and the flat vertical faces of the impact limiters. The corresponding length scales for these surfaces are the impact limiter diameter, overpack diameter, and impact limiter diameter, respectively. Noting that $Gr \times Pr$ is expressed as $L^3 \Delta TZ$, where Z (from Table 3.2.7) is at least 2.6×10^5 at a conservatively high upper bound system exterior surface temperature of 340 °F, it is apparent that the turbulent condition is always satisfied for ΔT in excess of a few degrees Fahrenheit. Under turbulent conditions, the more conservative heat transfer corre lation for horizontal cylinders (i.e., $h = 0.18 \Delta T^{1/3}$) is utilized for thermal analyses on all exposed system surfaces.

Including both convective and radiative heat loss from the system exterior surfaces, the following relationship for surface heat flux is developed:

$$q_s = 0.18(T_s - T_A)^{4/3} + \sigma \times \varepsilon \times [(T_s + 460)^4 - (T_A + 460)^4]$$

where:

T_s, T_A = surface, ambient temperatures (°F)
q_s = surface heat flux (Btu/ft^2-hr)
ε = surface emissivity (see Table 3.2.4)
σ = Stefan-Boltzman Constant (0.1714×10^{-8} Btu/ft^2-hr-°R^4)

3.4.1.1.8 Determination of Solar Heat Input

The intensity of solar radiation incident on an exposed surface depends on a number of time varying parameters. The solar heat flux strongly depends upon the time of the day as well as on latit ude and day of the year. Also, the presence of clouds and other atmospheric conditions (dust, haze, etc.) can significantly attenuate solar intensity levels. Rapp [3.4.2] has discussed the influence of such factors in considerable detail.

The HI-STAR System thermal analysis is based upon insolation levels specified in 10CFR71, Subpart

F, which are for a 12-hour daytime period. During normal transport conditions, the HI -STAR System is cyclically subjected to solar heating during the 12-hour daytime period followed by cooling during the 12-hour nighttime. However, due to the large mass of metal and the size of the system, the inherent dynamic time lag in the temperature response is substantially larger than the 24-hour heating-cooling time period. Accordingly, the HI-STAR System cask model includes insolation at exposed surfaces averaged over a 24-hour time period. A bounding solar absorption coefficient of 1.0 is applied to cask exterior surfaces. The 10CFR71 mandated 12-hour average incident solar radiation levels are summarized in Table 3.4.7. The combined incident insolation heat flux absorbed by exposed cask surfaces and decay heat load from the MPC is rejected by natural convection and radiation to ambient air.

3.4.1.1.9 Effective Thermal Conductivity of Radial Channels - Holtite Region

In order to minimize heat transfer resistance limitations due to the poor thermal conductivity of the Holtite-A neutron shield material, a large number of thick radial channels formed from high strength and conductivity carbon steel material are embedded in the neutron shield region. These radial channels form highly conductive heat transfer paths for efficient heat removal. Each channel is welded to the outside surface of the outermost intermediate shell and at the overpack enclosure shell, thereby providing a continuous path for heat removal to the ambient environment.

The effective thermal conductivity of the composite neutron shieldin g and radial channels region is determined by combining the heat transfer resistance of individual components in a parallel network. In determining the heat transfer capability of this region to the outside ambient environment for normal transport conditions, *no credit is taken for conduction through the neutron shielding material.* Thus, heat transport from the outer intermediate shell surface to the overpack outer shell is conservatively based on heat transfer through the carbon steel radial channel legs a lone. Thermal conductivity of the parallel neutron shield and radial channel leg region is given by the following formula:

$$K_{ne} = \frac{K_R N_R t_R \ln\left[\frac{r_B}{r_A}\right]}{2\pi L_R} + \frac{K_{ns} N_R t_{ns} \ln\left[\frac{r_B}{r_A}\right]}{2\pi L_R}$$

where (in consistent U.S. units):

K_{ne}	=	effective thermal conductivity of neutron shield region
r_A	=	inner radius of neutron shielding
r_B	=	outer radius of neutron shielding
K_R	=	effective thermal conductivity of carbon steel radial channel leg
N_R	=	total number of radial channel legs (also equal number of neutron shield sections)
t_R	=	minimum (nominal) thickness of each radial channel leg
L_R	=	effective radial heat transport length through radial channel leg

K_{ns}	=	neutron shield thermal conductivity
t_{ns}	=	neutron shield circumferential thickness (between two radial channel legs)

The radial channel leg to outer intermediate shell surface weld thickness is equal to half the plate thickness. The additional weld resistance is accounted for by reducing the plate thickness in the weld region for a short radial span equal to the weld size. Conductivity of the radi al carbon steel channel legs based on the full thickness for the entire radial span is correspondingly reduced. Figure 3.4.4 depicts a resistance network developed to combine the neutron shield and radial channel legs resistances to determine an effective conductivity of the neutron shield region. Note that in the resistance network analogy only the annulus region between overpack outer enclosure inner surface and intermediate shells outer surface is considered in this analysis. The effective thermal conductivity of neutron shield region is provided in Table 3.4.8.

3.4.1.1.10 Effective Thermal Conductivity of the Eccentric MPC to Overpack Gap

During horizontal shipment of the HI-STAR System under normal transport conditions, the MPC will rest on the inside surface of the overpack. In the region of line contact, the resistance to heat transfer across the gap will be negligibly small due to a vanishingly small gap thickness. The resistance to heat transfer at other regions along the periphery of the MPC will, however, increase in direct proportion to the thickness of the local gap. This variation in gap thickness can be accounted for in the thermal model by developing a relation for the total heat transferred across the gap as given below:

$$Q_E = 2\int_0^{\pi} \frac{K_{He}}{g(\theta)} L\, R_o\, \Delta T\, d\theta$$

where:

Q_E	=	total heat transfer across the gap (Btu/hr)
K_{He}	=	helium conductivity Btu/ft-hr-°F
L	=	length of MPC (ft.)
R_o	=	MPC radius (ft.)
θ	=	angle from point of line contact
$g(\theta)$	=	variation of gap thickness with angle (ft.)
ΔT	=	temperature difference across the gap (°F)

A corresponding relationship for heat transferred across a uniform gap is given by:

$$Q_c = \frac{K_{eff}}{(R_I - R_0)} 2\pi\, R_0\, L\, \Delta T$$

where R_1 is the inside radius of the overpack and K_{eff} is the effective thermal conductivity of an equivalent concentric MPC/overpack gap configuration. From these two relationships, the ratio of effective gap conductivity to helium thermal conductivity in the MPC/overpack region i s shown below:

$$\frac{K_{eff}}{K_{He}} = \frac{R_1 - R_0}{\pi} \int_0^{\pi} \frac{1}{g(\theta)} d\theta$$

Based on an analysis of the geometry of a thin gap between two eccentrically positioned cylinders, the following relationship is developed for variation of the gap thickness with position:

$$g(\theta) = (R_1 - R_0)(1 - \cos\theta) + \varepsilon \cos\theta$$

The above equation conservatively accounts for imperfect contact by postulating a minimum gap ε at the point where the two surfaces would ideally form a line of perfect contact. The relatively thin MPC shell is far more flexible than the much thicker overpack inner shell, and will ovalize to yield greater than line contact. The substantial weight of the fuel basket and contained fuel assemblies will also cause the MPC shell to conform to the overpack inner shell. An evaluation based on contact along a line would therefore be reasonable and conservative. However, a minimum gap is assumed to further increase conservatism in this calculation.

Based on an applied gap of 0.02-inch, which is conservative compared to contact along a line, the effective gap thermal conductivity determined from analytical integration [3.4.7] is in excess of 200% of the conductivity of helium gas. In the HI-STAR analysis, a conservative effective gap conductivity equal to twice the helium gas conductivity is applied to the performance evaluation.

3.4.1.1.11 Effective Thermal Conductivity of MPC Basket-to-Shell Aluminum Heat Conduction Elements

~~As shown in MPC Drawings 1395 and 1401,~~ *The HI-STAR MPCs feature an option to install* full-length heat conduction elements fabricated from aluminum alloy 1100 ~~are placed~~ in the large MPC basket-to-shell gaps ~~to provide uninterrupted metal pathways to transport heat from the basket periphery to the MPC shell.~~ Due to the high aluminum alloy 1100 thermal conductivity (about 15 times that of Alloy X), a significant rate of net heat transfer is possible along the thin plates. *For conservatism, heat dissipation by the Aluminum Heat Conduction Elements (AHCEs) is ignored in normal transport analyses. This overstates the initial fuel temperature for hypothetical fire accident evaluation. To conservatively compute fuel temperature in a hypothetical fire condition, the presence of heat conduction elements in AHCE equipped MPCs is duly recognized.* Figure 3.4.12 shows a mathematical idealization of a heat conduction element inserted between basket periphery panels and the MPC shell. The aluminum insert is shown to cover the MPC basket Alloy X peri pheral panel and MPC shell surfaces (Regions I and III depicted in Figure 3.4.12) along the full -length of the basket. Heat transport to and from the aluminum insert is conservatively postulated to occur across a thin helium gap as shown in the figure (i.e., no credit is considered for aluminum insert to Alloy X metal-to-metal contact). Aluminum surfaces inside the hollow region are sandblasted prior to fabrication to result in a rough surface finish which has a significantly higher emissivity compared to smooth surfaces of rolled aluminum. The untreated aluminum surfaces directly facing Alloy X panels have a smooth finish to minimize contact resistance.

Net heat transfer resistance from the hot basket periphery panel to the relatively cooler MPC shell along the aluminum heat conduction element pathway is a sum of three individual resistances in regions labeled I, II, and III. In Region I, heat is transported from the basket to the aluminum insert surface directly facing the basket panel across a thin helium resistance gap. Longitudinal transport of heat (in the z direction) in the aluminum plate (in Region I) will result in an axially non-uniform temperature distribution. Longitudinal one-dimensional heat transfer in the Region I aluminum plate is analytically formulated to result in the following ordinary differential equation for the non-uniform temperature distribution:

$$t\,K_{Al}\frac{\partial^2 T}{\partial z^2} = -\frac{K_{He}}{h}(T_h - T) \qquad \text{(Equation a)}$$

Boundary Conditions

$$\frac{\partial T}{\partial z} = 0 \text{ at } z = 0$$
$$T = T_h\text{' at } z = P \qquad \text{(Equation b)}$$

where (see Figure 3.4.12):

$T(z)$	=	non-uniform aluminum metal temperature distribution
t	=	conduction element thickness
K_{Al}	=	conduction element conductivity
K_{He}	=	helium conductivity
h	=	helium gap thickness
T_h	=	hot basket temperature
T_h'	=	conduction element Region I boundary temperatu re at z = P
P	=	conduction element Region I length

Solution of this ordinary differential equation subject to the imposed boundary condition is:

$$(T_h - T) = (T_h - T_h') \left[\frac{e^{\frac{z}{\sqrt{\alpha}}} + e^{-\frac{z}{\sqrt{\alpha}}}}{e^{\frac{P}{\sqrt{\alpha}}} + e^{-\frac{P}{\sqrt{\alpha}}}} \right] \qquad \text{(Equation c)}$$

where α is a dimensional parameter equal to htK_{Al}/K_{He}. The net heat tra nsfer (Q_l) across the Region I helium gap can be determined by the following integrated heat flux to a conduction element of length L as:

$$Q_l = \int_0^P \frac{K_{He}}{h} (T_h - T) (L) \, dz \qquad \text{(Equation d)}$$

Substituting the analytical temperature distribution result obtained in Equation c into Equation d and then integrating, the following expression for net heat transfer is obtained:

$$Q_l = \frac{K_{He} L \sqrt{\alpha}}{h} \left(1 - \frac{1}{e^{\frac{P}{\sqrt{\alpha}}} + e^{-\frac{P}{\sqrt{\alpha}}}} \right) (T_h - T_h') \qquad \text{(Equation e)}$$

Based on this result, an expression for Region I resistance is obtained as shown below:

$$R_I = \frac{T_h - T_{h'}}{Q_I} = \frac{h}{K_{He} L \sqrt{\alpha}} \left(1 - \frac{1}{e^{\frac{P}{\sqrt{\alpha}}} + e^{-\frac{P}{\sqrt{\alpha}}}} \right)^{-1} \qquad \text{(Equation f)}$$

Similarly, a Region III resistance expression can be analytically determined as shown below:

$$R_{III} = \frac{(T_c' - T_c)}{Q_{III}} = \frac{h}{K_{He} L \sqrt{\alpha}} \left(1 - \frac{1}{e^{\frac{P}{\sqrt{\alpha}}} + e^{-\frac{P}{\sqrt{\alpha}}}} \right)^{-1} \qquad \text{(Equation g)}$$

A Region II resistance expression can be developed from the following net heat transfer equation in the vertical leg of the conduction element as shown below:

$$Q_{II} = \frac{K_{Al} L t}{W} (T_h' - T_c') \qquad \text{(Equation h)}$$

Hence,

$$R_{II} = \frac{T_h' - T_c'}{Q_{II}} = \frac{W}{K_{Al} L t} \qquad \text{(Equation i)}$$

This completes the analysis for the total thermal resistance attributable to the heat conduction elements equal to sum of the three individual resistances. The total resistance is smeared across the basket-to-MPC shell region as an effective uniform annular gap conductivity (see Figure 3.4.2). Note that heat transport along the conduction elements is an independent conduction path in parallel with conduction and radiation mechanisms in the large helium gaps. Helium conduction and radiation between the MPC basket and the MPC shell is accounted for separately in the ANSYS MPC models described earlier in this section. Therefore, the total MPC basket-to-MPC shell peripheral gaps conductivity will be the sum of the conduction elements effective conductivity and the helium conduction-radiation gap effective conductivity.

3.4.1.1.12 FLUENT Model for HI-STAR Temperature Field Computation

In the preceding subsections, the series of analytical and numerical models to define the thermal characteristics of the various elements of the HI-STAR System are presented. The thermal modeling begins with the replacement of the SNF cross section and surrounding fuel cell space by a solid lamina

with an equivalent conductivity. Since radiation is an important constituent of the heat transfer process in the SNF/storage cell space and the rate of radiation heat transfer is a strong function of the surface temperatures, it is necessary to treat the equivalent lamina conductivity as a function of temperature. In fact, because of the relatively large range of temperatures which will exist in a loaded HI-STAR System under the design basis heat loads, it is necessary to include the effect of variation in the thermal conductivity of materials with temperature throughout the system finite volume model. The presence of significant radiation effect in the storage cell spaces adds to the imperative to treat the equivalent lamina conductivity as temperature-dependent.

FLUENT finite volume simulations have been performed to establish the equivalent thermal conductivity as a function of temperature for the limiting (thermally most resistive) BWR and PWR spent fuel types. By utilizing the most limiting SNF (established through a simplified analytical process for comparing conductivities) the numerical idealization for the fuel space conductivity is ensured to be conservative for all non-limiting fuel types.

Having replaced the interior of the cell spaces by solid prismatic (square) columns possessing a temperature-dependent conductivity essentially renders the basket into a non-homogeneous three-dimensional solid where the non-homogeneity is introduced by the honeycomb basket structure. The basket panels themselves are a composite of Alloy X cell wall, Boral neutron absorber, and Alloy X sheathing metal. A conservative approach to replace this composite section with an equivalent "solid wall" is described in a preceding subsection.

In the next step, a planar section of the MPC is considered. The MPC, externally radially symmetric, contains a non-symmetric basket lamina wherein the equivalent fuel space solid squares are separated by the "equivalent" solid metal walls. The space between the basket and the MPC, called the peripheral gap, is filled with helium gas and aluminum heat conduction elements (shown in MPC Drawings 1395 and 1401). The equivalent thermal conductivity of this MPC section is computed using a finite element procedure on ANSYS, as described previously. To the "helium-conduction-radiation" based peripheral gap conductivity, the effective conductivity of aluminum conduction elements is added to obtain a combined effective conductivity. At this stage in the thermal analysis, the SNF/basket/MPC assemblage has been replaced with a two-zone (Figure 3.4.2) cylindrical solid whose thermal conductivity is a strong function of temperature.

The idealization for the overpack is considerably more straightforward. The overpack is radially symmetric except for the Holtite region (discussed in Subsection 3.4.1.1.9). The procedure to replace the multiple shell layers, Holtite-A and radial connectors with an equivalent solid utilizes classical heat conduction analogies, as described in the preceding subsections.

In the final step of the analysis, the equivalent two-zone MPC cylinder, the equivalent overpack shell, the top and bottom plates, and the impact limiters are assembled into a comprehensive finite volume model. A cross section of this axisymmetric model implemented on FLUENT is shown in Figure 3.4.14. A summary of the essential features of this model is presented in the following:

- The overpack shell is represented by 840×9 elements. The effective thermal conductivity of the overpack shell elements is set down as a function of temperature based on the analyses described earlier.

- The overpack bottom plate and bolted closure plate are modele d by 312×9 axisymmetric elements.

- The two-zone MPC "solid" is represented by 1,144×9 axisymmetric elements.

- The space between the MPC "solid" and the overpack interior space is assumed to contain helium.

- Heat input due to insolation is applied to the impact limiter surfaces and the cylindrical surface of the overpack.

- The heat generation in the MPC solid basket region is assumed to be uniform in each horizontal plane, but to vary in the axial direction to correspond to the axial burnup distribution in the active fuel region postulated in Chapter 1.

The finite volume model constructed in this manner will produce an axisymmetric temperature distribution. The peak temperature will occur near the centerline and is expected to correspond to the axial location of peak heat generation. As is shown later, the results from the finite element solution bear out these observations.

3.4.1.1.13 Effect of Fuel Cladding Crud Resistance

In this subsection, a conservatively bounding estimate of the temperature d rop across a crud film adhering to a fuel rod during dry storage conditions is determined. The evaluation is performed for a BWR fuel assembly based on an upper bound crud thickness obtained from PNL-4835 report ([3.3.5], Table 3). The crud present on fuel assemblies is predominantly iron oxide mixed, with small quantities of other metals such as cobalt, nickel, chromium, etc. Consequently, the effective conductivity of the crud mixture is expected to be in the range of typical metal alloys. Metals have the rmal conductivities several orders of magnitude larger than that of helium. In the interest of extreme conservatism, however, a film of helium with the same thickness replaces the crud layer. The calculation is performed in two steps. In the first step, a crud film resistance is determined based on bounding maximum crud layer thickness replaced as a helium film on the fuel rod surfaces. This is followed by a peak local cladding heat flux calculation for the smaller GE 7×7 fuel assembly postulated to emit a conservatively bounding decay heat equal to 0.5kW. The temperature drop across the crud film obtained as a product of the heat flux and crud resistance terms is determined to be less than 0.1 °F. The calculations are presented below:

Bounding Crud Thickness (δ) = 130μm (4.26×10^{-4} ft)

(PNL-4835)

Crud Conductivity (K) = 0.1 Btu/ft-hr-°F (conservatively assumed as helium)

GE 7×7 Fuel Assembly:

Rod O.D.	=	0.563"
Active Fuel Length	=	150"
Heat Transfer Area	=	$(7\times7)\,(\pi \times 0.563) \times 150/144$
	=	$90.3\ ft^2$
Axial Peaking Factor	=	1.195 (Burnup distribution Table 1.2.15)
Decay Heat	=	500W (conservative assumption)

$$\text{Crud Resistance} = \frac{\delta}{K} = \frac{4.26\times10^{-4}}{0.1} = 4.26\times10^{-3}\,\frac{ft^2\text{-}hr\text{-}°F}{Btu}$$

$$\text{Peak Heat Flux} = \frac{(500\times3.417)\,Btu/hr}{90.3\,ft^2}\times1.195$$

$$= 18.92\times1.195 = 22.6\,\frac{Btu}{ft^2\text{-}hr}$$

Temperature drop (ΔT_c) across crud film:

$$= 4.26\times10^{-3}\,\frac{ft^2\text{-}hr\text{-}°F}{Btu}\times22.6\,\frac{Btu}{ft^2\text{-}hr}$$

$$= 0.096°F$$

(i.e., less than 0.1°F)

Therefore, it is concluded that deposition of cr ud does not materially change the SNF cladding temperature.

3.4.1.1.14 Maximum Time Limit During Wet Transfer

While loading an empty HI-STAR System for transport directly from a spent fuel pool, water inside the MPC cavity is not permitted to boil. Conse quently, uncontrolled pressures in the de -watering, purging, and recharging system that may result from two -phase condition, are completely avoided. This requirement is accomplished by imposing a limit on the maximum allowable time duration for fuel to be submerged in water after a loaded HI -STAR cask is removed from the pool and prior to the start of vacuum drying operations.

When the HI-STAR overpack and the loaded MPC under water -flooded conditions are removed from

the pool, the combined mass of the wat er, the fuel, the MPC, and the overpack will absorb the decay heat emitted by the fuel assemblies. This results in a slow temperature rise of the entire system with time, starting from an initial temperature of the contents. The rate of temperature rise is limited by the thermal inertia of the HI-STAR system. To enable a bounding heat-up rate determination for the HI-STAR system, the following conservative assumptions are imposed:

i. Heat loss by natural convection and radiation from the exposed HI-STAR surfaces to the pool building ambient air is neglected (i.e., an adiabatic temperature rise calculation is performed).

ii. Design Basis maximum decay heat input from the loaded fuel assemblies is imposed on the HI-STAR system.

iii. The smallest of the *minimum* MPC cavity-free volumes between the two MPC types is considered for flooded water mass determination.

iv. Fifty percent of the water mass in the MPC cavity is credited towards water thermal inertia evaluation.

Table 3.4.19 summarizes the weights and thermal inertias of several components in the loaded HI-STAR system. The rate of temperature rise of the HI-STAR and its contents during an adiabatic heat-up is governed by the following equation:

$$\frac{dT}{d\tau} = \frac{Q}{C_h}$$

where:

Q = decay heat load (Btu/hr) [equal to Design Basis maximum (between the two MPC types) 20.0 kW (i.e., 68,260 Btu/hr)]

C_h = combined thermal inertia of the loaded HI-STAR system (Btu/°F)

T = temperature of the contents (°F)

t = time after HI-STAR system is removed from the pool (hr)

A bounding heat-up rate for the HI-STAR system contents is determined to be equal to 2.19 °F/hr. From this adiabatic rate of temperature rise estimate, the maximum allowable time duration (t_{max}) for fuel to be submerged in water is determined as follows:

$$t_{max} = \frac{T_{boil} - T_{initial}}{dT/d\tau}$$

where:

T_{boil} = boiling temperature of water (equal to 212 °F at the water surface in the MPC cavity)

$T_{initial}$ = initial temperature of the HI-STAR contents when removed from the pool

Table 3.4.20 provides a summary of t_{max} at several initial HI-STAR contents temperatures.

As set forth in Section 7.4, in the unlikely event where the maximum allowable time provided in Table 3.4.20 is found to be insufficient to complete all wet transfer operations, a forced water circulation shall be initiated and maintained to remove the decay heat from the MPC cavity. In this case, relatively cooler water will enter via the MPC lid drain port connection and heated water will exit from the vent port. The minimum water flow rate required to maintain t he MPC cavity water temperature below boiling with an adequate subcooling margin is determined as follows:

$$M_W = \frac{Q}{C_{pw}(T_{max} - T_{in})}$$

where:

M_W = minimum water flow rate (lb/hr)

C_{pw} = water heat capacity (Btu/lb-°F)

T_{max} = maximum MPC cavity water mass temperature

T_{in} = temperature of water supply to MPC

With the MPC cavity water temperature limited to 150 °F, MPC inlet water maximum temperature equal to 125°F and at the design basis maximum heat load, the water flow rate is determined to be 2,731 lb/hr (5.5 gpm).

3.4.1.1.15 Cask Cooldown and Reflood Analysis During Fuel Unloading Operation

Before a loaded HI-STAR System can be unloaded (i.e., fuel removed from the MPC) the cask must be cooled from the operating temperatures and reflooded with water. Past i ndustry experience generally supports cooldown of cask internals and fuel from hot storage conditions by direct water quenching. However, the extremely rapid cooldown rates that are typical during water injection, to which the hot cask internals and fuel cladding are subjected to, may result in uncontrolled thermal stresses and failure in the structural members. Moreover, water injection results in large amounts of steam generation and unpredictable transient two-phase flow conditions inside the MPC cavity, which may result in over-pressurization of the MPC helium retention boundary and a potentially unacceptable reduction in the safety margins to prevent criticality. To avoid potential safety concerns

related to rapid cask cooldown by direct water quenching , the HI-STAR MPCs are designed to be cooled in a gradual manner, thereby eliminating thermal shock loads on the cask internals and fuel cladding.

In the unlikely event that a HI-STAR system is required to be unloaded, it will be transported back to the fuel handling building. Prior to reflooding the MPC cavity with water, a forced flow helium recirculation system with adequate flow capacity shall be operated to remove the decay heat and initiate a slow cask cooldown lasting for several days. The operating procedures in Section 7.2 provide a detailed description of the steps involved in the cask unloading. In this section, an analytical evaluation is presented to provide the basis for helium flow rates and time of forced cooling to meet the objective of eliminating thermal shock when the MPC cavity is eventually flooded with water.

Under a closed loop forced helium circulation condition, the helium gas is cooled via an external chiller, down to 100°F, and then introduced inside the MPC cavity from the drain line near the bottom baseplate. The helium gas enters the MPC basket from the bottom oversized flow holes and moves upward through the hot fuel assemblies, removing heat and cooling the MPC internals. The heated helium gas exits from the basket top and collects in the top plenum, from where it is expelled through the MPC lid vent connection to the helium recirculation and cooling system. The bulk average temperature reduction of the MPC contents as a function of time is principally dependent upon the rate of helium circulation. The temperature transient is governed by the following heat balance equation:

$$C_h \frac{dT}{d\tau} = Q_D - m C_p (T - T_i) - Q_c$$

Initial Condition: $T = T_o$ at $t = 0$

where:

T = MPC bulk average temperature (°F)

T_o = initial MPC bulk average temperature in the HI-STAR system (equal to 483°F [3.4.16])

t = time after start of forced circulation (hr)

Q_D = decay heat load (Btu/hr) (equal to Design Basis maximum 20.0 kW (i.e., 68,260 Btu/hr))

m = helium circulation rate (lb/hr)

C_p = helium heat capacity (Btu/lb-°F)

(equal to 1.24 Btu/lb-°F)

Q_c = heat rejection from cask exposed surfaces to ambient (Btu/hr) (conservatively neglected)

C_h = thermal capacity of the loaded MPC (Btu/ °F) (For a bounding upper bound 100,000 lb loaded MPC weight, and heat capacity of Alloy X equal to 0.12 Btu/lb-°F, the heat capacity is equal to 12,000 Btu/ °F)

T_i = MPC helium inlet temperature (°F)

The differential equation is analytically solved, yielding the following expression for time-dependent MPC bulk temperature:

$$T(t) = (T_i + \frac{Q_D}{m C_p})(1 - e^{-\frac{m C_p t}{C_h}}) + T_o e^{-\frac{m C_p t}{C_h}}$$

This equation is used to determine the minimum helium mass flow rate that would cool the MPC cavity down from initially hot conditions to less than 200°F. For example, to cool the MPC to less than 200°F in 72 hours would required a helium mass flow rate of 574 lb/hr (i.e., 859 SCFM).

Once the helium gas circulation has cooled the MPC internals to less than 200 °F, water can be injected to the MPC without risk of boiling and the associated thermal stress concerns. Because of the relatively long cooldown period, the thermal stress contribution to the total cladding stress would be negligible, and the total stress would therefore be bounded by the normal (dry) condition. The elimination of boiling eliminates any concern of over-pressurization due to steam production.

3.4.1.1.16 MPC Temperature Distribution Under Vacuum Conditions

The initial loading of SNF in the MPC requires that the water within the MPC be drained and replaced with helium. This operation on the HI -STAR MPCs will be carried out using a conventional vacuum drying approach. In this method, removal of the last traces of residual moisture from the MPC cavity is accomplished by evacuating the MPC for a short time after draining the MPC.

Prior to the start of the MPC draining operation, both the overpack annulus and the MPC are full of water. The presence of water in the MPC ensures that the fuel cladding temperatures are lower than design basis limits by large margins. As the heat generating active fuel length is uncovered during the draining operation, the fuel and basket mass will undergo a gradual heat up from the initially cold conditions when the heated surfaces were submerged under water.

A vacuum condition steady-state analysis has been performed, for Holtec MPCs, at conservatively higher than transport design basis heat loads (~~22.25 kW for MPC-24 and 21.4 kW for MPC-68~~ *29 kW*

for all MPCs) to demonstrate that fuel cladding temperature limits are not exceede d. The results of this analysis, therefore, bound HI-STAR vacuum condition temperatures. The bounding analysis demonstrates that the steady -state maximum temperatures in the vacuum condition will remain below short-term temperature limits.

3.4.1.1.17 Effects of Helium Dilution from Fuel Rod Gases

In this subsection, the generic cask transportation accident issue raised in a USNRC Spent Fuel Project Office (SFPO) staff guidance letter† is addressed. This issue directs cask designers to evaluate the impact of fission gas release into the canister, from a 100% fuel rods rupture accident, on the cask component temperatures and pressures *when the MNOP* is within 10% of the design pressure.* ~~:~~ *Although HI-STAR MNOP does not fall within the stipulated criteria,* ~~The~~ *the* impact ~~is~~ illustrated ~~from the limiting~~ *for a HI-STAR with an* MPC-24 *canister.* ~~design., in which the MNOP is within 10% of the design pressure.~~

Under a severe hypothetical accident scenario 100% of the fuel rods may rupture, releasing the rod fill gas (helium) and a portion of the gaseous fission products (^{3}H, ^{85}Kr, ^{129}I and ^{131}Xe). The gaseous fission products release fractions are stipulated in NUREG-1536. The released gases will mix with the MPC backfill gas and reduce its thermal conductivity. This reduction in conductivity will result in a small increase in MPC temperatures and pressures.

Appendix C of NUREG/CR-0497 [3.4.13] describes a method for calculating the effective thermal conductivity of a mixture of gases. The same method is also descr ibed by Rohsenow and Hartnett [3.2.2]. The following expression is provided by both references:

$$k_{mix} = \sum_{i=1}^{n} \left(\frac{k_i x_i}{x_i + \sum_{\substack{j=1 \\ j \neq i}}^{n} \varphi_{ij} x_j} \right)$$

where:

k_{mix} = thermal conductivity of the gas mixture (Btu/hr -ft-°F)
n = number of gases
k_i = thermal conductivity of gas component i (Btu/hr-ft-°F)
x_i = mole fraction of gas component i

In the preceding equation, the term φ_{ij} is given by the following:

† SFPO Director's Interim Staff Guidance Letter(s), W.F. Kane, (Interim Staff -Guidance-7), October 8, 1998.

* *MNOP is a regulatory term defined in NUREG-1617 as the maximum gauge pressure that would develop in the containment in a period of 1 year under the heat condition specified in 10 CFR 71.71(c)(1) in the absence of venting, external ancillary cooling or operational controls.*

$$\varphi_{ij} = \phi_{ij}\left[1 + 2.41\frac{(M_i - M_j)(M_i - 0.142 \cdot M_j)}{(M_i + M_j)^2}\right]$$

where M_i and M_j are the molecular weights of gas components i and j, and ϕ_{ij} is:

$$\phi_{ij} = \frac{\left[1 + \left(\frac{k_i}{k_j}\right)^{\frac{1}{2}}\left(\frac{M_i}{M_j}\right)^{\frac{1}{4}}\right]^2}{2^{\frac{3}{2}}\left(1 + \frac{M_i}{M_j}\right)^{\frac{1}{2}}}$$

Table 3.4.30 presents a summary of the gas mixture thermal conductivity calculations for an MPC-24 containing design basis PWR fuel assemblies.

Having calculated the gas mixture thermal conductivity, the effective thermal conductivity of the design basis PWR fuel assembly is calculated using the finite-volume model described in Subsection 3.4.1.1.2. Only the helium gas conductivity is changed, all other modeling assumptions are the same. The fuel assembly effective thermal conductivity with diluted helium is compared to that with undiluted helium in Table 3.4.31.

Next, the effective thermal conductivities of the MPC fuel basket and basket periphery regions are determined as described in Subsection 3.4.1.1.4. This calculation incorporates both the diluted h elium thermal conductivity and the effective thermal conductivity of the fuel assembly with diluted helium. The Rayleigh effect thermal conductivity multipliers are unchanged in this analysis. This is conservative because the released rod gases will increa se the average fluid density and decrease the gas thermal conductivity, consequently increasing the Rayleigh number. The effective thermal conductivities with diluted helium are compared to those with undiluted helium in Table 3.4.31.

The MPC fuel basket and basket periphery effective thermal conductivities are input to a finite-volume model of the HI-STAR System arranged for transport. The cask system temperature distribution with diluted MPC helium is determined using the finite-volume model, as described in Subsection 3.4.1.1.12. Design basis normal environmental conditions are applied to the model and a temperature field solution obtained. Cask system temperatures with diluted MPC helium are summarized in Table 3.4.32.

The slightly higher MPC cavity temperature with MPC helium dilution will result in a small perturbation in MPC internal pressure. Based on the temperature field obtained with helium dilution, the MPC internal pressure is determined using the Ideal Gas Law. The calculated MPC internal

pressure with helium dilution is presented in Table 3.4.33.

The analyses presented in this subsection are performed to determine the effect of a hypothetical rupture of all fuel rods in a HI-STAR System during a severe transportation accident. Under the extreme conditions, the MPC component temperatures and pressures are within design limits. Based on the results of these conservative calculations, it is determined that the effects of this severe hypothetical condition do not exceed the abilities of the HI -STAR System.

3.4.1.1.18 HI-STAR Temperature Field With Low Heat Emitting Fuel

The HI-STAR 100 thermal evaluations for BWR fuel are divided in two groups of fuel assemblies proposed for storage in MPC-68. These groups are classified as Low Heat Emitting (LHE) fuel assemblies and Design Basis (DB) fuel assemblies. The LHE group of fuel assemblies are characterized by low burnup, long cooling time, and short active fuel lengths. Consequently, their heat loads are dwarfed by the DB group of fuel assemblies. The Dresden-1 (6x6 and 8x8), *Quad*$^+$, and Humboldt Bay (7x7 and 6x6) fuel characteristics warrant their classification as LHE fuel. These characteristics, including burnup and cooling time limits imposed on this class of fuel, are presented in Table 2.1.6. This fuel (*except Quad*$^+$ is permitted to be loaded when encased in Damaged Fuel Containers (DFCs). As a result of interruption of radiation heat exchange between the fuel assembly and the fuel basket by the DFC boundary, this loading configuration is bounding for thermal evaluation. In Subsection 4.4.1.1.2, two canister designs for encasing LHE fuel are evaluated – a previously approved Holtec Design (Holtec Drawing-1783) and an existing canister in which some of the Dresden-1 fuel is currently stored (Transnuclear D-1 Canister). The most resistive fuel assembly determined by analytical evaluation is considered for thermal evaluation (see Table 4.4.6). The MPC -68 basket effective conductivity, loaded with the most resistive fuel assembly from the LHE group of fuel (*encased in a canister*) is provided in Table 4.4.7. To this basket, LHE fuel decay heat load, is applied and a HI -STAR 100 System temperature field obtained. The low heat load burden limits the initial peak cladding temperature to less than *530°F* which is substantially below the temperature limit for long-cooled fuel (~643°F).

A thoria rod canister designed to hold a maximum of 20 fuel rods arrayed in a 5x4 configuration is currently stored at the Dresden -1 spent fuel pool. The fuel rods contain a mixture of enriched UO_2 and Thorium Oxide in the fuel pellets. The fuel rods were originally constituted as part of an 8x8 fuel assembly and used in the second and third cycle of Dresden -1 operation. The maximum fuel burnup of these rods is quite low (~13,100 MWD/MTU). The thoria rod canister internal design is a honeycomb structure formed from 12 gage stainless steel plates. The rods are loaded in individual square cells and are isolated from each other by the cell walls. The few number of rods (18 per assembly) and very low burnup of fuel stored in these Dresden -1 canisters render them as miniscule sources of decay heat. The canister all-metal internal honeycomb construction serves as an additional means of heat dissipation in the fuel cell space. In accordance with

preferential fuel loading requirements, low burnup fuel shall be loaded toward the basket periphery (i.e., away from the hot central core of the fuel basket). All these considerations provide ample assurance that these fuel rods will be stored in a benign thermal environment and therefore remain protected during transport.

3.4.1.2 Test Model

A detailed analytical model for evaluating the thermal design of the HI-STAR System was developed using the FLUENT CFD code and the industry standard ANSYS modeling system as discussed in Subsection 3.4.1.1. Furthermore, the analysis incorporates many conservative assumptions in order to demonstrate compliance with specified temperature limits for operation with adequate margins. In view of these considerations, the HI-STAR thermal design complies with the thermal criteria set forth in the design basis for normal transport conditions. Additional experimental verification of the thermal design is therefore not required. Acceptance and periodic thermal testing for the HI-STAR System is discussed in Sections 8.1 and 8.2.

3.4.2 Maximum Temperatures Under Normal Transport Conditions

Both MPC-basket designs developed for the HI-STAR System have been analyzed to determine temperature distributions under normal transport conditions. In the HI-STAR System thermal analysis models developed on FLUENT, the overpack impact limiters are included in the finite volume geometry. However, no credit is considered for the presence of heat conducting aluminum honeycomb material. In other words, heat transmission through the ends is conservatively neglected in the analysis. The thermal results are therefore bounding with respect to impact limiter design. The MPC baskets are considered to be loaded at design-basis maximum heat load with PWR or BWR fuel assemblies, as appropriate.

As discussed in Subsection 3.4.1.1.1, the thermal analysis is performed using a submodeling process where the results of an analysis on an individual component are incorporated into the analysis of a larger set of components. Specifically, the submodeling process yields directly computed fuel temperatures from which fuel basket temperatures are indirectly calculated. This modeling process differs from previous analytical approaches wherein the basket temperatures were evaluated first and then a basket-to-cladding temperature difference calculation by Wooten-Epstein or other means provided a basis for cladding temperatures. Subsection 3.4.1.1.2 describes the calculation of an effective fuel assembly thermal conductivity for an equivalent homogenous region. It is important to note that the result of this analysis is a function for thermal conductivity versus temperature. This function for fuel thermal conductivity is then input to the fuel basket effective thermal conductivity calculation described in Subsection 3.4.1.1.4. This calculation uses a finite-element methodology, wherein each fuel cell region containing multiple finite-elements has temperature varying thermal conductivity properties. The resultant temperature varying fuel basket thermal conductivity computed by this basket-fuel composite model is then input to the fuel basket region of the FLUENT cask model.

Because the FLUENT cask model incorporates the results of the fuel basket submodel, which in turn incorporates the fuel assembly submodel, the peak temperature reported from the FLUENT model is the peak temperature in any component. In a dry storage cas k, the hottest components are the fuel assemblies. It should be noted that, because the fuel assembly models described in Subsection 3.4.1.1.2 include the fuel pellets, the FLUENT calculated peak temperatures reported in Tables 3.4.10 and 3.4.11 are actually peak pellet centerline temperatures which bound the peak cladding temperatures. We conservatively assume that the peak clad temperature is equal to the peak pellet centerline temperature.

For both the 24-PWR and 68-BWR assembly MPC-basket configurations, *baseline* converged temperature contours corresponding to *steady-state hot* conditions (100°F ambient, maximum design basis maximum decay heat and full insolation) *and AHCEs installed in the fuel basket peripheral spaces* are shown in Figures 3.4.16 and 3.4.17. Figures 3.4.19 and 3.4.20 show the axial temperature variation of the hottest fuel rod in the MPC-24 and MPC-68 basket designs, respectively. Figures 3.4.22 and 3.4.23 show the radial temperature profile in the MPC-24 and MPC-68 basket designs, respectively, in the horizontal plane where maximum fuel cladding temperature is indicated. Tables 3.4.10 and 3.4.11 summarize maximum calculated temperatures in different parts of the HI-STAR System at design-basis maximum decay heat loads. Tables 3.4.28 and 3.4.29 summarize the peak fuel cladding temperatures with heat loads lower than the design basis maximum. In Tables 3.4.22 and 3.4.23, maximum calculated temperatures in different parts of the HI-STAR System under *steady-state cold* conditions (-40°F ambient, maximum design basis maximum decay heat and no insolation) are summarized. *To confirm that the results provided herein are bounding for all MPCs (MPC-24, MPC-24E, MPC-32 and MPC-68) without the AHCEs in the MPC peripheral spaces, an alternate thermal model with certain excessive elements of conservatism moderated is deployed. The results of the alternate calculation confirm that the reported fuel temperatures are conservatively bounding.*

The following additional observations can be derived by inspecting the temperature field obtained from the finite element analysis:

- The maximum fuel cladding temperature is well within the PNL recommended temperature limit.
- The maximum temperature of basket structural material is well within the stipulated design temperatures.
- The maximum temperature of the Boral neutron absorber is below the material supplier's recommended limit.
- The maximum temperatures of the MPC helium retention boundary materials are well below their respective ASME Code limits.
- The maximum temperatures of the aluminum heat conduction elements are well below the

stipulated design temperature limits.

- The maximum temperature of the HI-STAR containment boundary materials is well below their respective ASME Code limits.

- The neutron shielding material (Holtite-A) will not experience temperatures in excess of its qualified limit.

The above observations lead us to conclude that the temperature field in the HI -STAR System with a fully loaded MPC containing design-basis heat emitting SNF complies with all regulatory and industry thermal requirements for normal conditions of transport. In other words, the thermal environment in the HI-STAR System will be conducive to safe transport of spent nuclear fuel.

3.4.2.1 Maximum Accessible Surface Temperatures

Access to the HI-STAR overpack cylindrical surface is restricted by the use of a personnel barrier (See Holtec Drawing 1809 in Chapter 1). Therefore, the HI -STAR System surfaces accessible during normal transport are the exposed impact limiter surfaces outside the personnel barrier. In this subsection, the exposed impact limiter surface temperatures are computed by including heat transmission from the hot overpack ends through the impact limiters. A conservatively bounding analysis is performed by applying the thermal conductivity of aluminum to the encased aluminum-honeycomb material in the impact limiter shells to the normal condition thermal model discussed earlier in this chapter. In this manner heat transport to the exposed surfaces from the hot overpack is maximized and accessible surface temperatures over estimated. The maximum exposed *cask* surface temperatures ~~of~~ *for a PWR MPC (*MPC-24*)* and *a BWR MPC (*MPC-68*)* ~~basket designs~~ *at design maximum heat loads* are 142°F and 139°F respectively. In Figure 3.4.28, a color contour map of the regions of HI-STAR System less than 185°F (358°K) is depicted for the hotter MPC-24 basket design. From this map, it is apparent that the accessible (impact limiter) surface temperatures are below the 10CFR71.43(g) mandated limit by a significant margin.

3.4.3 Minimum Temperatures

As specified in 10CFR71, the minimum ambient temperature conditions for the HI-STAR System are -20°F and a cold environment at -40°F. The HI-STAR System design does not have any minimum decay heat load restrictions for transport. Therefore, under zero decay heat load in combination with no solar input conditions, the temperature distribution will be uniformly equal to the imposed minimum ambient conditions. All HI-STAR System materials of construction would satisfactorily perform their intended function in the transport mode at this minimum postulated temperature condition. Evaluations in Chapter 2 demonstrate the acceptable structural performance of the overpack and MPC steel materials at low temperature. Shielding and criticality functions of the HI-STAR System materials (Chapters 5 and 6) are unaffected by exposure to this minimum temperature.

3.4.3.1 Post Rapid Ambient Temperature Drop Overpack Cooldown Event

In this section, the thermal response of the HI -STAR overpack to a rapid ambient temperature drop is analyzed and evaluated. The ambient temperature is postulated to drop from the maximum to minimum temperature under normal condition of transport in a very short time (100 °F to –40°F during a 1 hour period) and is assumed to hold steady at –40°F thereafter. The initial overpack condition prior to this rapid temperature drop corresponds to normal steady state transport with maximum design basis heat load. During this postulated cooldown event, the outer surface of the overpack will initially cool more rapidly than the bulk of metal away from the exposed surfaces. Consequently, it is expected that the through -thickness temperature gradients will increase for a period of time, reach a maximum and follow an asymptotic return to the initial steady condition through thickness temperature gradients as the overpack temperature field approaches the –40°F ambient steady condition. The results of the transient analysis reported in this sub -section verify these observations.

Noting that the state of thermal stress is influenced by changes in the overpack temperature field during the cooldown transient, a number of critical locations in the containment boundary depicted in Figure 3.4.24 are identified as pertinent to a structural integrity evaluation discussed in Subsection 2.6.2.3 of this SAR. Locations (1) and (2) are chosen to track the through -thickness temperature gradients in the overpack top forging which is directly exposed to the ambient. Locations (3) and (4) are chosen to track the overpack inner containment shell t hrough-thickness temperature gradient in a plane of maximum heat generation (i.e. active fuel mid-height) where the heat fluxes and corresponding temperature gradients are highest. Locations (A) and (B) are similarly chosen to track the temperature differe ntial in the multi-layered shells (outer-to-inner shells).

The normal transport condition thermal model discussed previously in this chapter is employed in the overpack cooldown transient analysis. This analysis is carried out by applying time-dependent thermal boundary conditions to the model and starting the transient solution in the FLUENT program. In the cooldown event, the ambient temperature is decreased from 100 °F to –40°F in 10°F steps every 4 minutes (i.e. a total of 14 steps lasting 56 minutes). The ambient temperature is held constant thereafter. The maximum design basis heat load cask (i.e. the MPC-24 design) was selected to maximize the thermal gradients (by Fourier's Law, thermal gradient is proportional to heat flow). The overpack cooldown ev ent is tracked by the thermal model for a period of 24 hours and results are reported in Figures 3.4.25 through 3.4.27 as discussed below.

In Figure 3.2.25, the overpack containment through -thickness temperature gradient responses are plotted. From this figure, it is evident that the exposed surface of the overpack forging (location (2)) initially cools at a faster rate than the recessed location (1). A similar but less pronounced result is observed in the multi-layered shells temperature changes depicted in Figure 3.4.26. This out-of-phase rate of cooling results in an increasing temperature gradient through the overpack metal layers. The thermal response of deeply recessed locations (3) and (4) show gradual temperature changes that follow each other close ly. In other words, while through -thickness temperature gradients in the forging are somewhat altered the overpack inner shell gradients are essentially unchanged during the cooldown period. A closer examination of the forging temperature gradient is there fore warranted.

In Figure 3.4.27, the time dependent forging through thickness temperature differential is depicted. The gradient increases to a maximum in a short time period followed by a slow return towards the starting state. In absolute terms, both the steady state and transient temperature gradients in the forging are quite modest. In the steady state the forging through thickness temperature gradient is approximately 3°F. This value reaches a maximum plateau of 7°F during the transient event (Figure 3.4.27). The incremental thermal stress arising from this short-term gradient elevation is computed and discussed in Subsection 2.6.2.3 of this SAR.

3.4.4 Maximum Internal Pressures

The MPC is initially filled with dry helium after fuel loading and prior to sealing the MPC lid port cover plates and closure ring. During normal transport conditions, the gas temperature within the MPC rises to its maximum operating temperature as determined by the thermal analysis methodology described earlier (see Subsection 3.4.1). The gas pressure inside the MPC will increase with rising temperature. The pressure rise is determined using the Ideal Gas Law which states that the absolute pressure of a fixed volume of entombed gas is proportional to its absolute temperature.

The HI-STAR Maximum Normal Operating Pressure (MNOP) is calculated for *10 CFR71.71(c)(1) heat condition (100°F ambient & insolation) and the HI-STAR Overpack passively cooled at design maximum heat load. For other lower than design maximum heat load scenarios, (e.g. transport with Trojan fuel) the MNOP results are confirmed to be bounding.* ~~a postulated 100% fuel rod failure and the release of fill and fission gases from the rods~~. In Tables 3.4.13 and 3.4.14, summary calculations for determining net free volume in the ~~MPC-24 and MPC-68~~ *PWR and BWR* canisters are presented. Based on a 30% release of the significant radioactive gases, a 100% release of the rod fill gas *from postulated cladding breaches*, the net free volume and the initial fill gas pressure (see Table 3.3.2), the *MNOP results are* ~~maximum MPC gas pressure for the 100% rod rupture condition is~~ given in Table 3.4.15. The overpack containment boundary MNOP for a hypothetical MPC breach condition is bounded by the MPC pressure results reported in this table.

3.4.5 Maximum Thermal Stresses

Thermal expansion induced mechanical stresses due to imposed non-uniform temperature distributions have been determined and reported in Chapter 2. Tables 3.4.17 and 3.4.18 summarize the HI-STAR System components temperatures, under steady-state hot conditions, for structural evaluation.

Additionally, Table 3.4.24 provides a summary of MPC helium retention boundary temperatures during normal transport conditions (steady state hot). Structural evaluations in Section 2.6 reference these temperature results to demonstrate the MPC helium retention boundary integrity.

3.4.6 Evaluation of System Performance for Normal Conditions of Transport

The HI-STAR System thermal analysis is based on detailed and complete heat transfer models that properly account for radiation, conduction and natural convection m odes of heat transfer. The thermal models incorporate many conservative assumptions that are listed below.

1. No credit for gap reduction between the MPC and overpack due to differential thermal expansion under hot condition is considered.

2. No credit is considered for MPC basket internal thermosiphon heat transfer. Under a perfectly horizontal transport condition, axial temperature gradients with peaking at active fuel mid-height induces buoyancy flows from both ends of the basket in each MPC cell. Buoy ancy flow in shallow horizontal channels has been widely researched and reported in the technical literature [3.4.10 to 3.4.12]. An additional mode of heat transport due to thermosiphon flow within the basket cells is initiated for any cask orientation oth er than a perfectly horizontal condition. In practice this is a highly likely scenario. However, in the interest of conservatism, no credit is considered for this mode of heat transfer.

3. An upper bound solar absorbtivity of unity is applied to all exposed surfaces.

4. No credit considered for radiative heat transfer between the Boral neutron absorber panels and the Boral pocket walls, or for the presence of helium in the pocket gaps.

5. No credit is considered for conduction through the neutron shieldi ng materials.

6. No credit is considered for contact between fuel assemblies and the MPC basket wall or between the MPC basket and the MPC basket supports. The fuel assemblies and MPC basket are conservatively considered to be in concentric alignment.

7. No credit considered for presence of highly conducting aluminum honeycomb material inside impact limiters.

8. The MPC basket axial conductivity is conservatively ~~assumed to be equal to the lower basket cross-sectional effective conductivity.~~ *limited to the fuel cladding only (i.e. axial heat transfer through fuel pellets is neglected).*

9. The MPC is assumed to be loaded with the SNF type which has the maximum equivalent thermal resistance of all fuel types in its category (BWR or PWR), as applicable.

10. The design basis maximum decay heat loads are used for all thermal-hydraulic analyses. For casks loaded with fuel assemblies having decay heat generation rates less than design basis, additional thermal margins of safety will exist.

11. Interfacial contact conductance of multi-layered intermediate shell contacting layers was conservatively determined to bound surface finish, contact pressure, and base metal

conductivity conditions.

12. *Turbulation of flow at grid spacers, top & bottom fittings are neglected.*

Temperature distribution results obtained from a conservatively developed thermal model show that maximum fuel cladding temperature limits are met with adequate margins. Margins during actual normal transport conditions are expected to be greater due to the many conservative assumptions incorporated in the analysis. The maximum local temperatures in the neutron shield and overpack seals are lower than design limits. The maximum local MPC basket temperature level is below the recommended limits for structural materials in terms of susceptibility to stress, corrosion and creep induced degradation. Furthermore, structural evaluation (Chapter 2) has demonstrated that stresses (including those induced due to imposed temperature gradients) are within ASME B&PV Code limits. Section 3.6 provides a discussion of compliance with the regulatory requirements and acceptance criteria listed in Section 3.0. As a result of the above -mentioned considerations, it is concluded that the HI -STAR thermal design is in compliance with 10CFR71 requirements for normal conditions of transport.

Table 3.4.1

CLOSED CAVITY NUSSELT NUMBER
RESULTS FOR HELIUM FILLED MPC PERIPHERAL VOIDS

	Case (i) Nusselt Number		Case (ii) Nusselt Number	
Temperature (°F)	MPC-24, *MPC-24E, MPC-32*	MPC-68	MPC-24, *MPC-24E, MPC-32*	MPC-68
200	6.93	4.72	5.45	3.46
450	5.44	3.71	4.09	2.58
700	4.60	3.13	3.36	2.12

Table 3.4.2

RELATIONSHIP BETWEEN HI-STAR SYSTEM REGIONS
AND MATHEMATICAL MODEL DESCRIPTIONS

HI-STAR System Region	Mathematical Model	Subsections
Fuel Assembly	Fuel Region Effective Thermal Conductivity	3.4.1.1.2
MPC	Effective Thermal Conductivity of Boral/Sheathing/Box Wall Sandwich	3.4.1.1.3
	Basket In-Plane Conductive Heat Transport	3.4.1.1.4
	Heat Transfer in MPC Basket Peripheral Region	3.4.1.1.5
	Effective Thermal Conductivity of MPC Basket-to-Shell Aluminum Heat Conduction Elements	3.4.1.1.11
Overpack	Effective Conductivity of Multi-Layered Intermediate Shell Region	3.4.1.1.6
	Effective Thermal Conductivity of Holtite Neutron Shielding Region	3.4.1.1.9
Ambient Environment	Heat Rejection from Overpack Exterior Surfaces	3.4.1.1.7
	Solar Heat Input	3.4.1.1.8
Assembled Cask Model	Overview of the Thermal Model	3.4.1.1.1
	Effective Conductivity of MPC to Overpack Gap	3.4.1.1.10
	FLUENT Model for HI-STAR	3.4.1.1.12

Table 3.4.3

THIS TABLE IS INTENTIONALLY DELETED.

Table 3.4.4

SUMMARY OF PWR FUEL ASSEMBLIES
EFFECTIVE THERMAL CONDUCTIVITIES

No.	Fuel	@ 200°F (Btu/ft-hr-°F)	@ 450°F (Btu/ft-hr-°F)	@ 700°F (Btu/ft-hr-°F)
1	W 17×17 OFA	0.182	0.277	**0.402**
2	W 17×17 Std	0.189	0.286	0.413
3	W 17×17 Vantage-5H	0.182	0.277	0.402
4	W 15×15 Std	0.191	0.294	0.430
5	W 14×14 Std	0.182	0.284	0.424
6	W 14×14 OFA	**0.175**	**0.275**	0.413
7	B&W 17×17	0.191	0.289	0.416
8	B&W 15×15	0.195	0.298	0.436
9	CE 16×16	0.183	0.281	0.411
10	CE 14×14	0.189	0.293	0.435
11	HN† 15×15 SS	0.180	0.265	0.370
12	W 14×14 SS	0.170	0.254	0.361
13	*B&W 15x15 Mark B-11*	*0.187*	*0.289*	*0.424*
14	*CE 14x14 (MP2)*	*0.188*	*0.293*	*0.434*

Note: Boldface values denote the lowest thermal conductivity in each column (excluding stainless steel clad fuel assemblies).

† Haddam Neck B&W or Westinghouse stainless steel clad fuel assemblies.

Table 3.4.5

SUMMARY OF BWR FUEL ASSEMBLIES EFFECTIVE THERMAL CONDUCTIVITIES

No.	Fuel	@ 200°F (Btu/ft-hr-°F)	@ 450°F (Btu/ft-hr-°F)	@ 700°F (Btu/ft-hr-°F)
1	Dresden 1 8×8*	0.119	0.201	0.319
2	Dresden 1 6×6	0.126	0.215	0.345
3	GE 7×7	0.171	0.286	0.449
4	GE 7×7R	0.171	0.286	0.449
5	GE 8×8	0.168	0.278	0.433
6	GE 8×8R	**0.166**	0.275	0.430
7	GE-10 8×8	0.168	0.280	0.437
8	GE-11 9×9	0.167	**0.273**	**0.422**
9	AC† 10×10 SS	0.152	0.222	0.309
10	Exxon 10×10 SS	0.151	0.221	0.308
11	Damaged Dresden 1 8×8 in a DFC§	0.107	0.169	0.254
12	Dresden-1 Thin Clad 6x6§	0.124	0.212	0.343
13	Humboldt Bay-7x7§	0.127	0.215	0.343
14	Damaged Dresden-1 8x8 (in TND-1 canister) §	0.107	0.168	0.252
15	8x8 Quad+ Westinghouse§	0.164	0.278	0.435

Note: Boldface values denote the lowest thermal conductivity in each column (excluding Dresden and LaCrosse clad fuel assemblies).

---

† Allis-Chalmers stainless steel clad fuel assemblies.

§ Low heat emitting fuel assemblies excluded from list of fuel assemblies (zircaloy clad) evaluated to determine the most resistive SNF type.

Table 3.4.6

MPC BASKET EFFECTIVE THERMAL CONDUCTIVITY RESULTS
FROM ANSYS MODELS

Basket	@200°F (Btu/ft-hr-°F)	@450°F (Btu/ft-hr-°F)	@700°F (Btu/ft-hr-°F)
MPC-24* (Zircaloy Clad Fuel)	~~1.108~~ *1.111*	1.495	~~1.954~~ *1.955*
MPC-68 (Zircaloy Clad Fuel)	~~0.959~~ *1.111*	~~1.188~~ *1.347*	~~1.432~~ *1.591*
MPC-24 (Stainless Steel Clad Fuel) *(Note 1)*	~~0.995~~ *0.897*	~~1.321~~ *1.213*	~~1.700~~ *1.577*[(a)]
MPC-68 (Stainless Steel Clad Fuel) *(Note 1)*	~~0.931~~ *1.070*	~~1.125~~ *1.27*	~~1.311~~ *1.451*[(b)]
MPC-68 (Dresden-1 8x8 in canisters)	~~0.861~~ *0.999*	~~1.055~~ *1.203*	~~1.242~~ *1.396*
MPC-32 (Zircaloy Clad Fuel)	*1.015*	*1.271*	*1.546*
MPC-32 (Stainless Steel Clad Fuel) (Note 1)	*0.806*	*0.987*	*1.161*[(c)]
MPC-24E (Zircaloy Clad Fuel)	*1.216*	*1.637*	*2.133*
MPC-24E (Stainless Steel Clad Fuel) (Note 1)	*0.991*	*1.351*	*1.766*[(d)]

(a) ~~13%~~ *19%* lower effective thermal conductivity than corresponding zircaloy -fueled basket
(b) 9% lower effective thermal conductivity than corresponding zircaloy -fueled basket
(c) 25% lower effective thermal conductivity than corresponding zircaloy-fueled basket
(d) 17% lower effective thermal conductivity than corresponding zircaloy-fueled basket
Note-1: Evaluated for a conservatively bounding configuration (fuel in a damaged fuel canister)

** The MPC-24 basket has an option for an enlarged cell opening. Both basket configurations (i.e. original and enlarged cell opening) are evaluated. T he bounding numerical results are reported herein.*

Table 3.4.7

INSOLATION DATA SPECIFIED BY 10C FR71, SUBPART F

Surface Type	12-Hour Total Insolation Basis	
	(g-cal/cm^2)	(Watts/m^2)
Horizontally Transported Flat Surfaces		
- Base	None	None
- Other Surfaces	800	774.0
Non-Horizontal Flat Surfaces	200	193.5
Curved Surfaces	400	387.0

Table 3.4.8

EFFECTIVE THERMAL CONDUCTIVITY OF THE NEUTRON SHIELD/RADIAL CHANNELS REGION

Condition/Temperature (°F)	**Thermal Conductivity (Btu/ft-hr-°F)**
Normal Condition:	
200	1.953
450	1.812
700	1.645
Fire Condition:	
200	3.012
450	2.865
700	2.689

Table 3.4.9

THIS TABLE IS INTENTIONALLY DELETED.

Table 3.4.10

HI-STAR SYSTEM NORMAL TRANSPORT† MAXIMUM TEMPERATURES
~~(MPC-24)~~ *(PWR MPCs)*

	Bounding ~~Calculated Maximum~~ **Temperature [°F]**	**Normal Condition Temperature Limit [°F]**
Fuel Cladding	701	720
MPC Basket Centerline	667	725
MPC Basket Periphery	430	725
MPC Outer Shell Surface	315	450
MPC/Overpack Helium Gap Outer Surface	291	400
Radial Neutron Shield Inner Surface	271	300
Overpack Enclosure Shell Surface	222	350
Axial Neutron Shield	292	300
Impact Limiter Exposed Surface	121	176
Overpack Closure Plate††	163	400
Overpack Bottom Plate††	295	350

† Steady-state hot (100°F ambient) with maximum decay heat and insolation.

†† Overpack closure plate and vent/drain port plug seals normal condition design temperature is 400°F. The maximum seals temperatures are bounded by the reported closure plate and bottom plate maximum temperatures. Consequently, a large margin of safety exists to permit safe operation of seals in the overpack helium retention boundary.

Table 3.4.11

HI-STAR SYSTEM NORMAL TRANSPORT† MAXIMUM TEMPERATURES
(MPC-68)

	~~Calculated Maximum Temperature~~ *Bounding Temperature* [°F]	**Normal Condition Temperature Limit [°F]**
Fuel Cladding	713	749
MPC Basket Centerline	697	725
MPC Basket Periphery	365	725
MPC Outer Shell Surface	306	450
MPC/Overpack Gap Outer Surface	282	400
Radial Neutron Shield Inner Surface	264	300
Overpack Enclosure Shell Surface	217	350
Axial Neutron Shield	255	300
Impact Limiter Exposed Surface	121	176
Overpack Closure Plate††	162	400
Overpack Bottom Plate††	256	350

† Steady-state hot (100°F ambient) with maximum decay heat and insolation.

†† Overpack closure plate and vent/drain port plug seals normal condition design temperature is 400°F. The maximum seals temperatures are bounded by the reported closure plate and bottom plate maximum temperatures. Consequently, a large margin of safety exists to permit safe operation of seals in the overpack helium retention boundary.

Table 3.4.12

THIS TABLE IS INTENTIONALLY DELETED.

Table 3.4.13

SUMMARY OF BOUNDING MINIMUM *PWR*
~~MPC-24~~ *MPCs* FREE VOLUME CALCULATIONS

Item	**MPC-24 Volume (ft^3)**	*MPC-24E Volume (ft^3)*	*MPC-32 Volume (ft^3)*
Cavity Volume	368.3	*368.3*	*367.9*
Basket Metal Volume	47.0	*48.3*	*29.6*
Bounding Fuel Assemblies Volume	78.8	*78.8*	*105.0*
Basket Supports and Fuel Spacers Volume	6.1	*6.1*	*9.0*
Aluminum Conduction Elements†	5.9	*5.9*	*5.9*
Net Free Volume	230.5 (6529 liters)	*229.3 (6490 liters)*	*218.4 (6184 liters)*

† Bounding 1,000 lbs aluminum weight.

Table 3.4.14

SUMMARY OF BOUNDING MINIMUM
MPC-68 FREE VOLUME CALCULATIONS

Item	**Volume (ft^3)**
Cavity Volume	367.2
Basket Metal Volume	45.5
Bounding Fuel Assemblies Volume	93.0
Basket Supports and Fuel Spacers Volume	11.3
Aluminum Conduction Elements[†]	5.9
Net Free Volume	211.5 (5989 liters)

[†] Bounding 1,000 lbs aluminum weight.

Table 3.4.15

SUMMARY OF MAXIMUM NORMAL OPERATING PRESSURE[†]
FOR HORIZONTAL TRANSPORT CONDITIONS

Condition	**Pressure (psig)**	*Bounding* **MPC Cavity Bulk Temperature (°F)**
MPC-24:		
Initial Backfill (at 70°F)	~~28.3~~ *42.8*	483
Normal Condition	~~61.8~~ *87.7*	
With ~~100%~~ *3%* Rods Rupture[(Note 1)]	~~98.9~~ *88.8*	
MPC-68:		
Initial Backfill (at 70°F)	~~28.5~~ *42.8*	468
Normal Condition	~~61.0~~ *86.0*	
With ~~100%~~ *3%* Rods Rupture[(Note 1)]	~~89.3~~ *86.9*	
MPC-24E:		
Initial Backfill (at 70°F)	*42.8*	*483*
Normal Condition	*87.7*	
With 3% Rods Rupture[(Note 1)]	*88.8*	
MPC-32:		
Initial Backfill (at 70°F)	*42.8*	*483*
Normal Condition	*87.7*	
With 3% Rods Rupture[(Note 1)]	*89.3*	

Note 1: NUREG-1617 requires an assumption for normal transport that 3% of the rods are breached with release of 100% fill gas and 30% fission gas to containment.

[†] Pressure analysis *in accordance with heat condition specified in 10 CFR 71.71(c)(1) in the absence of venting, external ancillary cooling or operational controls.* ~~is based on release of 100% of the rods fill gas and 30% of the significant radioactive gases from a ruptured rod.~~

Table 3.4.16

THIS TABLE IS INTENTIONALLY DELETED.

Table 3.4.17

~~MPC-24~~*PWR MPCs* NORMAL HORIZONTAL TRANSPORT CONDITION
HI-STAR SYSTEM COMPONENTS *BOUNDING* TEMPERATURE [°F] SUMMARY

	MPC Basket Axial Mid-Length	**MPC Basket Axial Ends**
Overpack enclosure shell	222	147
Overpack inner shell	291	163
MPC shell	315	164
Basket periphery	430	166
Basket center	667	177

Table 3.4.18

MPC-68 NORMAL HORIZONTAL TRANSPORT CONDITION
HI-STAR SYSTEM COMPONENTS TEMPERATURE [°F] SUMMARY

	MPC Basket Axial Mid-Length	**MPC Basket Axial Ends**
Overpack enclosure shell	217	146
Overpack inner shell	282	161
MPC shell	306	163
Basket periphery	365	164
Basket center	697	175

Table 3.4.19

SUMMARY OF LOADED HI-STAR SYSTEM
BOUNDING COMPONENT WEIGHTS AND THERMAL INERTIAS

Component	Weight (lbs)	Heat Capacity (Btu/lb-°F)	Thermal Inertia (Btu/°F)
Holtite-A	11,000	0.39	4,290
Carbon Steel	140,000	0.1	14,000
Alloy-X MPC (empty)	35,000	0.12	4,200
Fuel	40,000	0.056	2,240
MPC Cavity Water[†]	6,500	1.0	6,500
			31,230 (Total)

[†] Based on smallest MPC-68 cavity net free volume with 50% credit for flooded water mass.

Table 3.4.20

MAXIMUM ALLOWABLE TIME DURATION
FOR WET TRANSFER OPERATIONS

Initial Temperature (°F)	**Time Duration (hr)**
115	44.3
120	42.0
125	39.7
130	37.4
135	35.2
140	32.9
145	30.6
150	28.3

Table 3.4.21

THIS TABLE IS INTENTIONALLY DELETED.

Table 3.4.22

HI-STAR SYSTEM ~~MAXIMUM~~ *BOUNDING* TEMPERATURES [°F]
UNDER STEADY-STATE COLD† CONDITIONS (~~MPC-24~~ *PWR MPCs*)

Fuel Cladding	620
MPC Basket Centerline	586
MPC Basket Periphery	329
MPC Outer Shell Surface	190
MPC/Overpack Gap Outer Surface	165
Radial Neutron Shield Inner Surface	141
Overpack Enclosure Shell Surface	96
Axial Neutron Shield	165
Impact Limiter Exposed Surface	-40

† -40°F ambient temperature with maximum decay heat and no insolation.

Table 3.4.23

HI-STAR SYSTEM MAXIMUM TEMPERATURES [°F]
UNDER STEADY-STATE COLD† CONDITIONS (MPC-68)

Fuel Cladding	621
MPC Basket Centerline	605
MPC Basket Periphery	254
MPC Outer Shell Surface	178
MPC/Overpack Gap Outer Surface	153
Radial Neutron Shield Inner Surface	130
Overpack Enclosure Shell Surface	88
Axial Neutron Shield	123
Impact Limiter Exposed Surface	-40

† -40°F ambient temperature with maximum decay heat and no insolation.

Table 3.4.24

SUMMARY OF MPC HELIUM RETENTION BOUNDARY *BOUNDING* TEMPERATURE DISTRIBUTION DURING NORMAL STORAGE CONDITIONS

Location	**Figure 2.6.20 Designation**	~~**MPC-24**~~ *PWR MPCs* **[°F]**	**MPC-68 [°F]**
MPC Lid Inside Surface at Centerline	A	176	173
MPC Lid Outside Surface at Centerline	B	171	169
MPC Lid Inside Surface at Periphery	C	164	163
MPC Lid Outside Surface at Periphery	D	162	161
MPC Baseplate Inside Surface at Centerline	E	301	260
MPC Baseplate Outside Surface at Centerline	F	295	256
MPC Baseplate Inside Surface at Periphery	G	267	239
MPC Baseplate Outside Surface at Periphery	H	267	239
MPC Shell Maximum	I	315	306

Table 3.4.25

SUMMARY OF 10×10 ARRAY BWR FUEL ASSEMBLY TYPES
EFFECTIVE THERMAL CONDUCTIVITIES †

Fuel	**k_{eff} at 200°F [Btu/(ft-hr-°F)]**	**k_{eff} at 450°F [Btu/(ft-hr-°F)]**	**k_{eff} at 700°F [Btu/(ft-hr-°F)]**
GE-12/14	0.166	0.269	0.412
Atrium-10	0.164	0.266	0.409
SVEA-96	0.164	0.269	0.416

† The conductivities reported in this table are obtained by the simplified method described in the beginning of Subsection 3.4.1.1.2.

Table 3.4.26

COMPARISON OF ATRIUM-10[†] AND BOUNDING[††] BWR FUEL ASSEMBLY EFFECTIVE THERMAL CONDUCTIVITIES

Temperature	Atrium-10 Assembly		Bounding BWR Assembly	
°F	Btu/(ft-hr-°F)	W/m-K	Btu/(ft-hr-°F)	W/m-K
200	0.225	0.389	0.171	0.296
450	0.345	0.597	0.271	0.469
700	0.504	0.872	0.410	0.710

[†] The reported effective thermal conductivity has been obtained from a rigorous finite -element modeling of the Atrium-10 assembly.

[††] The bounding BWR fuel assembly effective thermal conductivity applied in the MPC-68 basket thermal analysis.

Table 3.4.27

THIS TABLE IS INTENTIONALLY DELETED.

Table 3.4.28

~~MPC-24~~ *PWR MPCs BOUNDING* PEAK FUEL CLADDING TEMPERATURE AS A FUNCTION OF TOTAL HEAT LOAD

Total MPC Decay Heat Load (kW)	Peak Fuel Cladding Temperature (°F)
20.0†	700.6
19.0	678.9
17.0	633.9
15.5	598.8

† Design Basis Maximum.

Table 3.4.29

MPC-68 PEAK FUEL CLADDING TEMPERATURE
AS A FUNCTION OF TOTAL HEAT LOAD

Total MPC Decay Heat Load (kW)	Peak Fuel Cladding Temperature (°F)
18.5[†]	712.7
17.0	674.0
15.5	634.1

[†] Design Basis Maximum.

Table 3.4.30

SUMMARY OF THERMAL CONDUCTIVITY CALCULATIONS
FOR MPC HELIUM DILUTED BY RELEASED ROD GASES

Component Gas	**Molecular Weight (g/mole)**	**Mole Fraction**	**Thermal Conductivity (Btu/hr-ft-°F)**
MPC and Fuel Rod Backfill Helium	4	0.817	0.098 @ 200°F 0.129 @ 450 °F 0.158 @ 700°F
Rod Tritium	3	8.007×10^{-5}	0.119 @ 200 0.148 @ 450°F 0.177 @ 700°F
Rod Krypton	85	0.016	6.76×10^{-3} @ 200°F 8.782×10^{-3} @ 450°F 0.011 @ 700°F
Rod Xenon	131	0.160	3.987×10^{-3} @ 200°F 5.258×10^{-3} @ 450°F 6.471×10^{-3} @ 700°F
Rod Iodine	129	6.846×10^{-3}	2.496×10^{-3} @ 200°F 3.351×10^{-3} @ 450°F 4.201×10^{-3} @ 700°F
Mixture of Gases (diluted helium)	N/A	1.000	0.053 @ 200°F 0.069 @ 450°F 0.085 @ 700°F

Table 3.4.31

COMPARISON OF COMPONENT EFFECTIVE THERMAL CONDUCTIVITIES WITH AND WITHOUT MPC HELIUM DILUTION

	Effective Thermal Conductivity (Btu/hr-ft-°F)		
	Value at 200°F	**Value at 450°F**	**Value at 700°F**
Fuel Assembly with Undiluted Helium	0.257	0.406	0.604
Fuel Assembly with Diluted Helium	0.160	0.278	0.458
MPC Fuel Basket with Undiluted Helium	1.108	1.495	1.954
MPC Fuel Basket with Diluted Helium	0.933	1.303	1.758
Basket Periphery with Undiluted Helium†	0.3136	0.4456	0.6459
Basket Periphery with Diluted Helium†	0.2286	0.3550	0.5538

† These thermal conductivity values do not include the contribution of the aluminum heat conduction elements.

Table 3.4.32

MPC-24 HYPOTHETICAL 100% RODS RUPTURE ACCIDENT
MAXIMUM TEMPERATURES

	Calculated Maximum Temperature (°F)	**Accident Condition Temperature Limit (°F)**
Fuel Cladding	743	1058
MPC Basket Centerline	709	950
MPC Basket Periphery	444	950
MPC Outer Shell Surface	314	775
MPC/Overpack Helium Gap Outer Surface	291	500
Radial Neutron Shield Inner Surface	271	N/A
Overpack Enclosure Shell Surface	222	1350
Overpack Closure Plate	176	700
Overpack Bottom Plate	296	700

Table 3.4.33

MPC-24 HYPOTHETICAL 100% RODS RUPTURE ACCIDENT PRESSURES

Calculated Accident Pressure (psig)	**Accident Condition Design Pressure (psig)**
~~102.1~~ *133.5*	~~125~~ *200*

Table 3.4.34

PLANT SPECIFIC BWR FUEL TYPES EFFE CTIVE THERMAL CONDUCTIVITY *

Fuel	@200°F [Btu/ft-hr-°F]	@450°F [Btu/ft-hr-°F]	@700F° [Btu/ft-hr-°F]
Oyster Creek (7x7	0.165	0.273	0.427
Oyster Creek (8x8)	0.162	0.266	0.413
TVA Browns Ferry (8x8)	0.160	0.264	0.411
SPC-5 (9x9)	0.149	0.245	0.380

* The conductivities reported in this table are obtained by a simplified analytical method described in Subsection 3.4.1.1.2.

(a) TYPICAL FUEL CELL

(b) SOLID REGION OF
EFFECTIVE CONDUCTIVITY

FIGURE 3.4-1; HOMOGENIZATION OF THE STORAGE CELL CROSS-SECTION

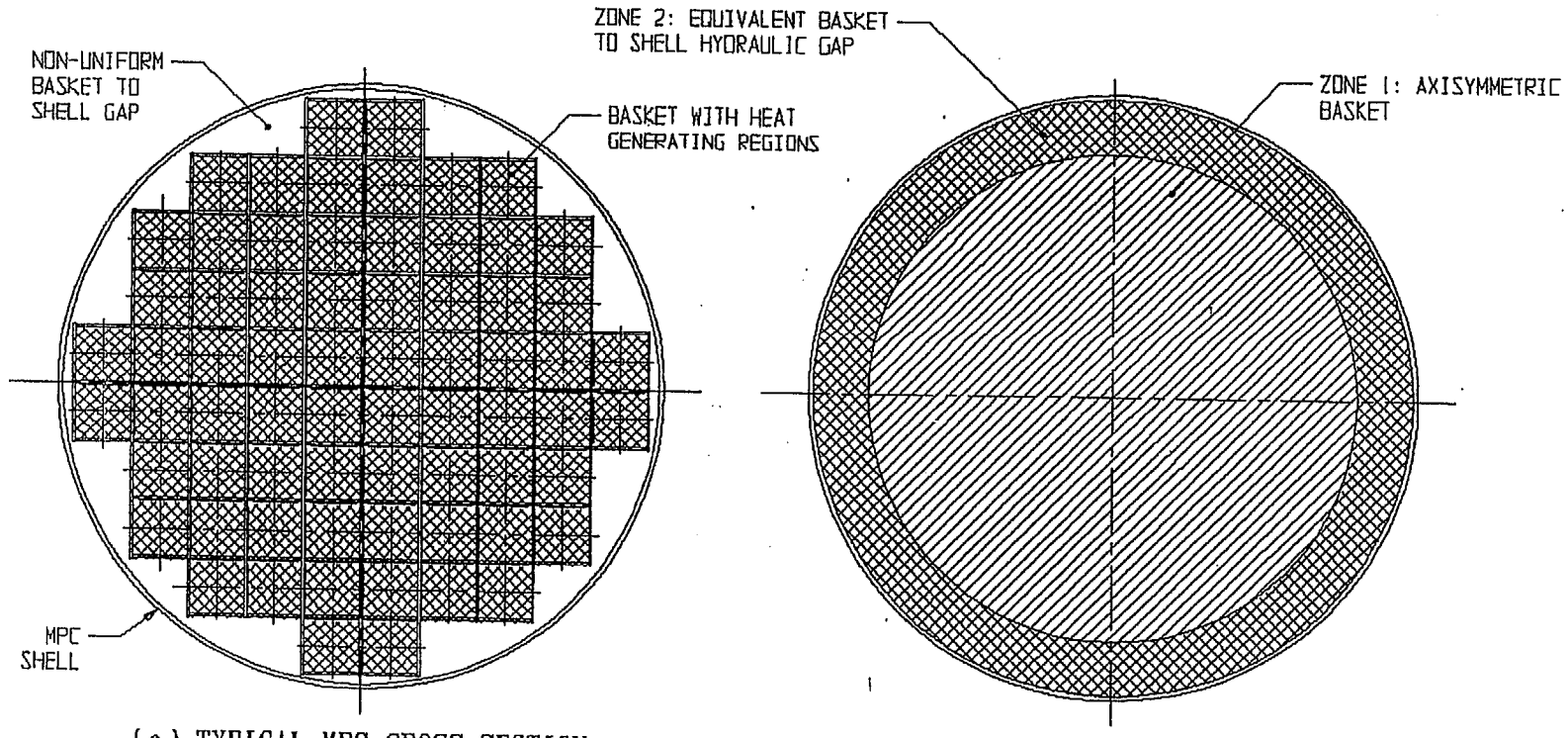

(a) TYPICAL MPC CROSS-SECTION

(b) EQUIVALENT TWO ZONE MODEL

FIGURE 3.4.2; MPC CROSS-SECTION REPLACED WITH AN EQUIVALENT TWO ZONE AXISYMMETRIC BODY

\PROJECTS\5014\HI951251\CH_3\3_4_2

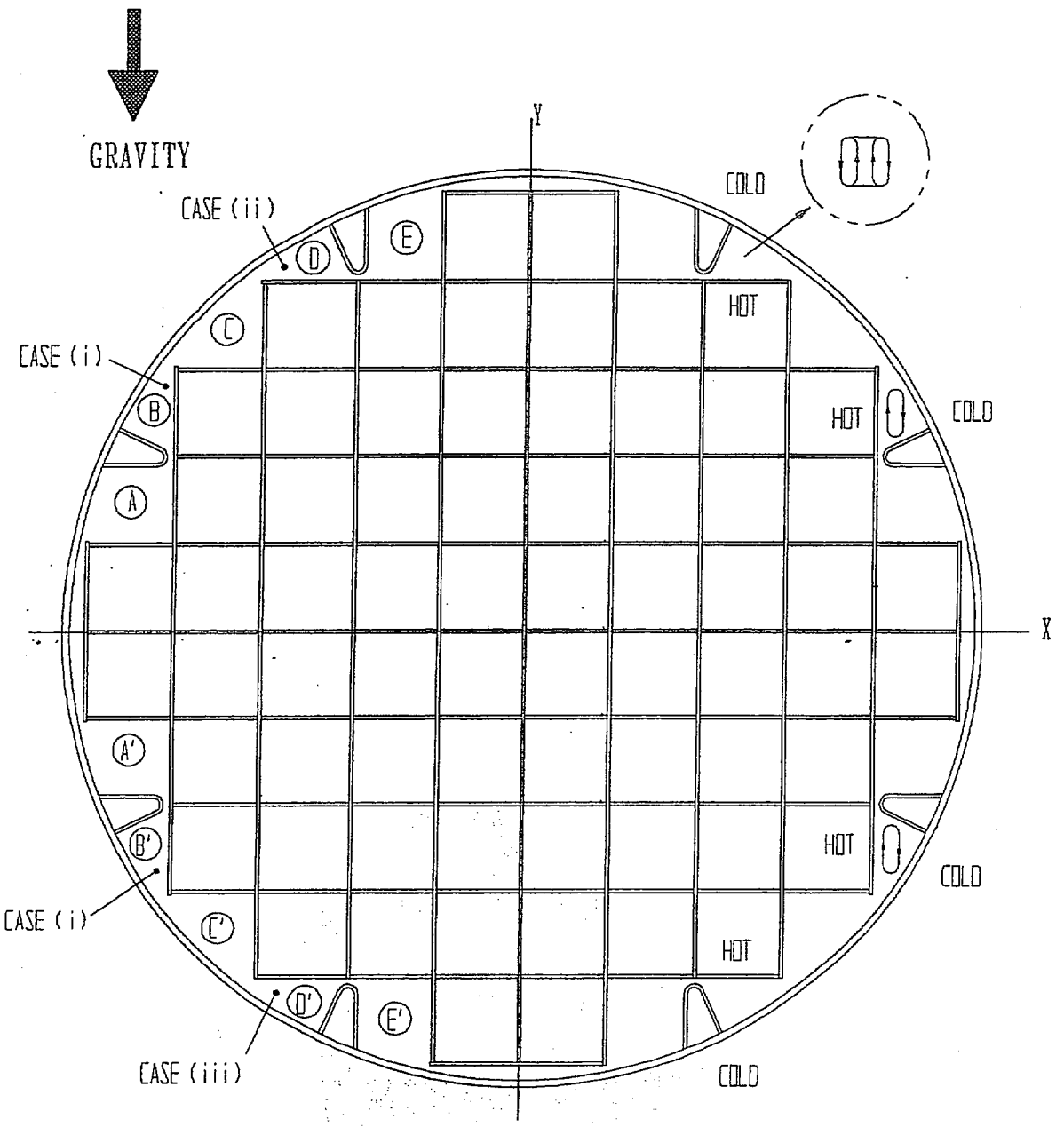

FIGURE 3.4.3; NATURAL CONVECTION IN MPC BASKET PERIPHERY REGION

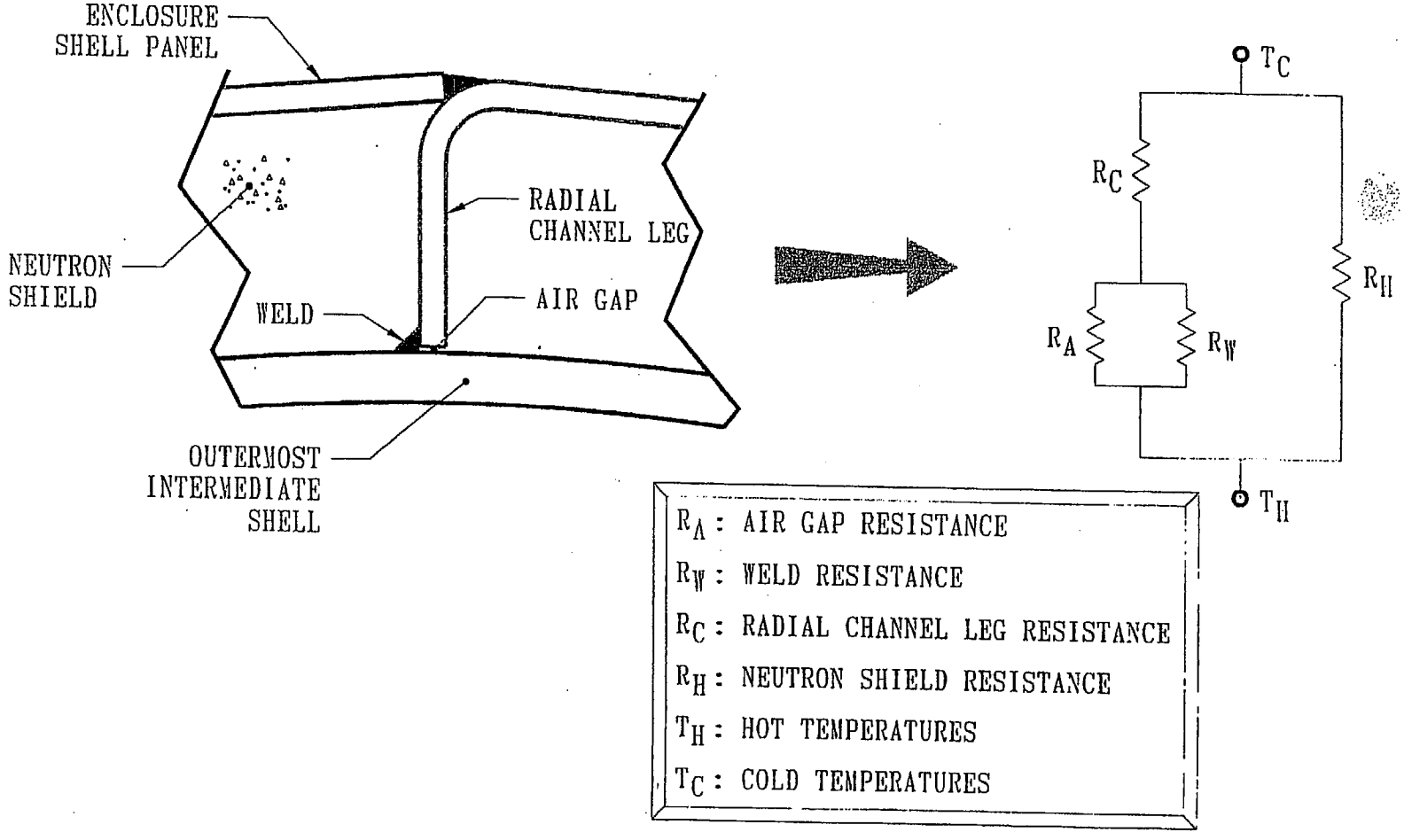

FIGURE 3.4.4; NEUTRON SHIELD REGION RESISTANCE NETWORK ANALOGY FOR EFFECTIVE CONDUCTIVITY CALCULATION

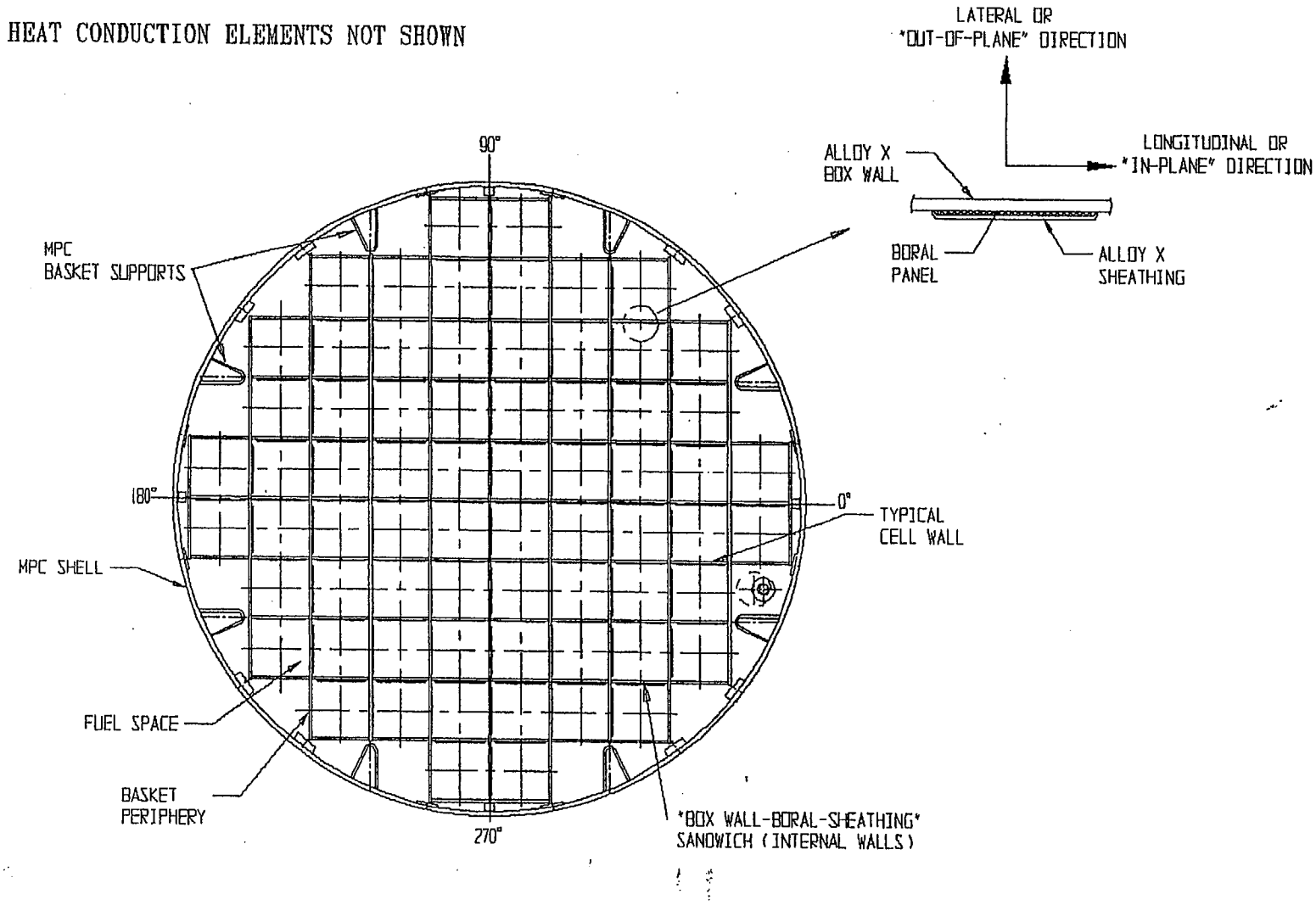

FIGURE 3.4.5; TYPICAL MPC BASKET PARTS IN A CROSS-SECTIONAL VIEW

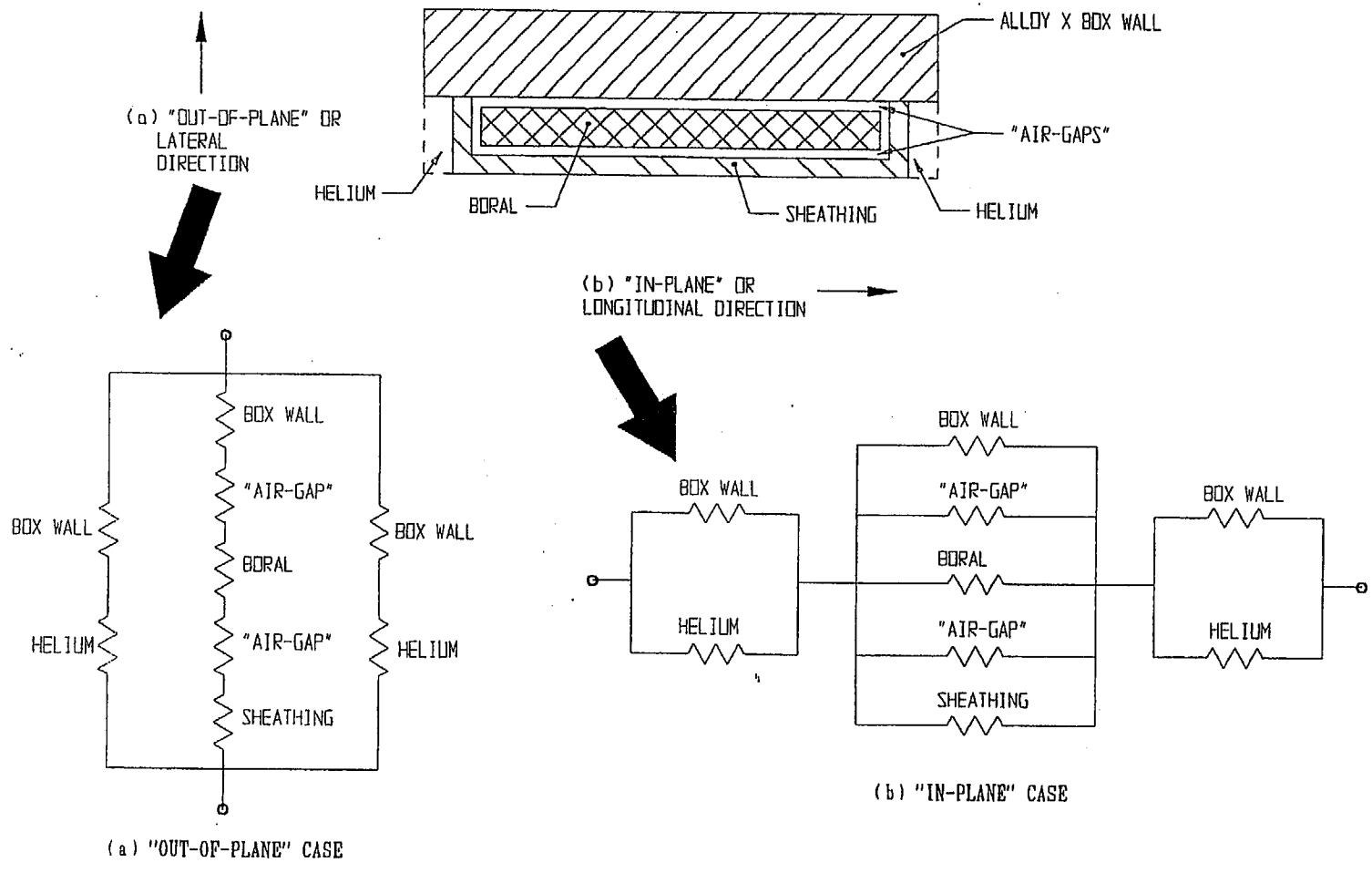

FIGURE 3.4.6; RESISTANCE NETWORK MODEL OF A "BOX WALL-BORAL-SHEATHING" SANDWICH

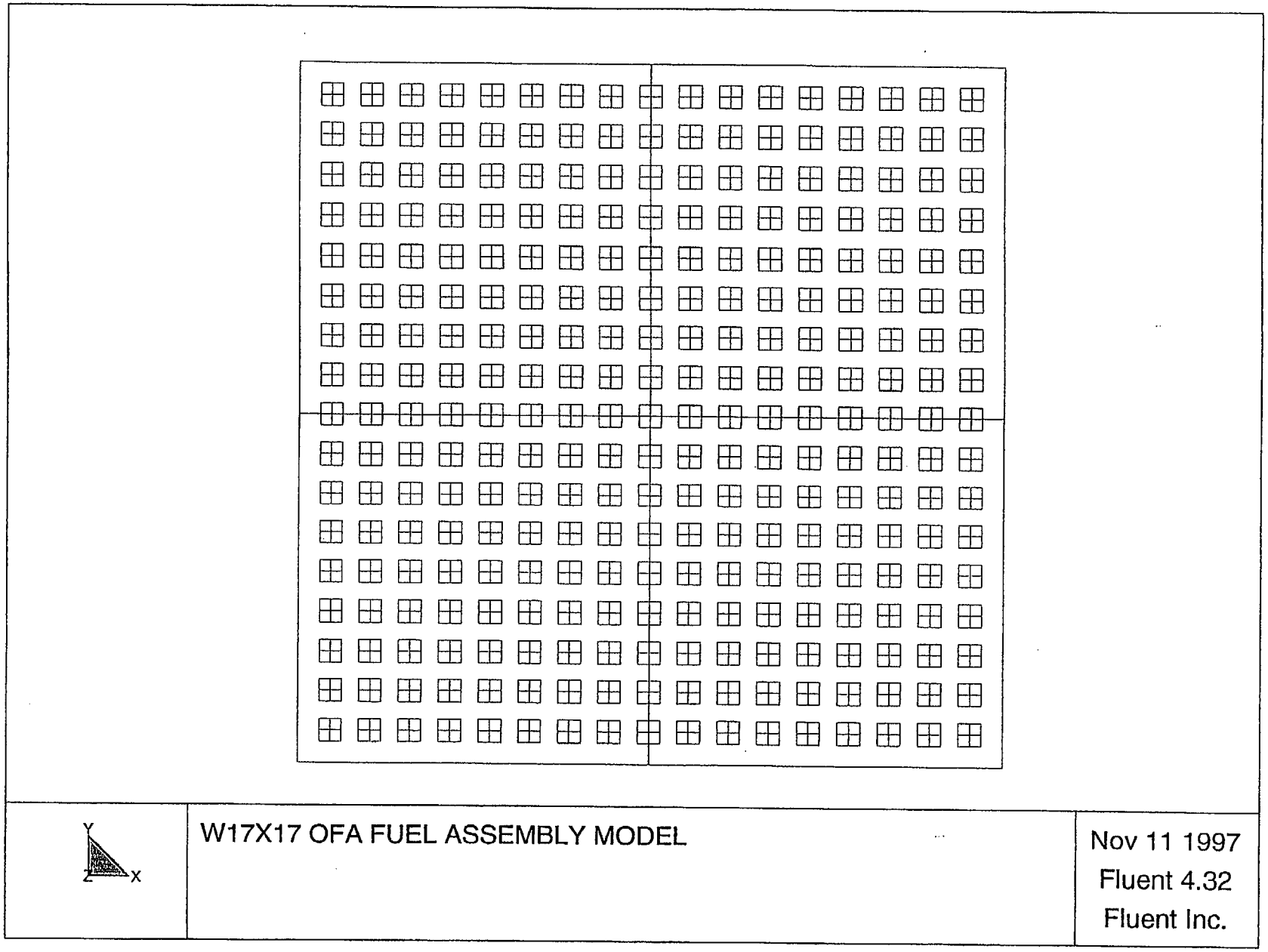

FIGURE 3.4.7: WESTINGHOUSE 17x17 OFA PWR FUEL ASSEMBLY MODEL

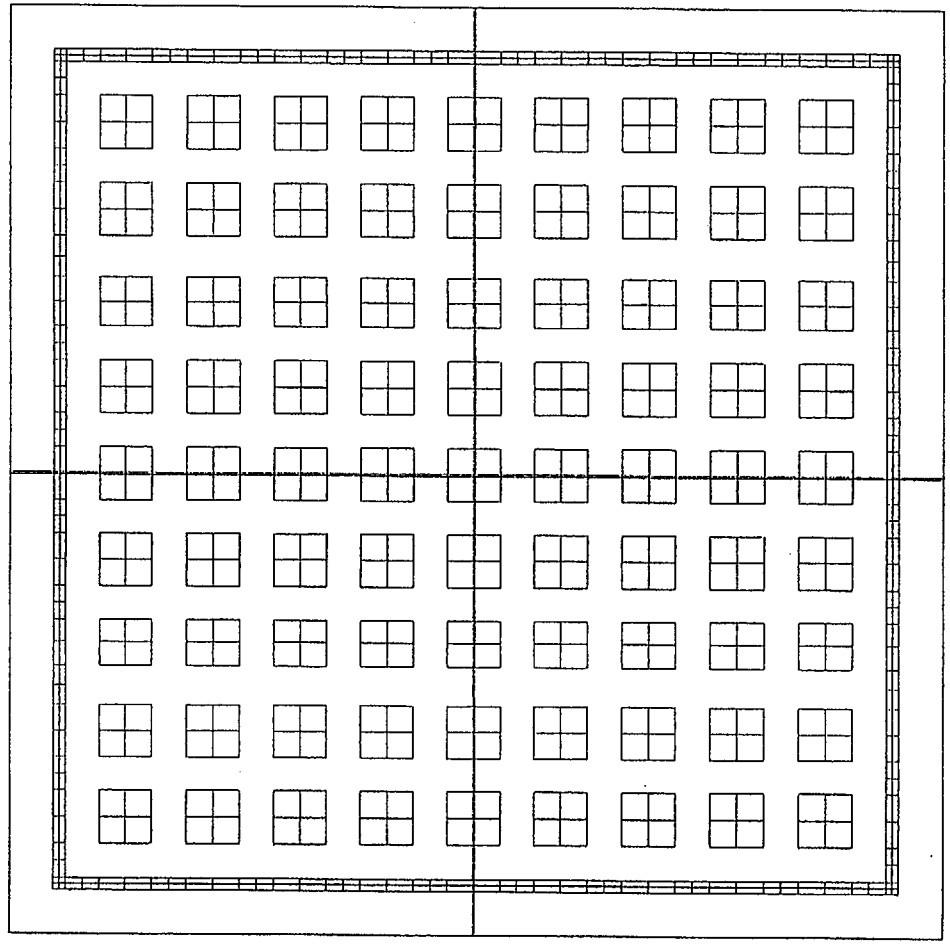

Y Z X	GE11-9X9 CHANNELED FUEL ASSEMBLY MODEL	Nov 11 1997 Fluent 4.32 Fluent Inc.

FIGURE 3.4.8: GENERAL ELECTRIC 9x9 BWR FUEL ASSEMBLY MODEL

FIGURE 3.4.9

THIS FIGURE IS INTENTIONALLY DELETED.

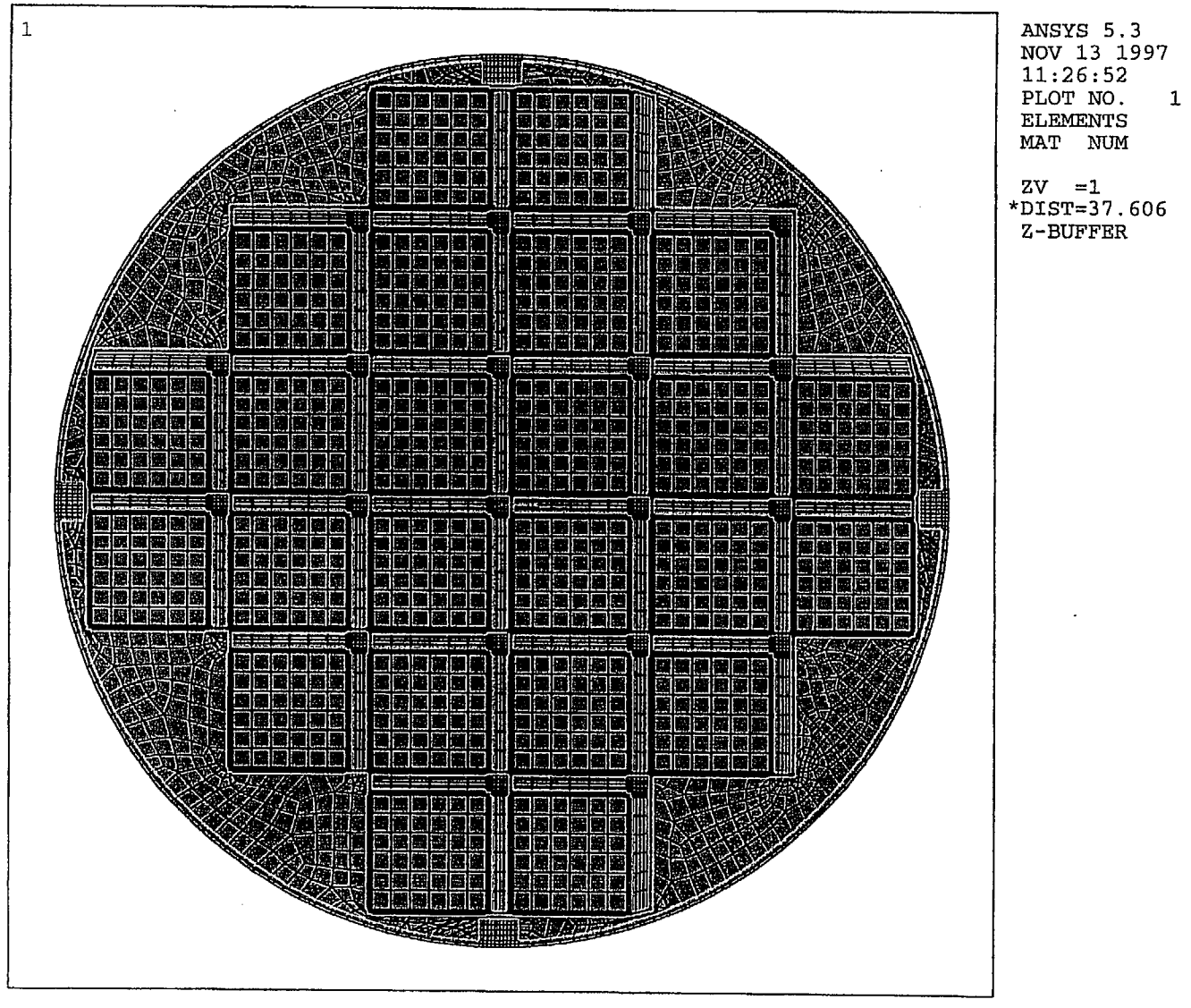

FIGURE 3.4.10; MPC-24 BASKET CROSS-SECTION ANSYS FINITE ELEMENT MODEL

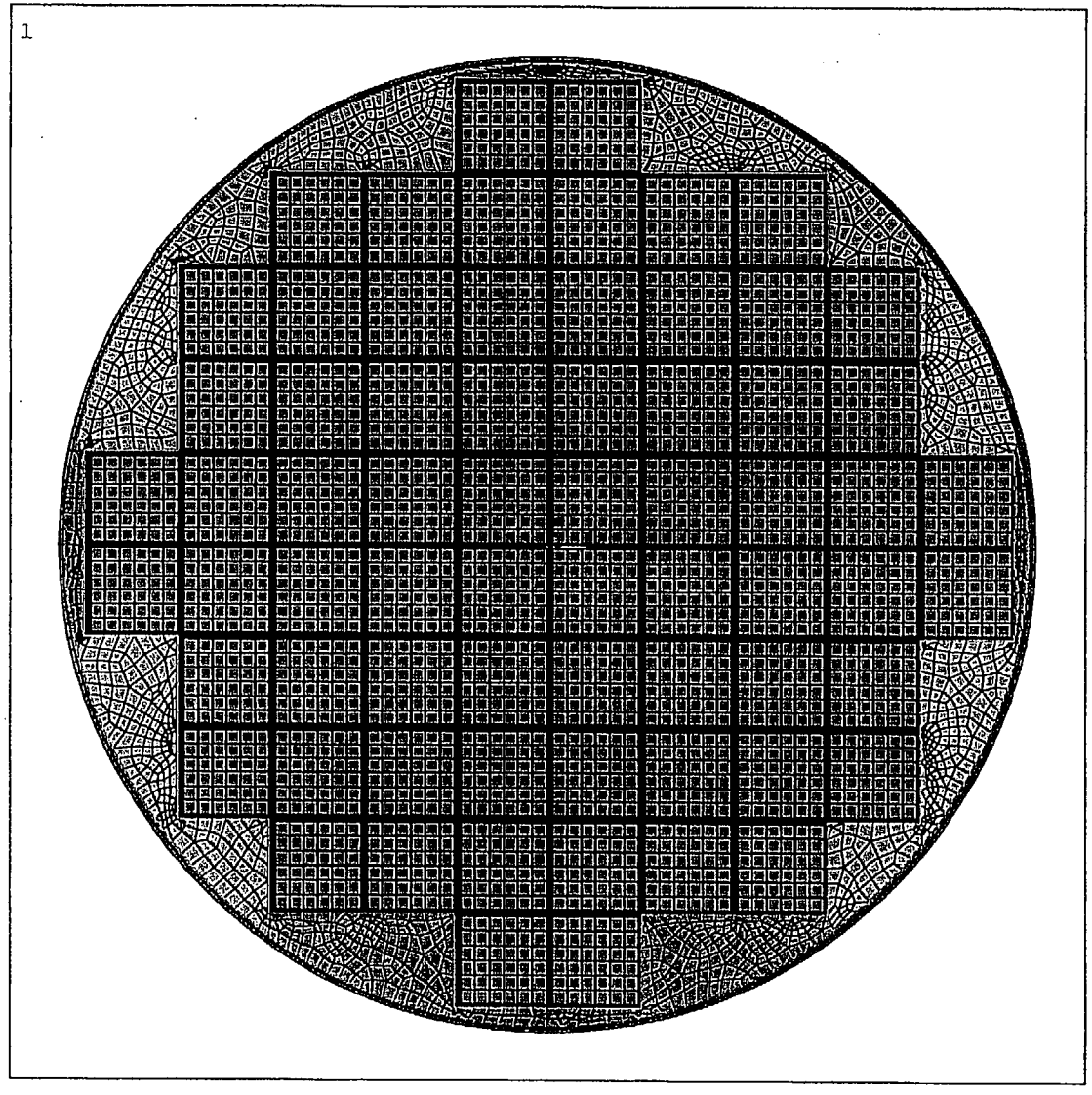

FIGURE 3.4.11; MPC-68 BASKET CROSS-SECTION ANSYS FINITE ELEMENT MODEL

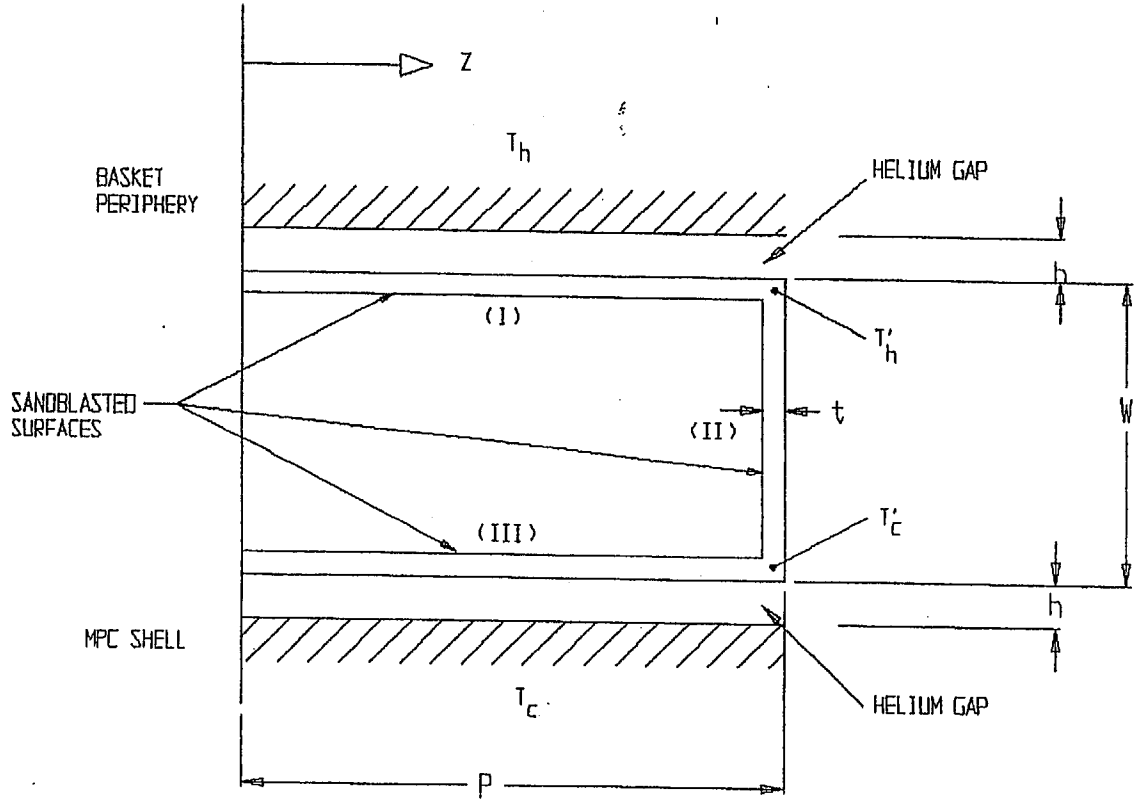

FIGURE 3.4-12; ILLUSTRATION OF AN MPC BASKET TO SHELL ALUMINUM HEAT CONDUCTION ELEMENT

\5014\HI951251\CH_3\3_4_12

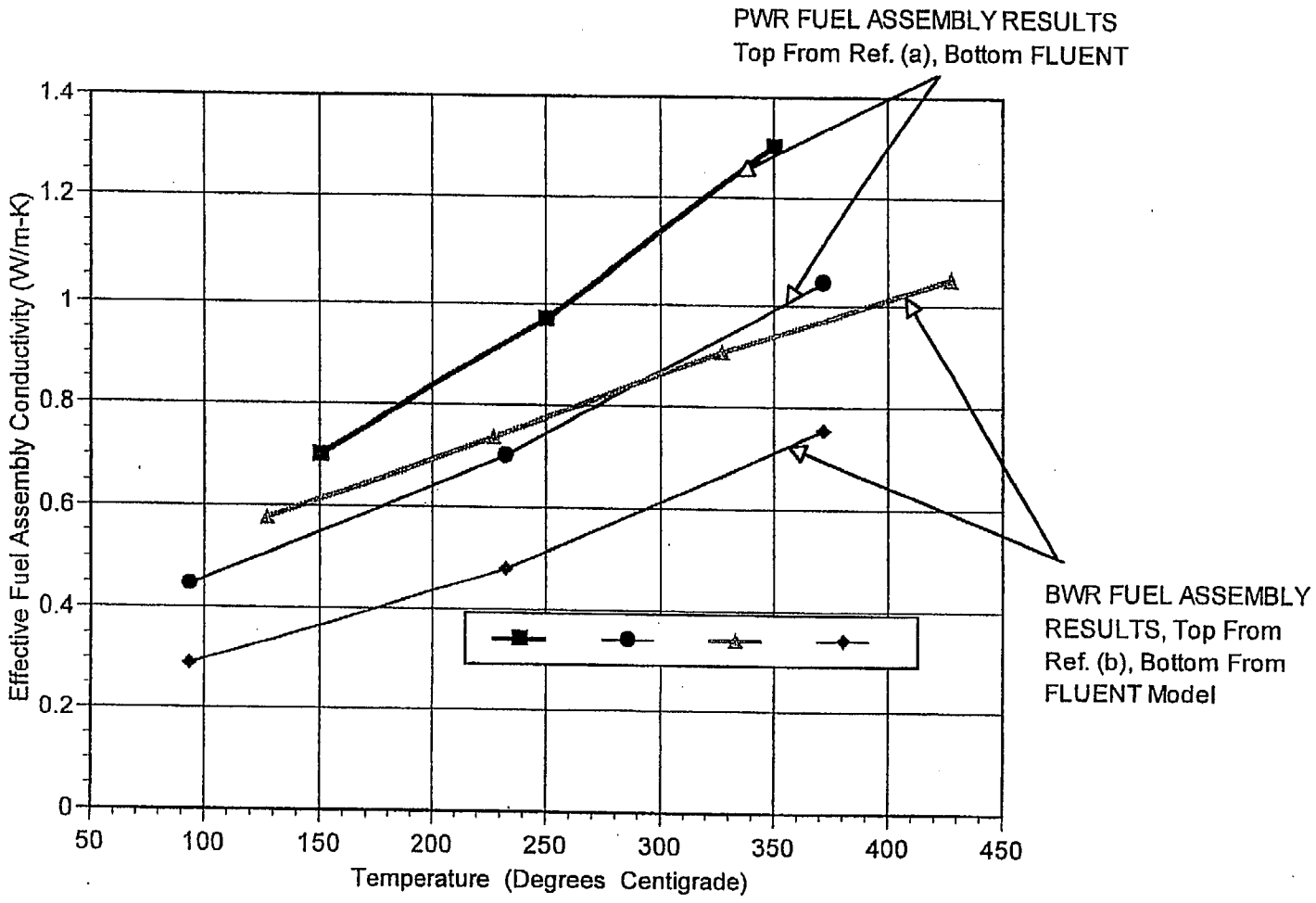

(a) "Determination of SNF Peak Temperatures in the Waste Package", Bahney & Doering, *HLRWM Sixth Annual Conf.*, Pages 671-673, (April 30 - May 5, 1995)
(b) "A Method for Determining the Spent-Fuel Contribution to Transport Cask Containment Requirements", *Sandia Report SAND90-2406*, page II-132, (1992)

FIGURE 3.4.13: COMPARISON OF FLUENT BASED FUEL ASSEMBLY EFFECTIVE CONDUCTIVITY RESULTS WITH PUBLISHED TECHNICAL DATA

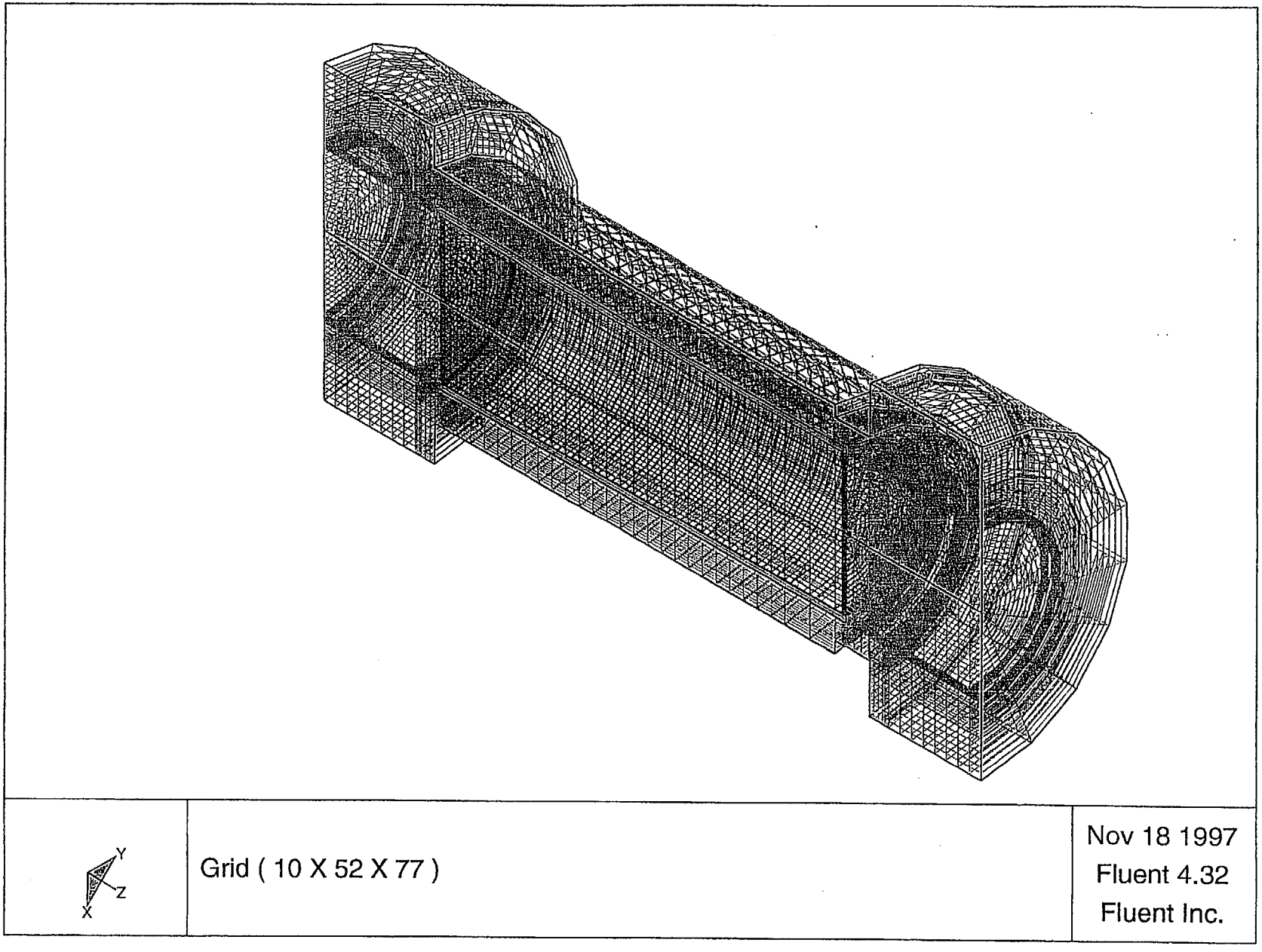

FIGURE 3.4.14: HI-STAR 100 SYSTEM FINITE ELEMENT MESH FOR THERMAL ANALYSIS

FIGURE 3.4.15

THIS FIGURE IS INTENTIONALLY DELETED.

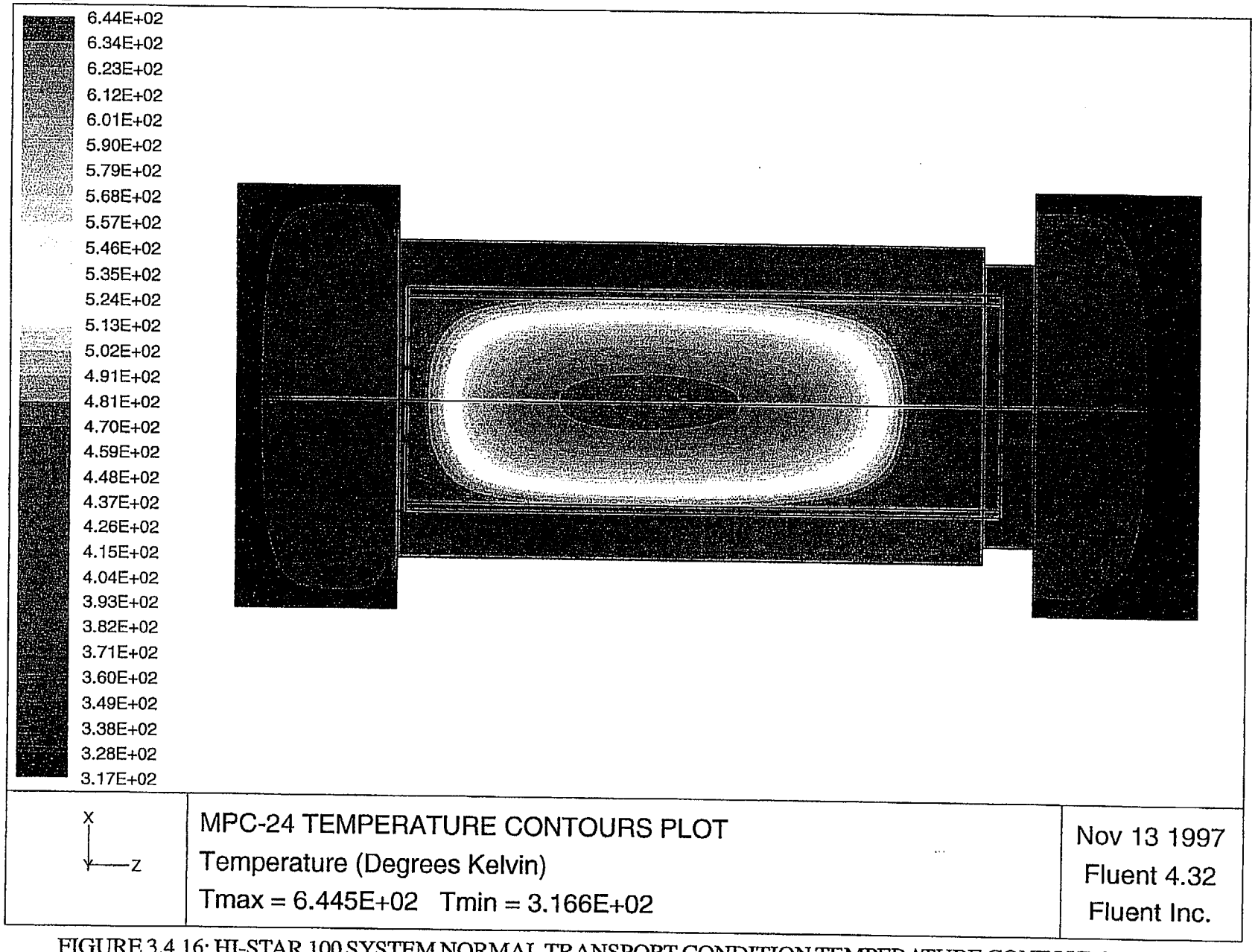

FIGURE 3.4.16: HI-STAR 100 SYSTEM NORMAL TRANSPORT CONDITION TEMPERATURE CONTOURS PLOT (MPC-24 BASKET)

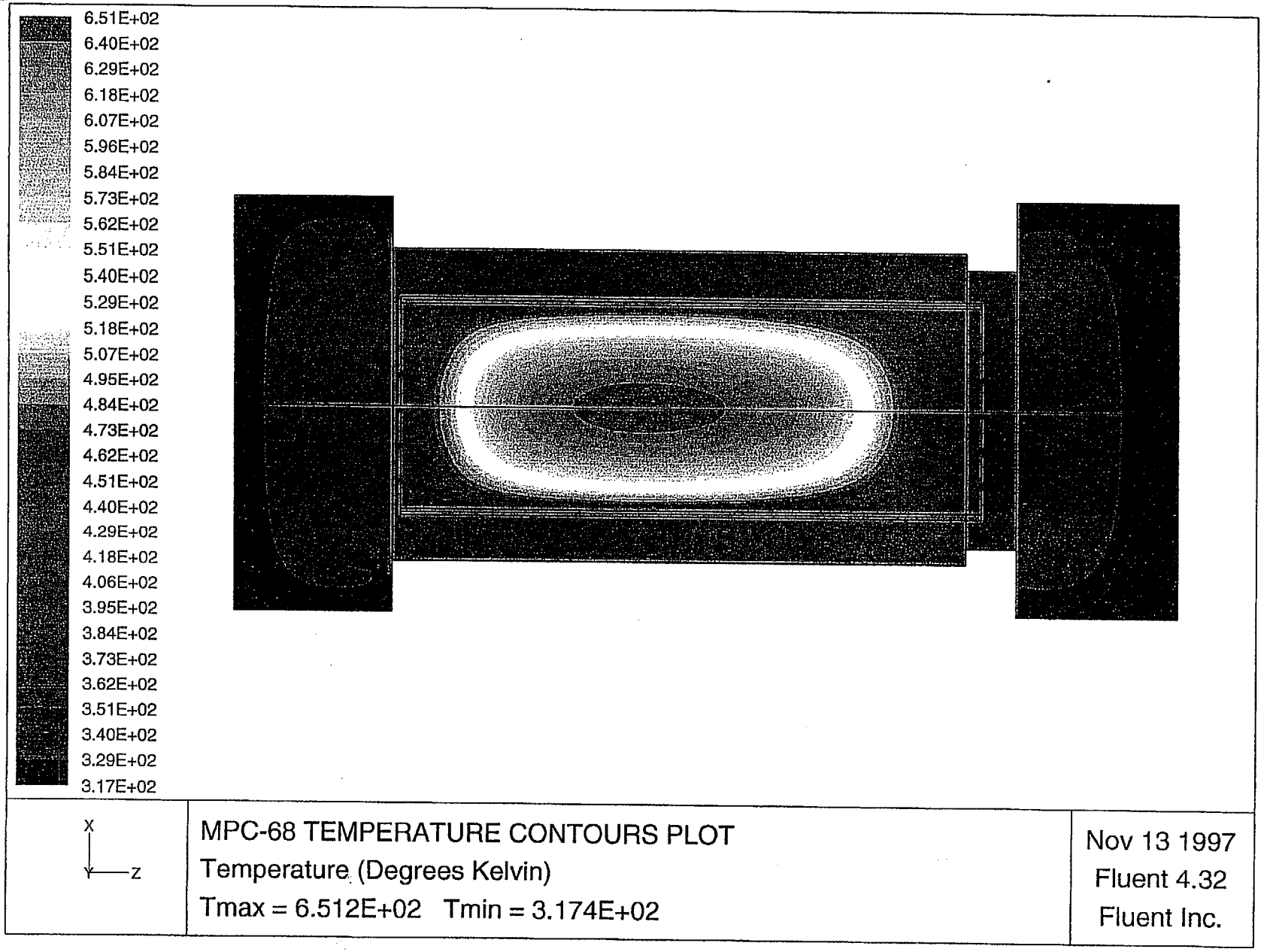

FIGURE 3.4.17: HI-STAR 100 SYSTEM NORMAL TRANSPORT CONDITION TEMPERATURE CONTOURS PLOT (MPC-68 BASKET)

FIGURE 3.4.18

THIS FIGURE IS INTENTIONALLY DELETED.

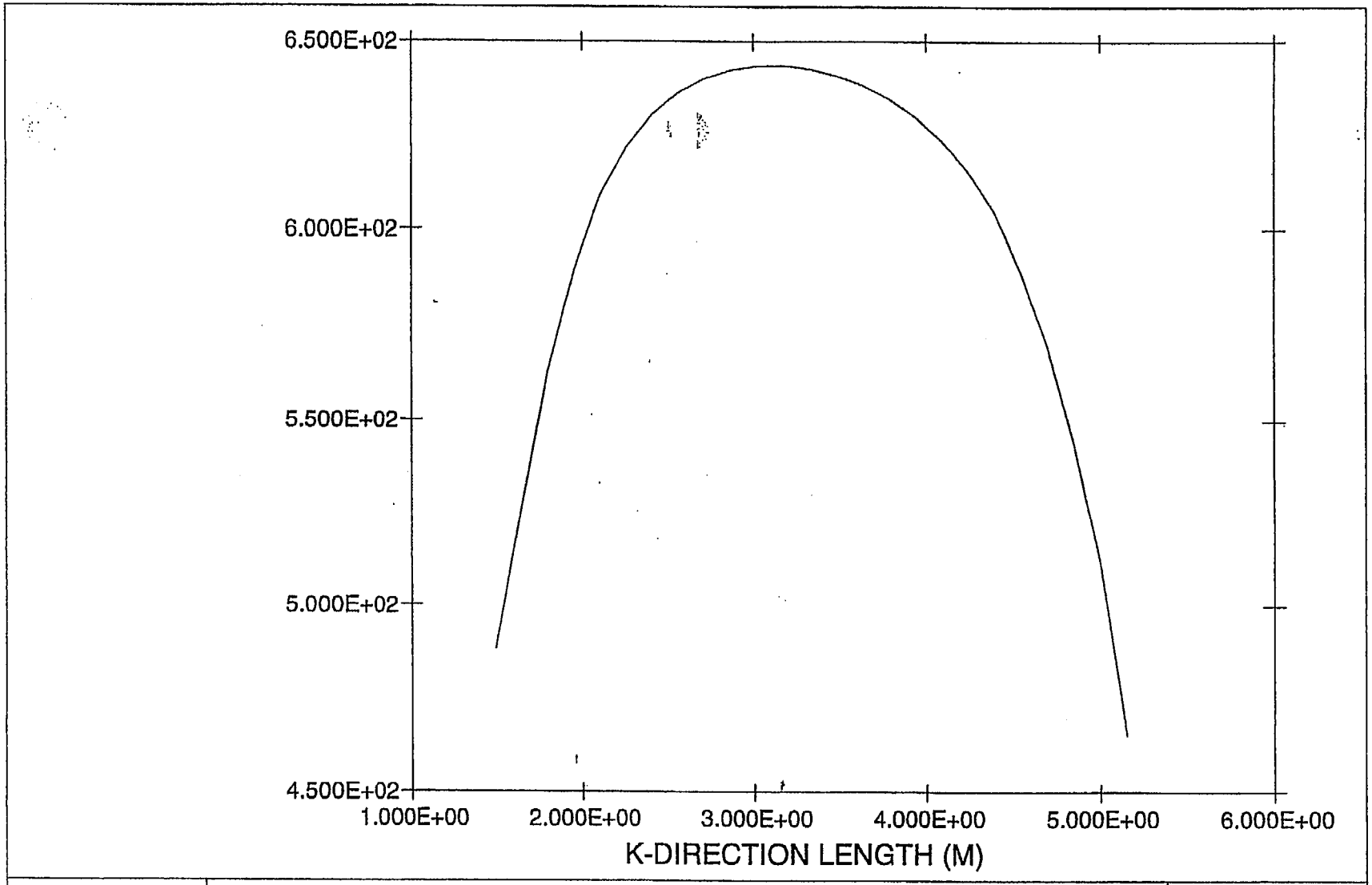

FIGURE 3.4.19: MPC-24 HOTTEST ROD TEMPERATURE PROFILE

Temperature (Kelvin) Vs. Axial Length (Meters)

May 24 1998
Fluent 4.32
Fluent Inc.

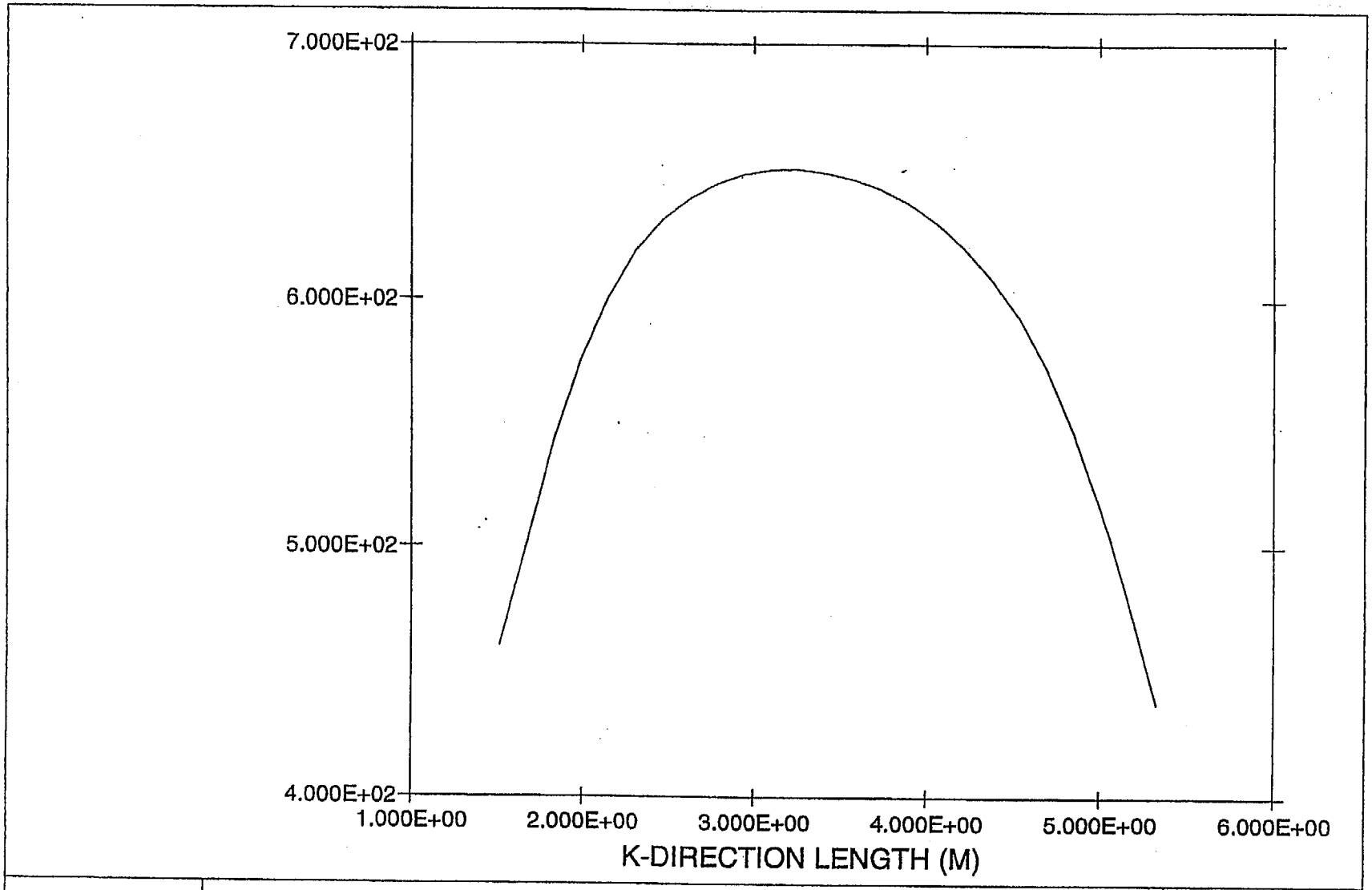

FIGURE 3.4.20: MPC-68 HOTTEST ROD TEMPERATURE PROFILE

Temperature (Kelvin) Vs. Axial Length (Meters)

May 24 1998
Fluent 4.32
Fluent Inc.

FIGURE 3.4.21

THIS FIGURE IS INTENTIONALLY DELETED.

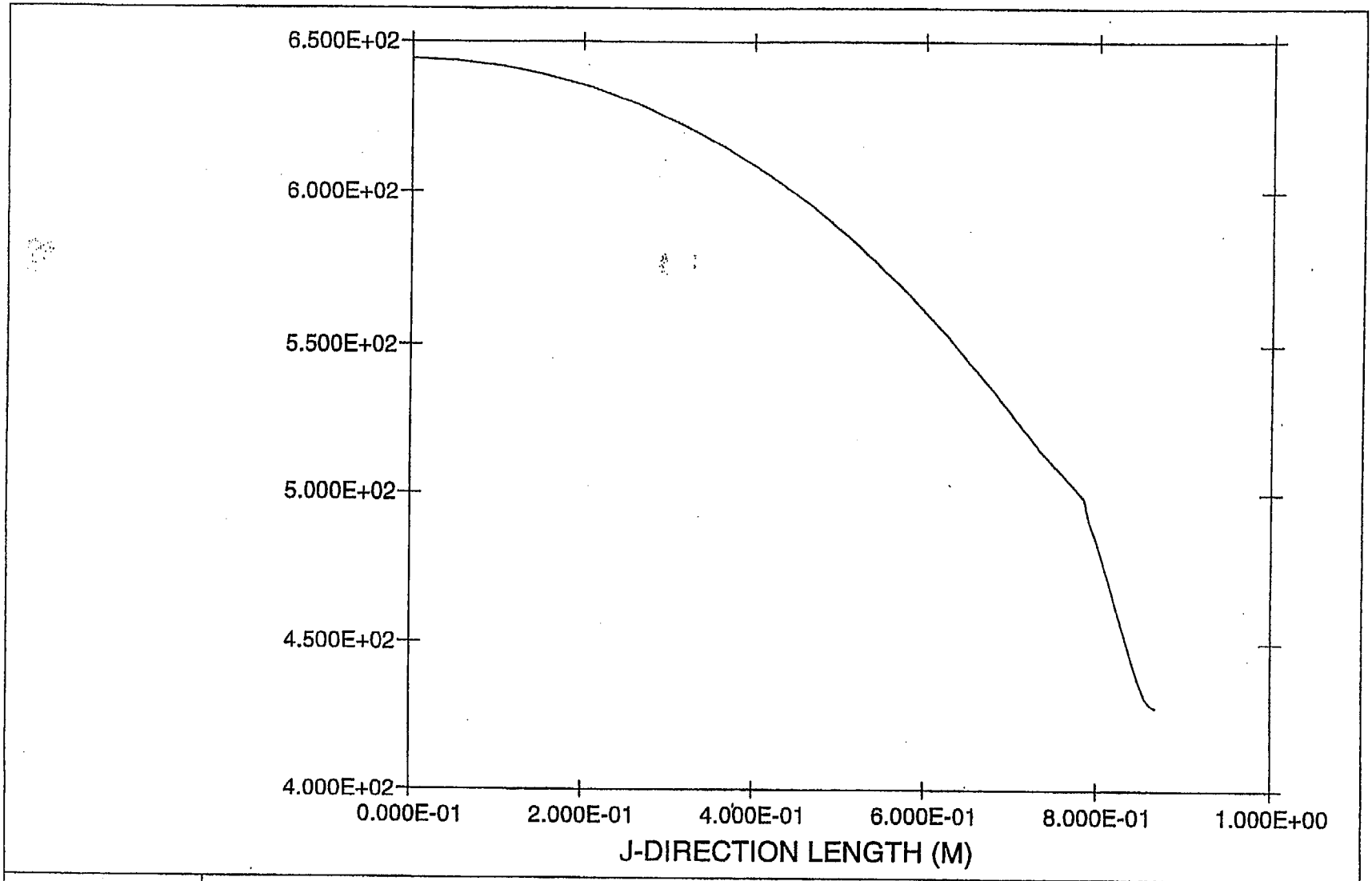

FIGURE 3.4.22: MPC-24 RADIAL TEMPERATURE PROFILE

Temperature (Kelvin) Vs. Radial Distance (Meters)

May 24 1998
Fluent 4.32
Fluent Inc.

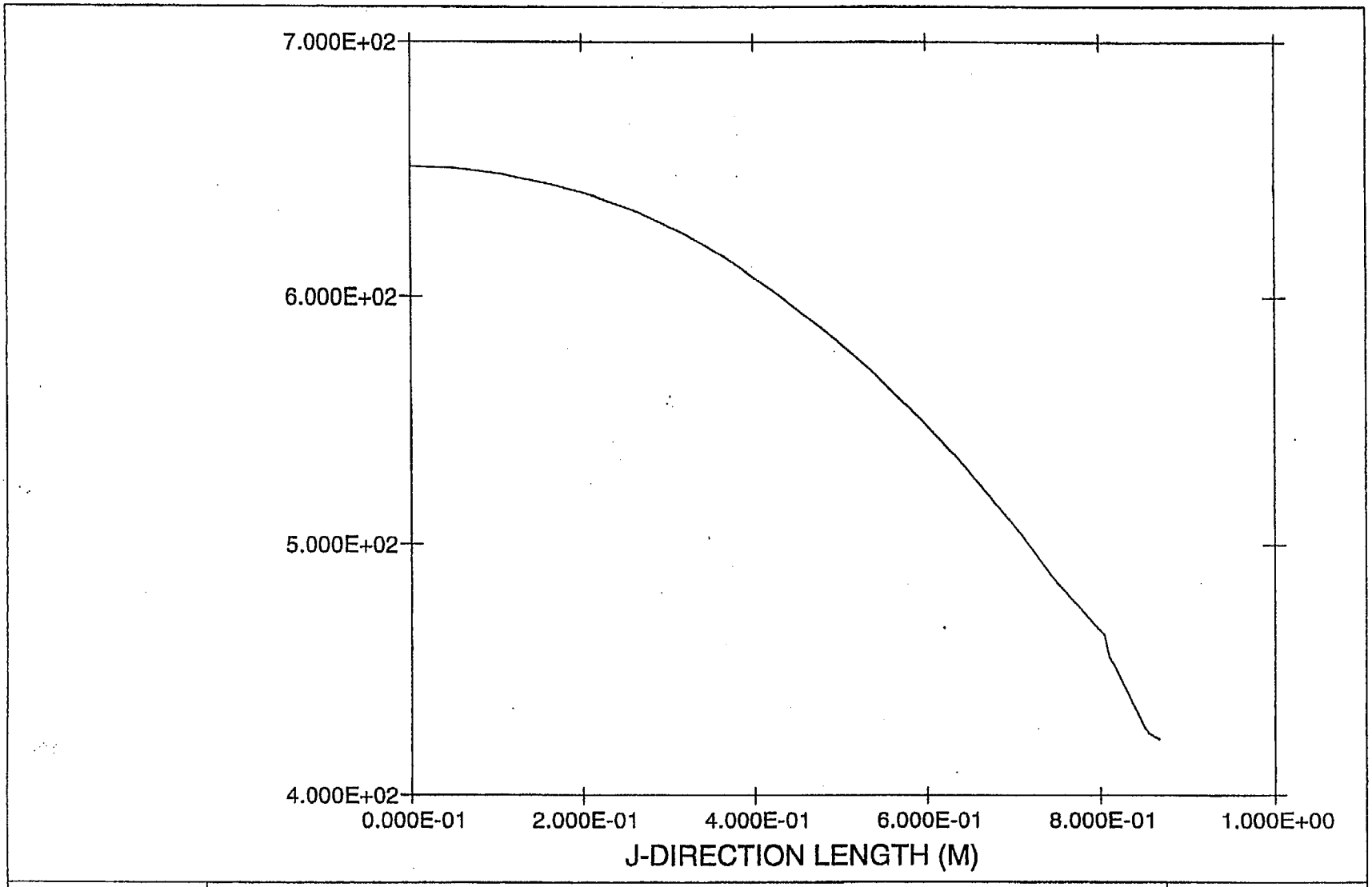

FIGURE 3.4.23: MPC-68 RADIAL TEMPERATURE PROFILE

Temperature (Kelvin) Vs. Radial Position (Meters)

May 24 1998
Fluent 4.32
Fluent Inc.

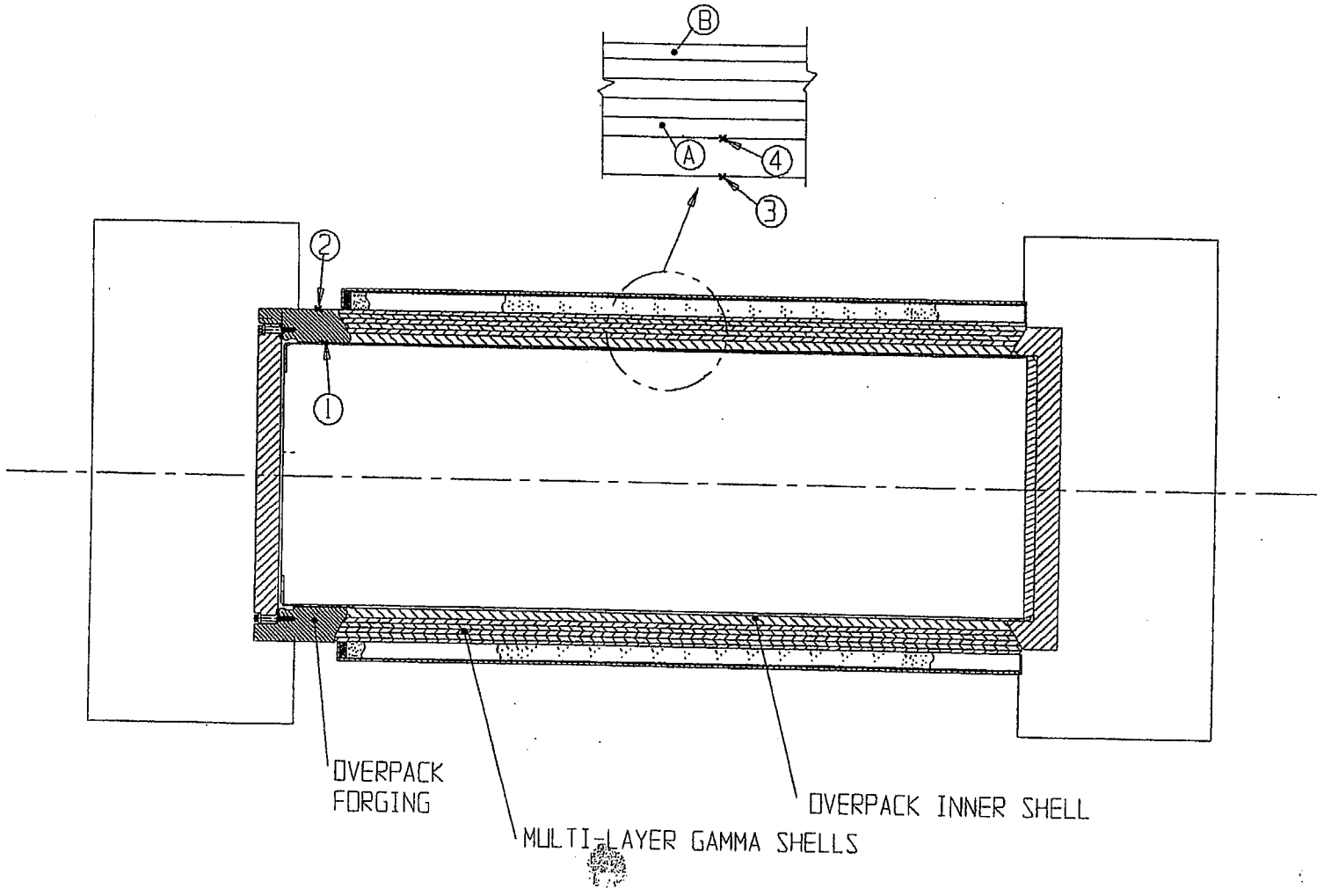

FIGURE 3.4.24; HI-STAR 100 PACKAGE CONTROL LOCATIONS TRACKED IN THE COOLDOWN EVENT

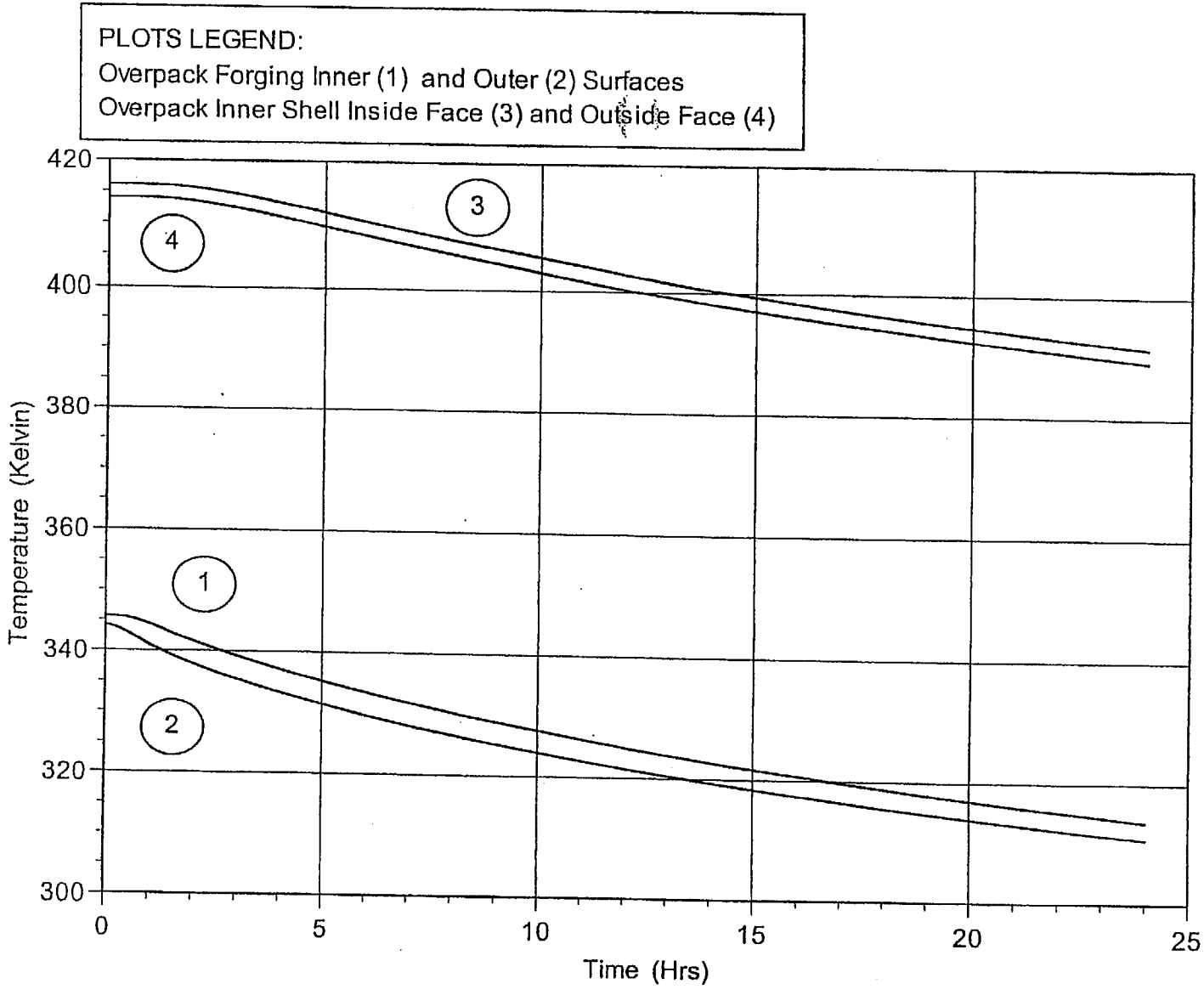

FIGURE 3.4.25: CONTAINMENT BOUNDARY COOLDOWN TEMPERATURE PROFILES

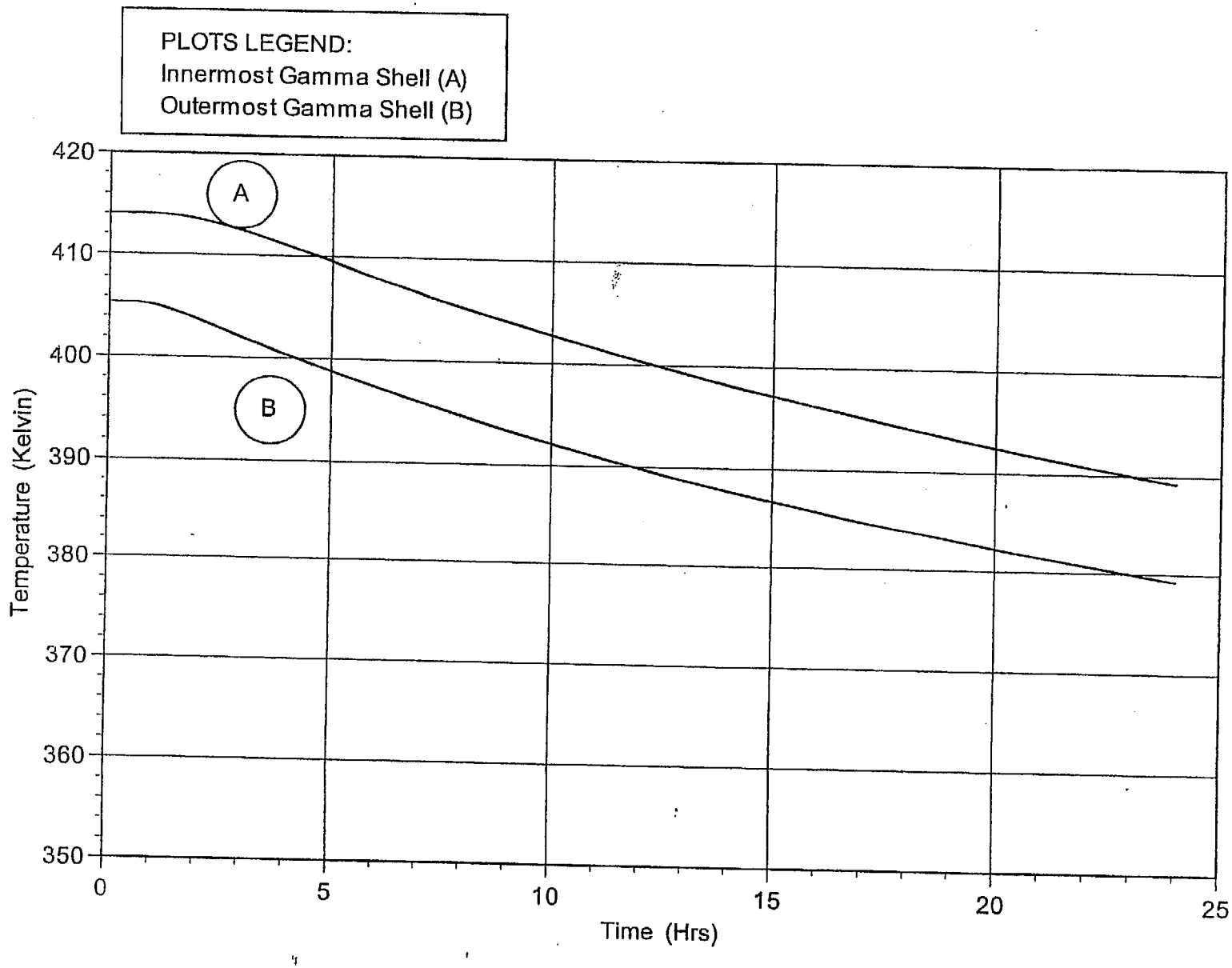

FIGURE 3.4.26: MULTI-LAYERED SHELLS COOLDOWN TEMPERATURE PROFILES

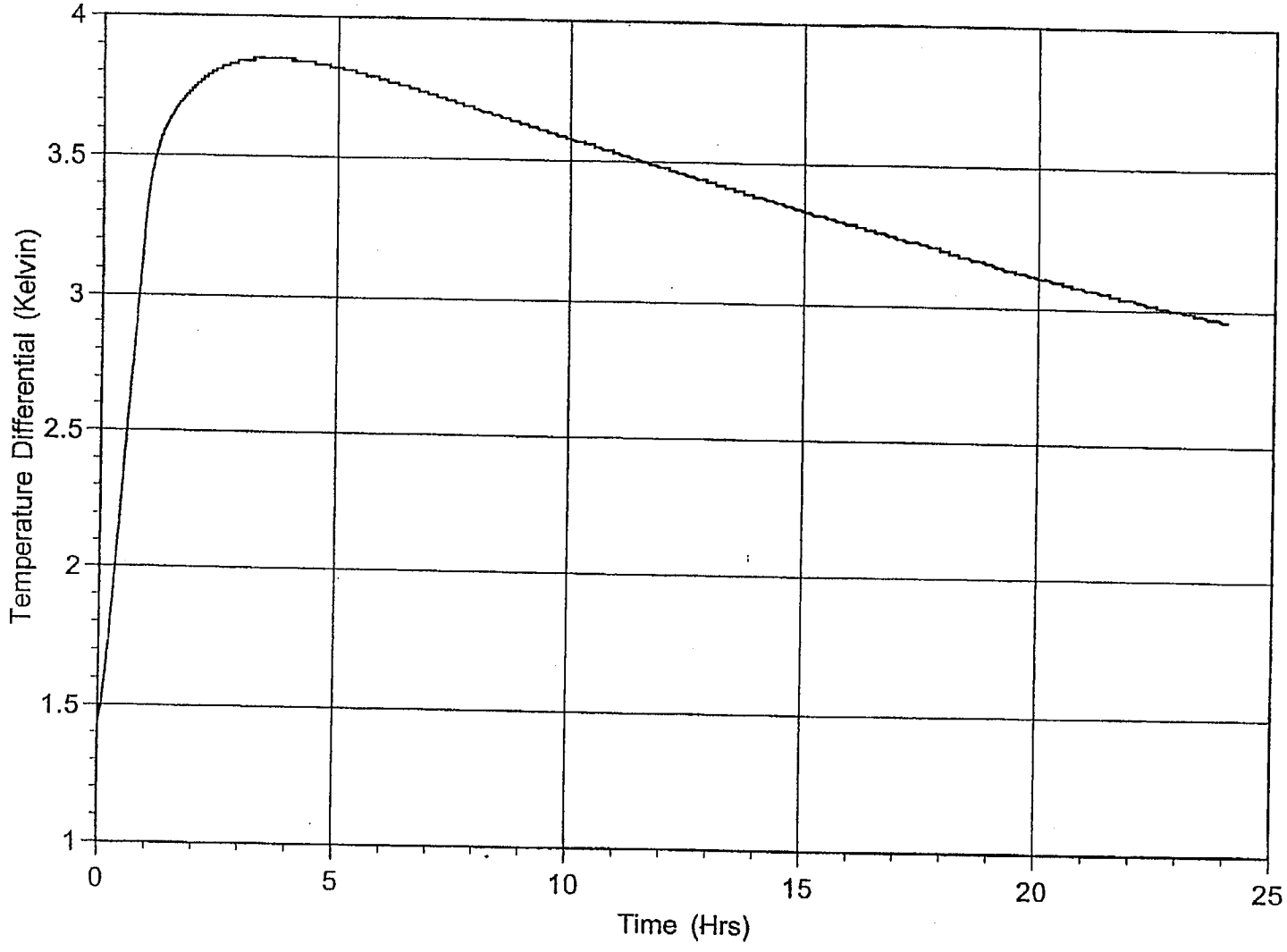

FIGURE 3.4.27: OVERPACK FORGING THROUGH THICKNESS TEMPERATURE GRADIENT DURING COOLDOWN TRANSIENT

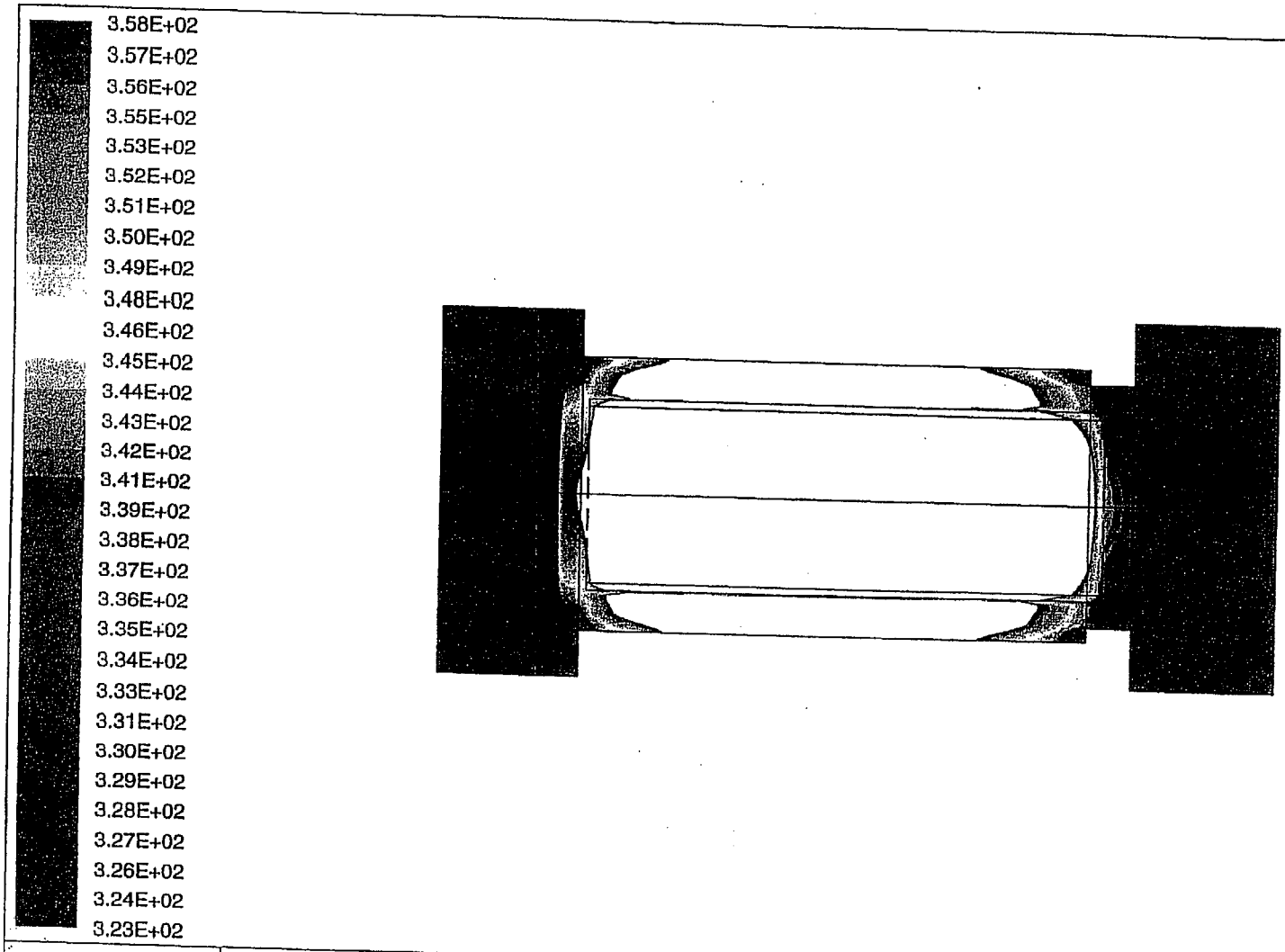

FIGURE 3.4.28: IMPACT LIMITERS SURFACE TEMPERATURE MAP
Temperature (Degrees Kelvin)
Tmax = 3.580E+02 Tmin = 3.232E+02

Feb 04 1999
Fluent 4.32
Fluent Inc.

3.5 HYPOTHETICAL ACCIDENT THERMAL EVALUATION

As mandated by 10CFR71 requirements, the HI-STAR System is subjected to a sequence of hypothetical accident conditions. The objective is to determine and assess the cumulative damage sustained by the system. The accident scenarios specified in order are: (1) a 30 foot free drop onto an unyielding surface; (2) a 40-inch drop onto a mild steel bar; and (3) exposure to a 30-minute fire at 1475°F. The initial conditions for the fire accident specify steady state at an ambient temperature between -20°F and 100°F [3.5.1]. In the HI-STAR System hypothetical fire accident evaluation, full effects of insolation before, during, and after the fire are considered. The effects of the first two drop accidents are evaluated in Chapter 2. In this section, the transient thermal response of the HI-STAR System to a 30-minute fire followed by a post-fire cooldown is determined. The fire accident evaluation is performed by consideration of a worst case combination of factors which conservatively overestimate heat input to the HI-STAR System during the fire followed by an underestimation of the ability of the cask to reject heat to the environment after the fire.

The impact limiters are designed to crush and absorb energy during the hypothetical drops. In the hypothetical fire accident evaluation, the impact limiter is assumed to be crushed to the bounding maximum condition of a solid block of highly conducting aluminum, resulting in increased heat input to the overpack ends through the reduced impact limiter thickness during the fire. The fire condition thermal analysis results are therefore bounding with respect to impact limiter design and amount of crush experienced during a hypothetical drop accident.

A puncture event may locally buckle some of the radial connector plates through the neutron shielding, thereby reducing the ability of the system to reject heat after the fire. As described in Section 2.7, the puncture bar is 6 inches in diameter and correspondingly has a face area of approximately 28.3 in^2. The enclosure shell area is greater than 52,200 in^2. Therefore, while the puncture bar would directly impact less than 0.06% of the exposed area, a conservative 10% reduction in the neutron shield region effective thermal conductivity is considered during the post-fire cooldown phase.

During the initial 30-minute fire event, some of the neutron shield will be exposed to high temperatures. Therefore, in determining heat input to the system, a conservative value maximizing the heat input is utilized for the neutron shield thermal conductivity. During the post-fire cooldown phase, no credit is considered for conduction through the neutron shield material. During the fire, a 10CFR71 mandated cask surface emissivity is considered to maximize radiant heat input to the cask. Destruction of the painted surfaces due to exposure to intense heat during the fire event is a credible possibility. Therefore, the lower emissivity of exposed carbon steel is conservatively considered for post-fire cooldown analysis.

The initial condition prior to the start of the fire accident is based on the bounding normal transport condition MPC basket temperature distribution. The smallest of the ~~two~~ *four* baskets *(MPC-24, MPC-24E, MPC-32 and MPC-68)* average density and heat capacity are applied to the fire transient analysis. Thus, maximum basket heat load coincident with minimum thermal inertia provides a

conservatively bounding response of the HI-STAR System to a fire accident condition.

The temperature history of a number of critical control points in the HI-STAR System are monitored during the 30-minute fire and the subsequent relaxation of temperature profiles during the post-fire cooldown phase. The impact of transient temperature excursions on HI-STAR System materials is assessed in this section.

3.5.1 Thermal Model

3.5.1.1 Analytical Model

A thermal transient simulation model to determine the fire condition temperature response is developed on the FLUENT CFD code [3.1.2]. The basic underlying finite volume model is based on the steady-state FLUENT model developed and described in Section 3.4. This basic model is modified by incorporating time dependent thermal loads on the exposed surfaces of the HI-STAR System for determining transient responses at every computational cell defined in the FLUENT model.

The HI-STAR System configuration during a hypothetical fire accident is schematically depicted in Figure 3.5.1. The initial thermal condition of the HI-STAR System prior to the accident condition is the normal transport steady-state temperature distribution. The HI-STAR System is then subjected to a 1475°F fire environment for 30 minutes. During this fire event, the impact limiters installed on both ends are assumed to be in a fully crushed state. This is a conservative assumption which results in an increased heat input to the overpack due to the higher thermal conductivity and reduced thickness of the crushed impact limiter. After 30 minutes, the ambient temperature is restored to 100°F and the HI-STAR System is allowed to proceed through a post-fire cooldown phase. During this entire transient event (fire and post-fire cooldown), the temperature history of several control points in the HI-STAR System is monitored. These points are schematically depicted in Figure 3.5.1.

Heat input to the HI-STAR System while it is engulfed in a fire is from a combination of radiation and forced convection heat transfer to all overpack/impact limiter exposed surfaces. This can be expressed by the following equation:

$$q_F = h_{fc}\,(T_F - T_s) + \sigma\,\varepsilon\,[(T_F + 460)^4 - (T_s + 460)^4]$$

where:

- q_F = surface heat input flux (Btu/ft^2-hr)
- T_F = fire condition temperature (1475°F)
- T_S = transient surface temperature (°F)
- h_{fc} = forced convection heat transfer coefficient [Btu/ft-hr-°F]
- ε = surface emissivity = 0.9 (per 10CFR71)
- σ = Stefan-Boltzmann Constant (0.1714×10^{-8} Btu/ft^2-hr-°R^4)

The forced convection heat transfer coefficient is calculated to bound the convective heat flux contribution to the exposed cask surfaces due to a fire induced air flow velocity of 15 m/s. For the case of air flow past a heated cylinder, Jakob [3.5.2] recommends the following correlation for convective heat transfer, obtained from experimental data:

$$Nu_{fc} = 0.028\, Re^{0.8} [\, 1 + 0.4 (\frac{L_{st}}{L_{tot}})^{2.75} \,]$$

where:

L_{tot} = length traversed by flow
L_{st} = length of unheated section
K_f = thermal conductivity of air evaluated at the average film temperature
Re = flow Reynolds Number based on L_{tot}
Nu_{fc} = Nusselt Number ($h_{fc}\, L_{tot}/K_f$)

Consideration of the wide range of temperatures to which the exposed surfaces are subjected to during the fire and the temperature dependent trend of air properties requires a careful selection of parameters to determine a conservatively large bounding value of the convective heat transfer coefficient. In Table 3.5.1, a summary of the parameter selections with justifications provides an appropriate basis for application of this correlation to determine forced convection heating of the HI-STAR System during the short-term fire event.

After the 30-minute fire event, the ambient temperature is restored to 100°F. The HI-STAR System cools down during this post-fire cooldown phase. Heat loss from outside exposed surfaces of the overpack is determined by the following equations:

$$q_S = 0.18 (T_S - T_A)^{4/3} + \sigma\, \varepsilon\, [(T_S + 460)^4 - (T_A + 460)^4]$$

where:

q_s= surface heat loss flux (Btu/ft^2-hr)
T_S = transient surface temperature (°F)
T_A = ambient temperature (100°F)
ε = surface emissivity
σ = Stefan-Boltzmann Constant (0.1714×10^{-8} Btu/ft^2-hr-°R^4)

During the fire event, some region of Holtite will be overheated and thus lose its ability to conduct heat. In the fire transient analysis, full credit is given to conduction through Holtite to conservatively increase heat input to the overpack. In the post-fire cooldown phase, all of the Holtite is conservatively assumed to be lost (no conduction through Holtite material).

During the 30-foot drop and puncture accident events, the mechanical integrity of the HI-STAR System is maintained. From a thermal analysis standpoint, the impact limiters are crushed and there is at most localized damage to radial channels. While the resulting localized damage would not significantly degrade the heat transfer ability of the Holtite region, a 10% effective conductivity reduction is conservatively (as described earlier in Section 3.5) applied during the post-fire cooldown

phase. In Table 3.5.2, a summary of inputs used in the determination of the effect of a hypothetical fire accident is provided.

3.5.1.2 Test Model

For determining the transient response of the HI-STAR System under a hypothetical fire accident condition, a detailed finite volume model has been developed on the validated and benchmarked FLUENT code. The dynamic model features several conservative assumptions to bound temperature excursions during the heat up and cooldown phases of the accident. Accordingly, development of a separate test model to verify the results is not considered necessary. Evaluation of the HI-STAR System thermal design in the event of a hypothetical fire event is shown to be in compliance with 10CFR71 requirements.

3.5.2 System Conditions and Environment

The HI-STAR System is shown to maintain its mechanical integrity following a 30 foot drop and puncture accident with stresses within applicable ASME Code requirements. The impact limiters absorb the impact forces and are crushed in the drop event. Completely crushed impact limiters provide a conservatively limiting situation for increased heat absorption during the 30-minute fire. The effect of a puncture accident results in localized damage to the radial connectors embedded in Holtite neutron shielding. This will *not* reduce the heat transfer capability of the region containing Holtite by a significant factor. The fire is specified to be at a temperature of 1475°F and last for 30 minutes. Emissivity of all exposed surfaces is set to 0.9. Some of the Holtite will decompose and lose its ability to conduct heat during the fire event due to exposure to severe temperature conditions. Thermal analysis of the HI-STAR System is performed by postulating worst case conditions whereby increased heat absorption takes place during the 30-minute fire and a reduced ability of the HI-STAR System to reject heat takes place during the post-fire cooldown phase.

3.5.3 System Temperatures

The hypothetical fire accident condition is evaluated by imposing a 1475°F fire temperature for 30 minutes followed by a post-fire equilibrium phase that is followed for more than 30 hours. The temperature-time history of several control points is monitored. These points are selected because of their importance relating to safety evaluation. In Figures 3.5.2 to 3.5.4, the transient temperature profiles of the monitored points shown in Figure 3.5.1 are plotted. From these plots, the temperature of exposed surfaces is seen to increase rapidly and peak at about 1348°F at the end of the fire (i.e., 30 minutes). Figure 3.5.5 shows the peak axial fuel cladding temperature profile during post-fire cooldown. In the post-fire equilibrium phase, there is an initial rapid cooldown of the peak surface temperature followed by an asymptotic approach to the final steady-state condition. The closure bolts and mechanical seals peak temperatures are below short-term limits. The MPC basket center temperature rises sluggishly to a broad peak and then slowly decays to a final steady-state condition. Portions of Holtite neutron shielding material near the overpack enclosure shell experience a short duration high temperature excursion. The crushed aluminum alloy inside the impact limiter begins to

melt at 1105°F. The latent heat of melting of aluminum alloy during the melting phase would absorb the incident heat flux from the fire. This ablation mechanism will protect the cask by limiting the surface temperature excursion and restricting the amount of heat input to the overpack lid. In the HI-STAR System fire transient evaluation, credit for this protective feature is not considered.

The HI-STAR fire event model is depicted in Figure 3.5.6. Fire condition containment boundary through thickness temperature profiles are presented in Figures 3.5.7, 3.5.8, and 3.5.9 across Sections A-A, B-B, and C-C, as shown in Figure 3.5.6. The figures present through-thickness temperature profiles at the end of the 30-minute fire and 60 minutes after the start of the fire (30 minutes into the post-fire cooldown period).

In the fire event, the dominant heat input source is located on the outside of the cask. The temperature gradient, as seen in Figures 3.5.7, 3.5.8, and 3.5.9, is reversed from the normal condition, with the maximum temperature occurring at the outermost layer. From Figure 3.5.7, it is apparent that the overpack inner shell remains below the 500°F short-term design basis temperature limit. At the end of the 30-minute fire, the outermost layer of the multi-layered shells is heated to approximately 540°F. During the post-fire cooldown phase the temperature of this outer layer rapidly drops below 500°F, as shown on the 60-minute profile.

An examination of the overpack forging temperature profile (Section B-B, Figure 3.5.8) shows that the outer layers of the forging, directly adjacent to the surface exposed to the fire, are heated to in excess of 700°F during the fire. The bulk of the forging metal mass (in excess of 6 inches out of the total 8.5 inches) remains below the 700°F short-term design basis temperature limit. The portion of the overpack forging which is covered by the impact limiters remains below 700°F both during and after the fire. This is illustrated by the temperature profiles presented in Figure 3.5.9.

The following observations can be drawn from an examination of Figures 3.5.6 through 3.5.9:

- The containment boundary regions that are within the confines of the multi-layered shells remain below 500°F.

- The containment boundary regions that are within the confines of the impact limiters remain below 700°F.

- The bulk of the containment boundary in the regions that are directly exposed to the fire remain below 700°F.

The outer region of the HI-STAR 100 overpack consists of forty sector shaped annular spaces enclosed in half inch thick carbon steel plates. These annular spaces contain Holtite-A neutron absorber material. Holtite-A is a stable material under the environmental and thermal conditions corresponding to normal operation. Under a fire condition, the temperature in the enclosure shell cavity rises resulting in loosening of the water intermolecular bonds to the neutron shield material

leading to liberation of water vapor. *For conservatism, a 6% weight loss factor for the neutron shield when exposed to a direct fire is assumed.* ~~Information on stability of neutron shield materials when exposed to a direct fire (temperatures between 800°C to 900°C for thirty minutes) is provided in Appendix 1.B. From reported test data, weight loss under extreme conditions is relatively small (less than 6%).~~ Under a conservatively postulated scenario wherein all of the radial neutron shield material (approximately 12,850 lbs required to completely fill the forty spaces) is exposed to a direct fire, 771 lbs of water vapor (i.e 6% of neutron shield) generation in 30 minutes is required to be expelled from the neutron shield cavities. To protect the enclosure shell from overpressure, two rupture discs (each having the required vapor expulsion capacity) are incorporated in the HI-STAR overpack design. The rupture discs have a relatively low set pressure (30 psig) to relieve water vapor if the generation is rapid during a fire condition. ~~Appendix 2.AM demonstrates structural integrity of the enclosure shell at the 30 psig internal pressure.~~

3.5.4 Maximum Internal Pressure

Based on bounding transient temperature excursions calculated for the HI-STAR System during a hypothetical fire accident condition, maximum calculated cask internal pressures are reported in Table 3.5.3. Maximum pressure calculations assume 100% of the fuel rods rupture, releasing conservatively determined rod fill gas and fission gases volumes into the MPC cavity.

3.5.5 Maximum Thermal Stresses

Maximum thermal stresses generated during transient temperature excursions within the HI-STAR System are reported in Chapter 2.

3.5.6 Evaluation of System Performance for the Hypothetical Accident Thermal Conditions

The HI-STAR System was subjected to a hypothetical fire accident condition with the impact limiters crushed and enclosure shell punctured as a result of previously imposed drop and puncture accidents. However, mechanical integrity of the overpack intermediate and inner shells, mechanical seals, and MPC shell is retained. During the fire accident event, portions of neutron shielding material in the overpack enclosure shell experience high transient temperature excursions and thus partially lose the ability to conduct heat and shield neutrons. Portions of aluminum alloy inside the crushed impact limiters near the exposed surfaces melt, but do not ignite.

For assessing the impact of transient temperature excursions on the integrity of the HI-STAR System, the significant components and quantities of interest are the closure plate bolts temperatures, the mechanical seals temperatures, the neutron shield temperature, the peak pressure and the peak fuel cladding temperature. The closure plate bolts maintain their ability to hold the seals ~~(see structural evaluation Appendix 2.V)~~. The neutron shield material in the post-accident shielding analysis is conservatively assumed to be completely lost. The peak system pressure remains below the design basis accident pressure. The fuel cladding temperature peak does not exceed short-term accident limits. Consequently, the HI-STAR System integrity during the most severe fire event followed by a

post-fire cooldown phase is not compromised. In Table 3.5.4, a summary of peak HI-STAR System component temperatures during fire and post-fire accident conditions is provided. The calculated results demonstrate that the HI-STAR System is in compliance with 10CFR71 thermal requirements for hypothetical accident conditions of transport.

Table 3.5.1

SUMMARY OF TEMPERATURE-DEPENDENT FORCED CONVECTION HEAT TRANSFER CORRELATION PARAMETERS FOR AIR

Parameter	**Trend with Increasing Temperatures**	**Criteria to Maximize h_{fc}**	**Conservative Parameter Value**	**Evaluated At**
Temperature Range	100°F-1475°F	NA	NA	NA
Density	Decreases	Reynolds Number	High	100°F
Viscosity	Increases	Reynolds Number	Low	100°F
Conductivity (K_f)	Increases	h_{fc} Proportional to K_f	High	1475°F

Table 3.5.2

SUMMARY OF HYPOTHETICAL FIRE ACCIDENT INPUTS

		Steady-State Initial[†] Condition	**30-minute Fire**	**Post-Fire Equilibrium**
1.	Conduction through Holtite	No	Yes	No
2.	Holtite Region Conductivity Reduction (Loss of Radial Connectors)	No	No	Yes
3.	Insolation	Yes	Yes	Yes
4.	Radiation Heat Transfer	Yes	Yes	Yes
5.	Surface Convection	Natural	Forced	Natural
6.	Impact Limiters Installed[††]	Yes	Yes (crushed)	Yes (crushed)
7.	Surface Emissivity	0.85	0.9	0.66

[†] A bounding initial temperature condition is imposed for fire transient analysis.

[††] Based on minimum 15,000 lbs impact limiter weight modeled as a solid aluminum cap to maximize heat input to cask.

Table 3.5.3

MAXIMUM HI-STAR SYSTEM HYPOTHETICAL FIRE
CONDITION EVENT PRESSURES†

Condition	**Pressure (psig)**			
	MPC-24	**MPC-68**	***MPC-24E***	***MPC-32***
Without fuel rods rupture	~~70.7~~ *99.6*	~~70.0~~ *98.0*	*99.6*	*99.6*
With 100% fuel rods rupture	~~114.7~~ *143.3*	~~101.7~~ *129.9*	*143.9*	*161.6*

† Pressure analysis is based on release of 100% of the rods fill gas and 30% of the significant radioactive gases from a ruptured rod.

Table 3.5.4

MAXIMUM HI-STAR SYSTEM COMPONENTS AND MATERIALS
TEMPERATURES DURING AND AFTER HYPOTHETICAL FIRE CONDITION

Material/Component	**Initial Condition (°F)**	**During Fire (°F)**	**Post Fire Cooldown (°F)**	**Accident Limit (°F)**
Fuel cladding	708	708	751	1058
Overpack closure bolts	159	415	514	600
Overpack closure plate seals	160	392	490	1200
Drain port plug seal	259	645	662	932
Vent port plug seal	160	283	443	932
Holtite outer surface	223	1232	1232	N/A[†]
Holtite inner surface	259	604	604	N/A
MPC shell	309	313	419	775
Impact limiter surface	127	983	983	1105
Overpack outer enclosure	226	1348	1348	1350

[†] Holtite is conservatively assumed to be completely lost during the fire accident.

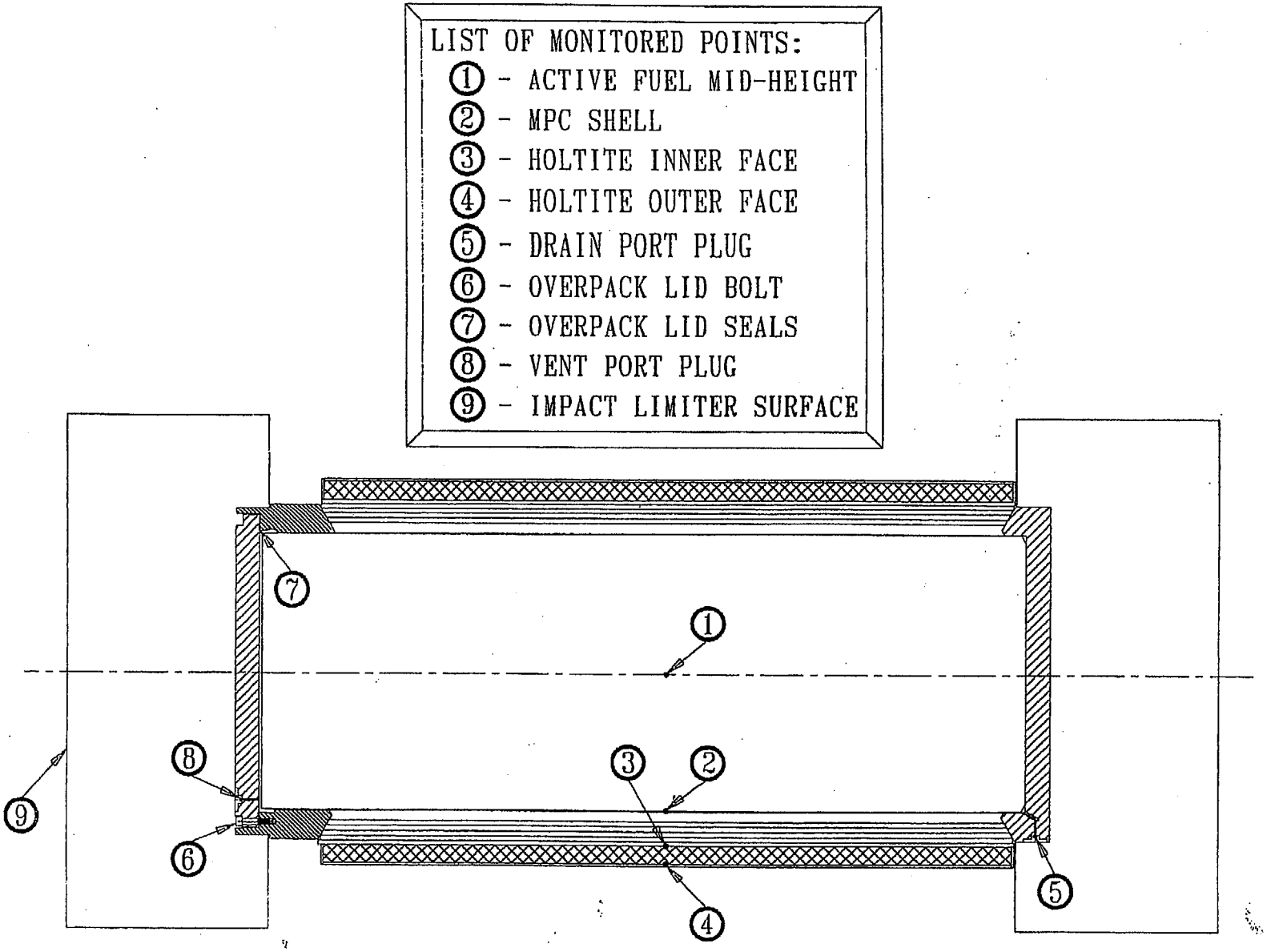

FIGURE 3.5.1; LOCATION OF HI-STAR 100 PACKAGE CONTROL POINTS MONITORED DURING HYPOTHETICAL FIRE ACCIDENT CONDITION

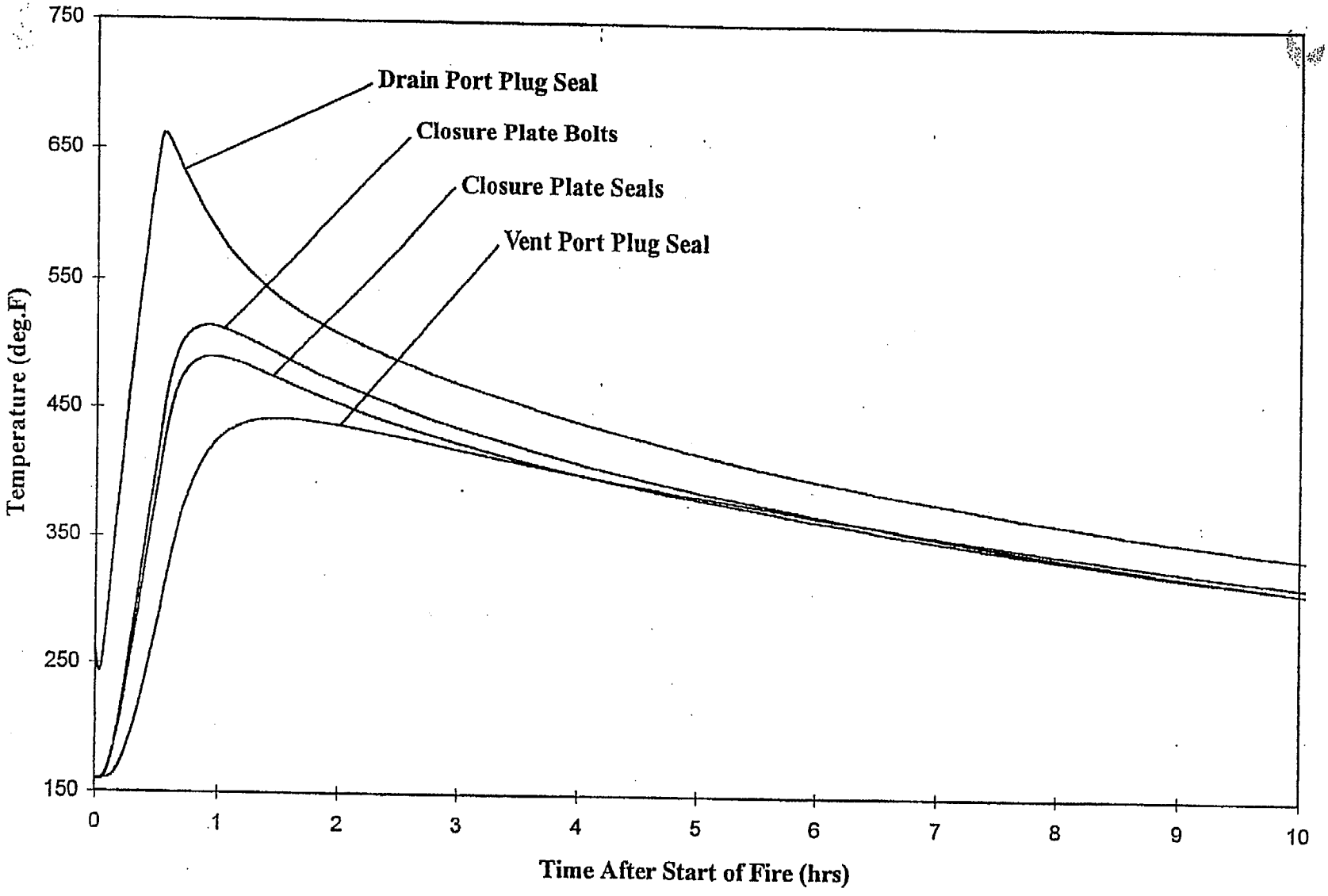

FIGURE 3.5.2; HI-STAR 100 PACKAGE CONTAINMENT BOUNDARY COMPONENTS FIRE ACCIDENT TRANSIENT TEMPERATURE RESPONSE

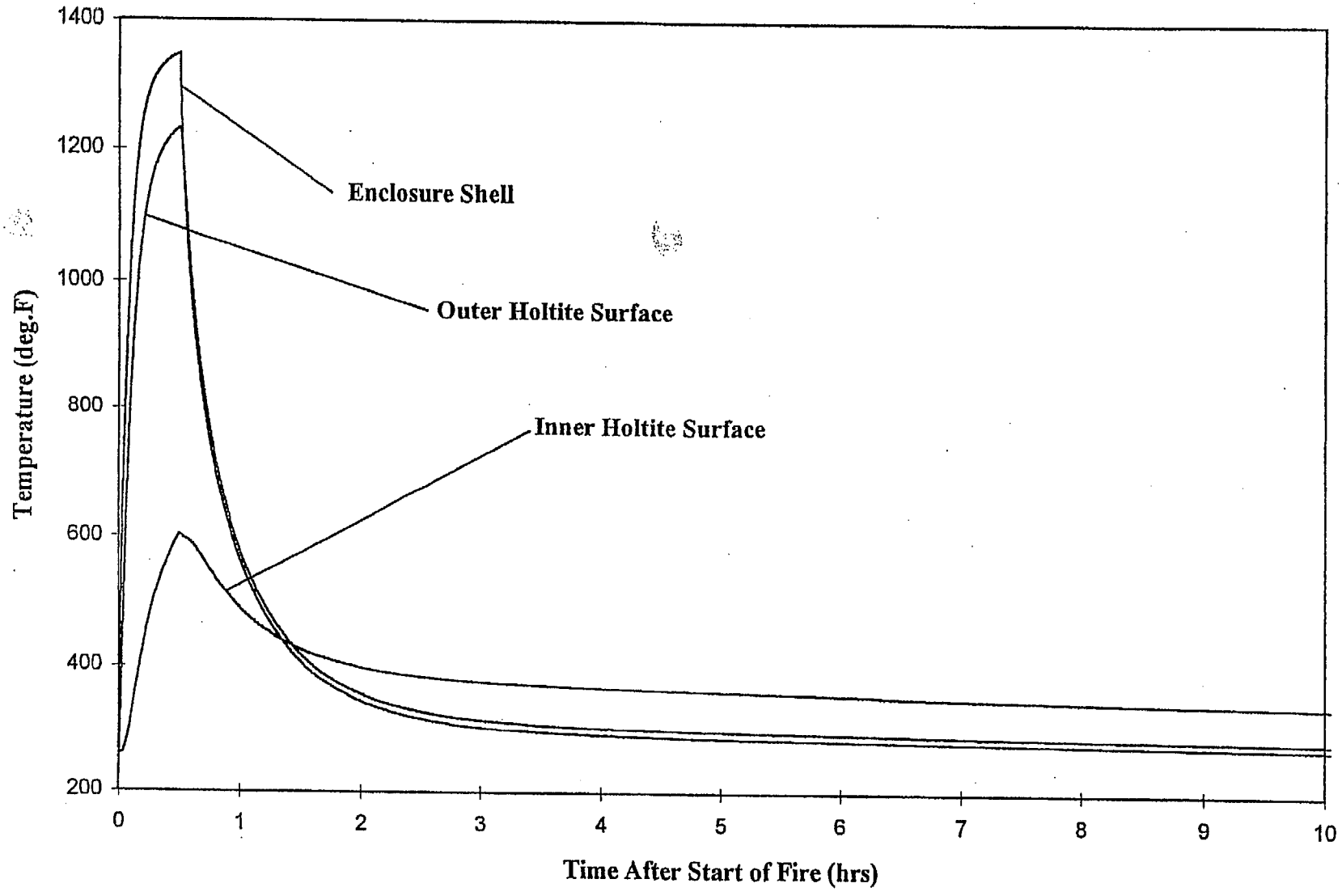

FIGURE 3.5.3; HI-STAR 100 PACKAGE NEUTRON SHIELDING REGION FIRE ACCIDENT TRANSIENT TEMPERATURE RESPONSE

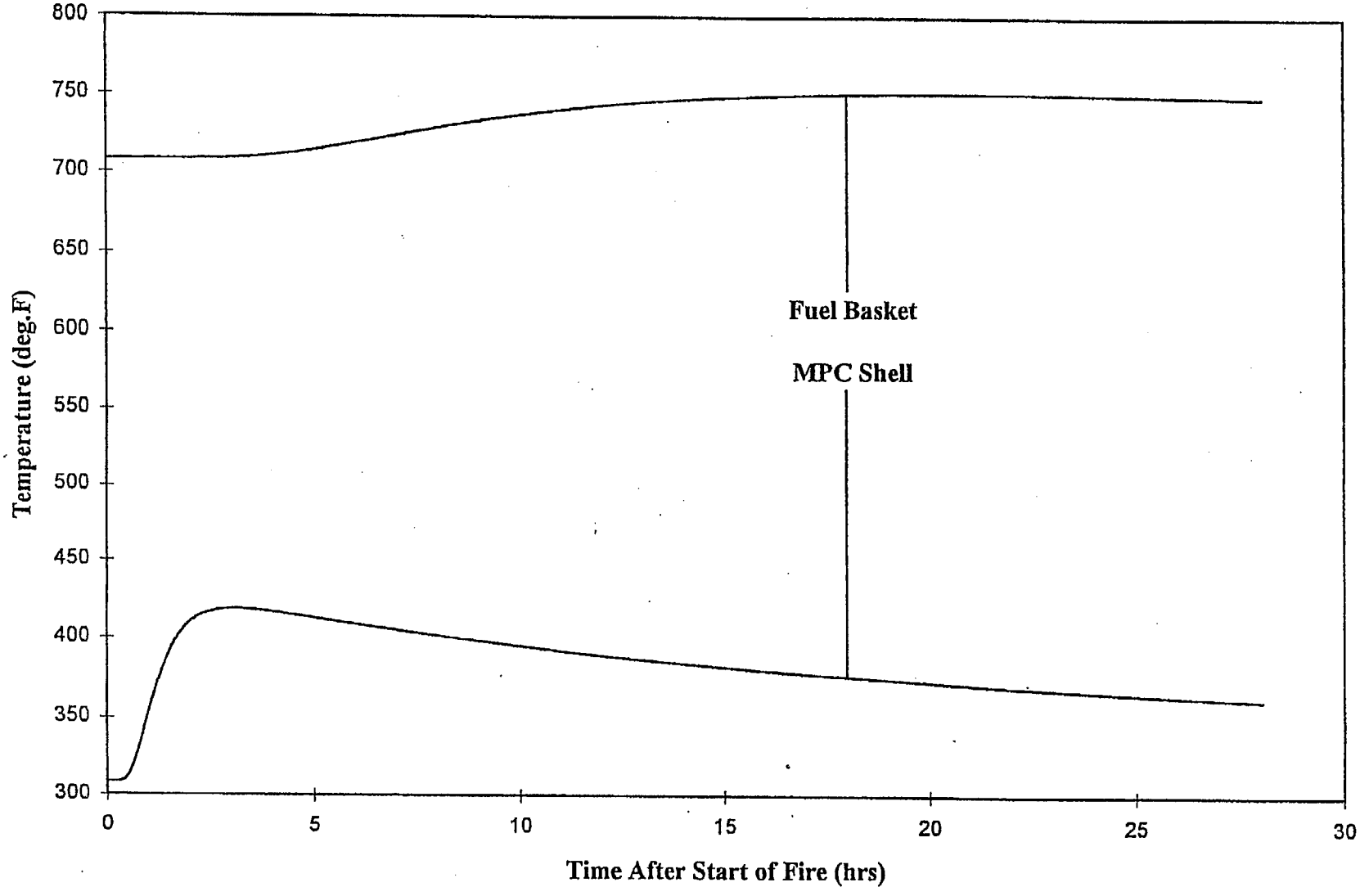

FIGURE 3.5.4; HI-STAR 100 PACKAGE MPC SHELL AND FUEL BASKET FIRE ACCIDENT TRANSIENT TEMPERATURE RESPONSE

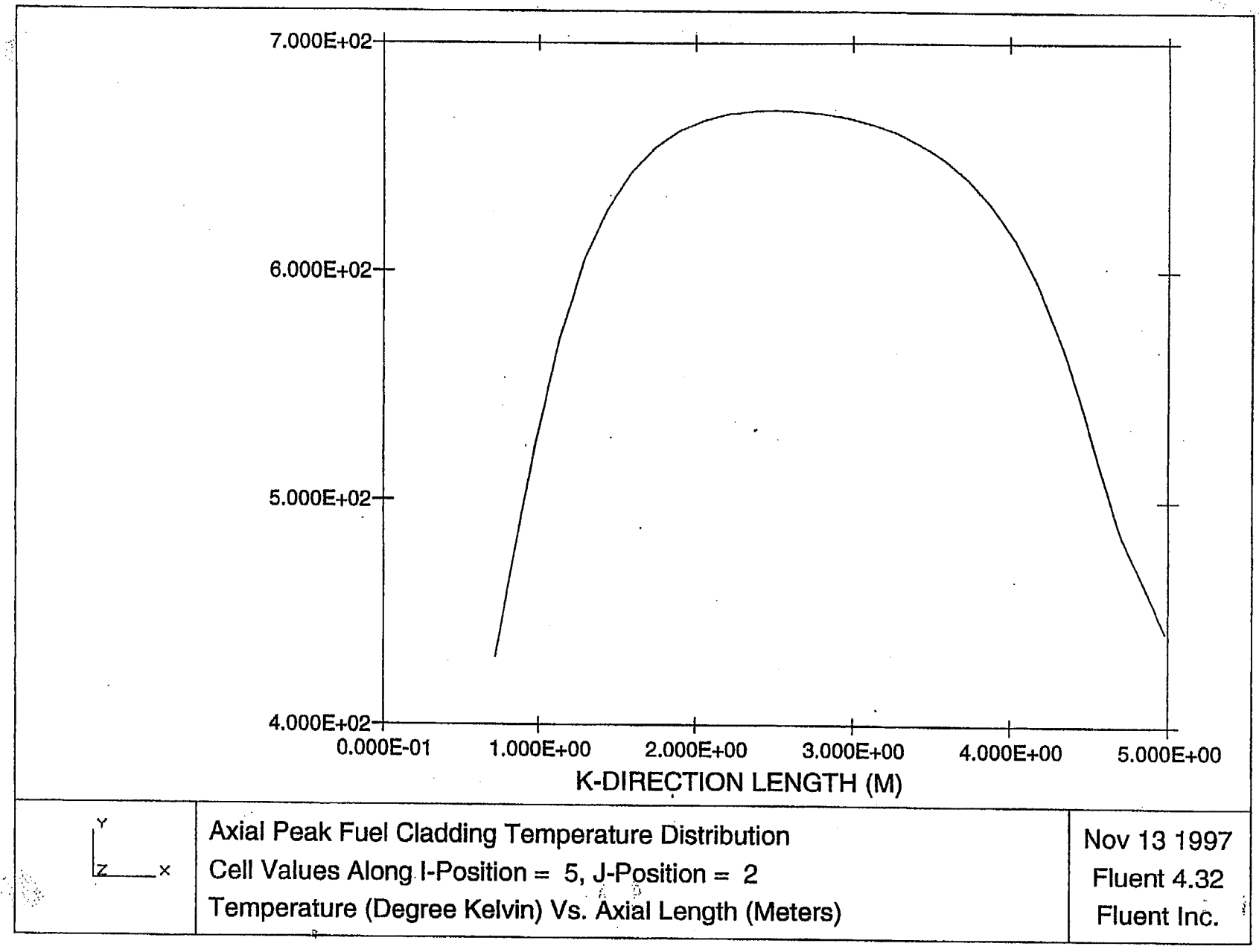

FIGURE 3.5.5: FUEL CLADDING PEAK AXIAL TEMPERATURE DISTRIBUTION DURING POST FIRE COOLDOWN

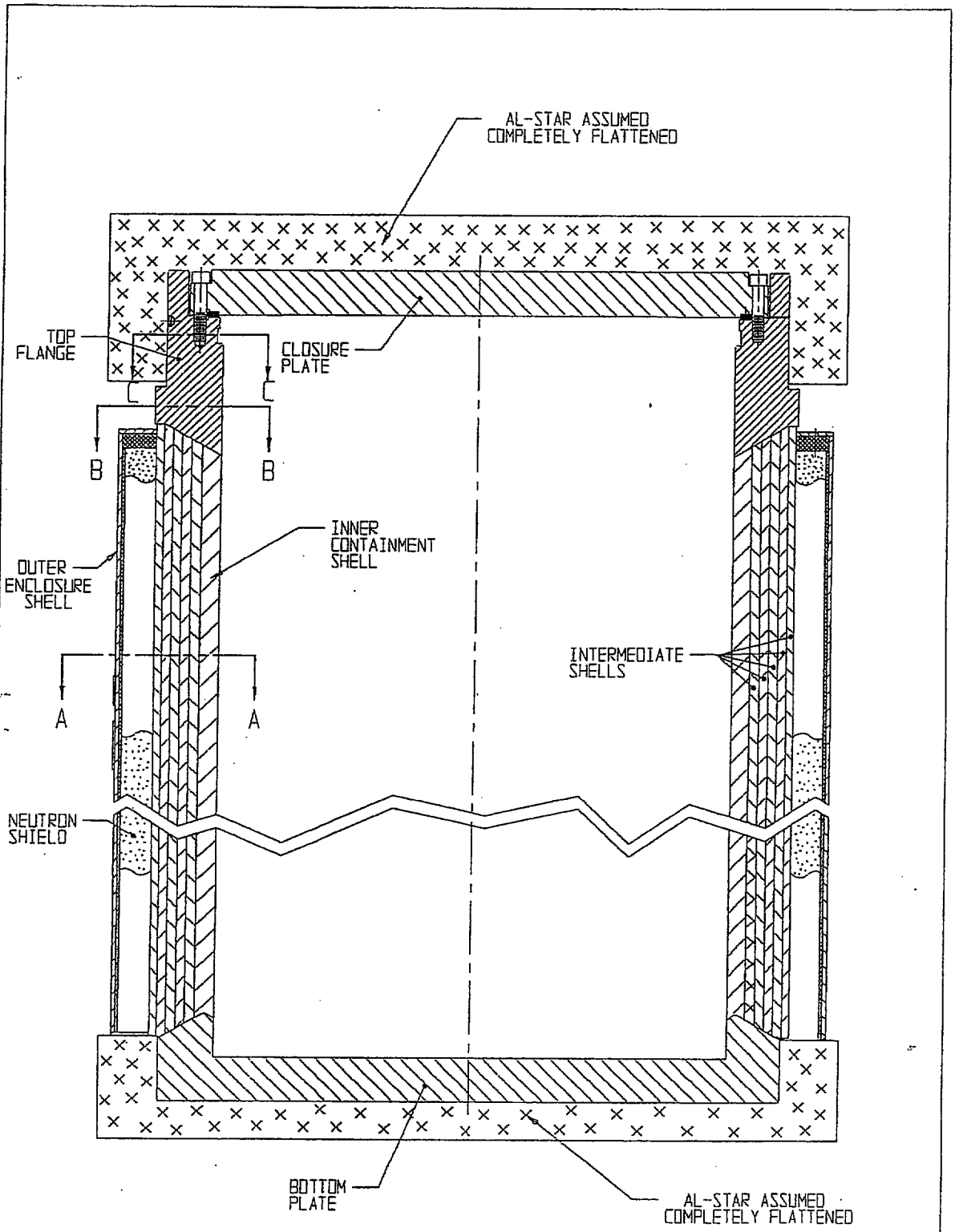

FIGURE 3.5.6; HI-STAR MODEL FOR TRANSPORT FIRE

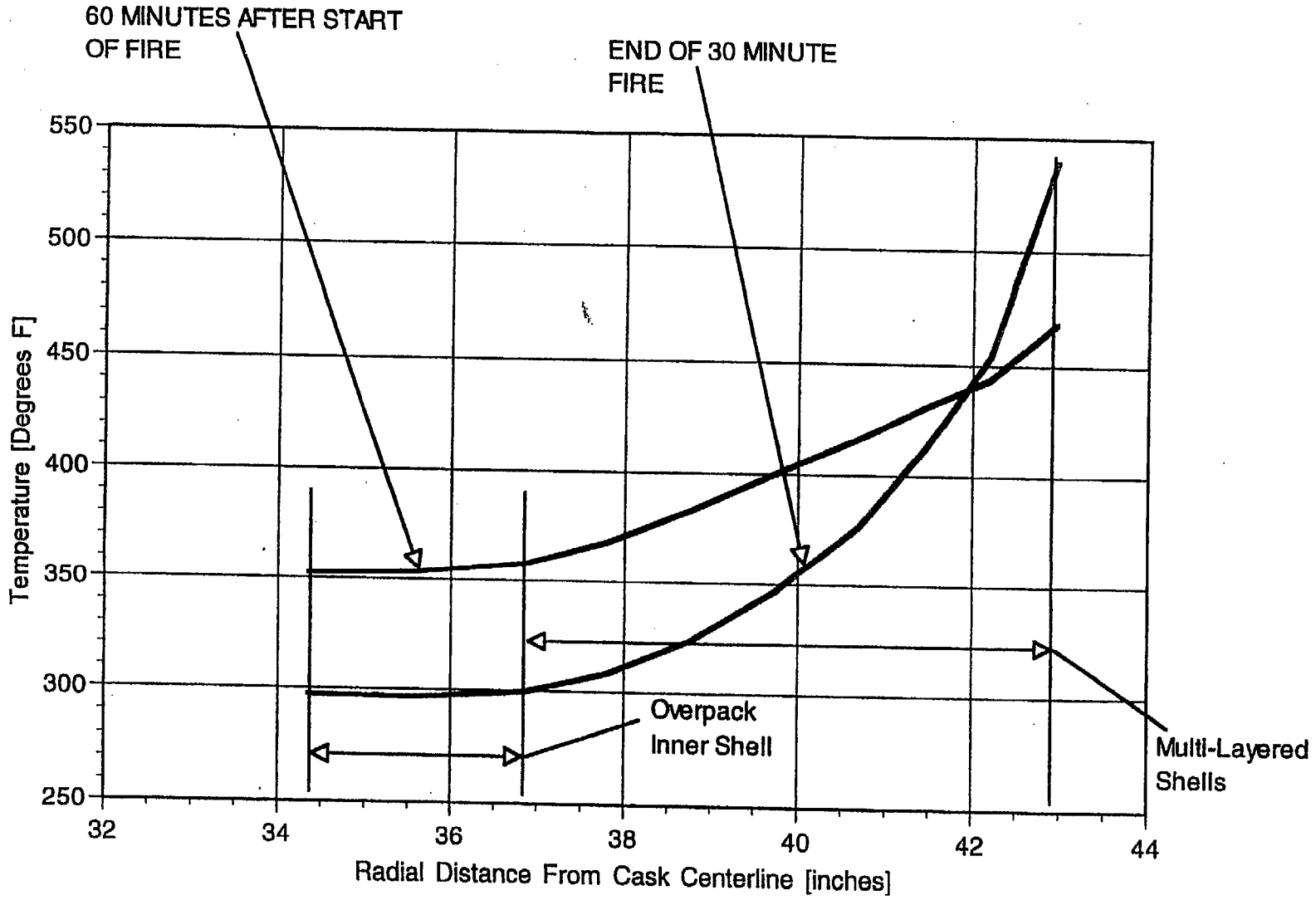

FIGURE 3.5.7: TRANSPORT FIRE CONDITION CONTAINMENT BOUNDARY AND LAYERED SHELLS TEMPERATURE DISTRIBUTIONS (SECTION A-A)

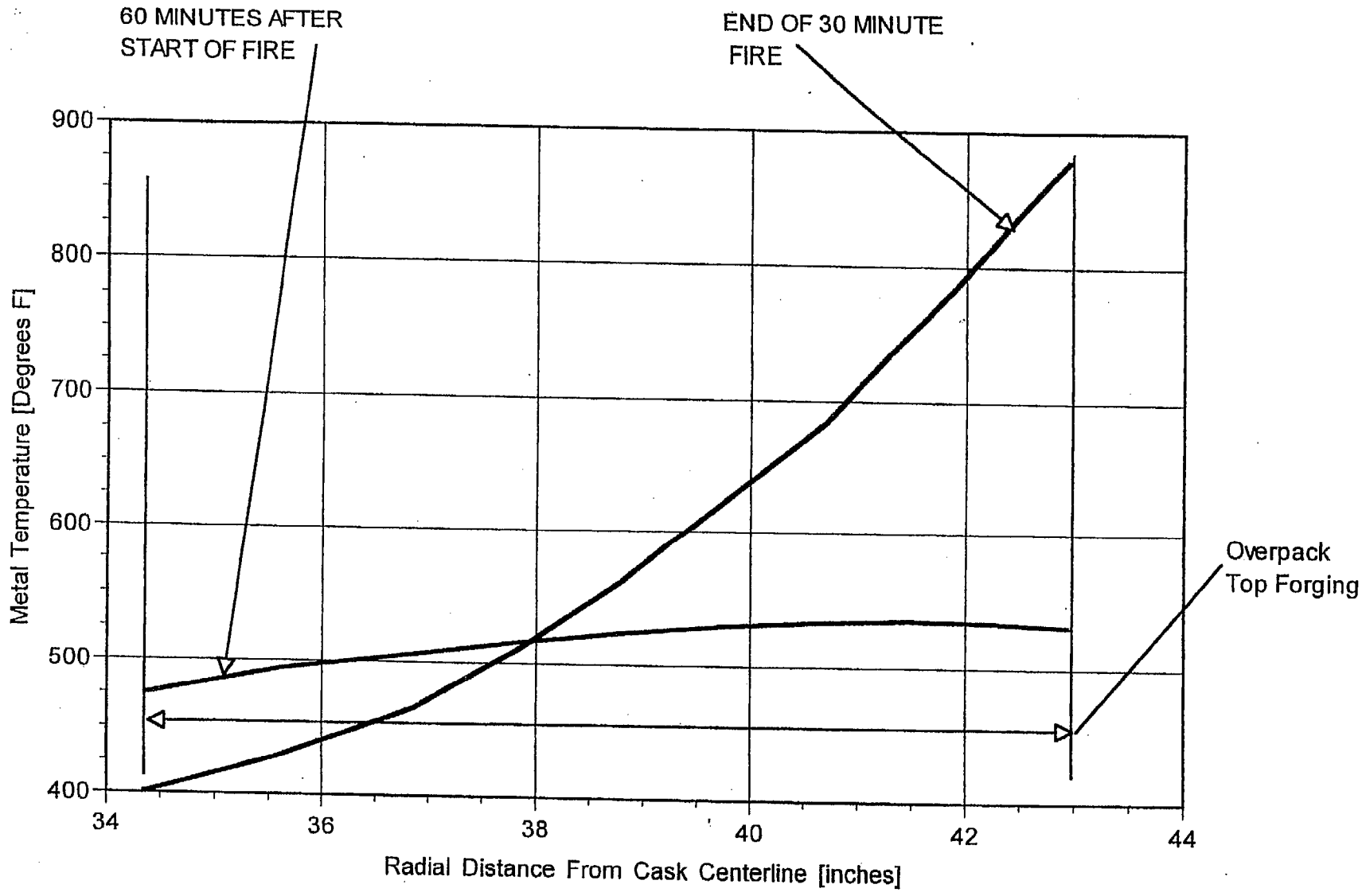

FIGURE 3.5.8: TRANSPORT FIRE CONDITION OVERPACK TOP FORGING TEMPERATURE DISTRIBUTIONS (SECTION B-B)

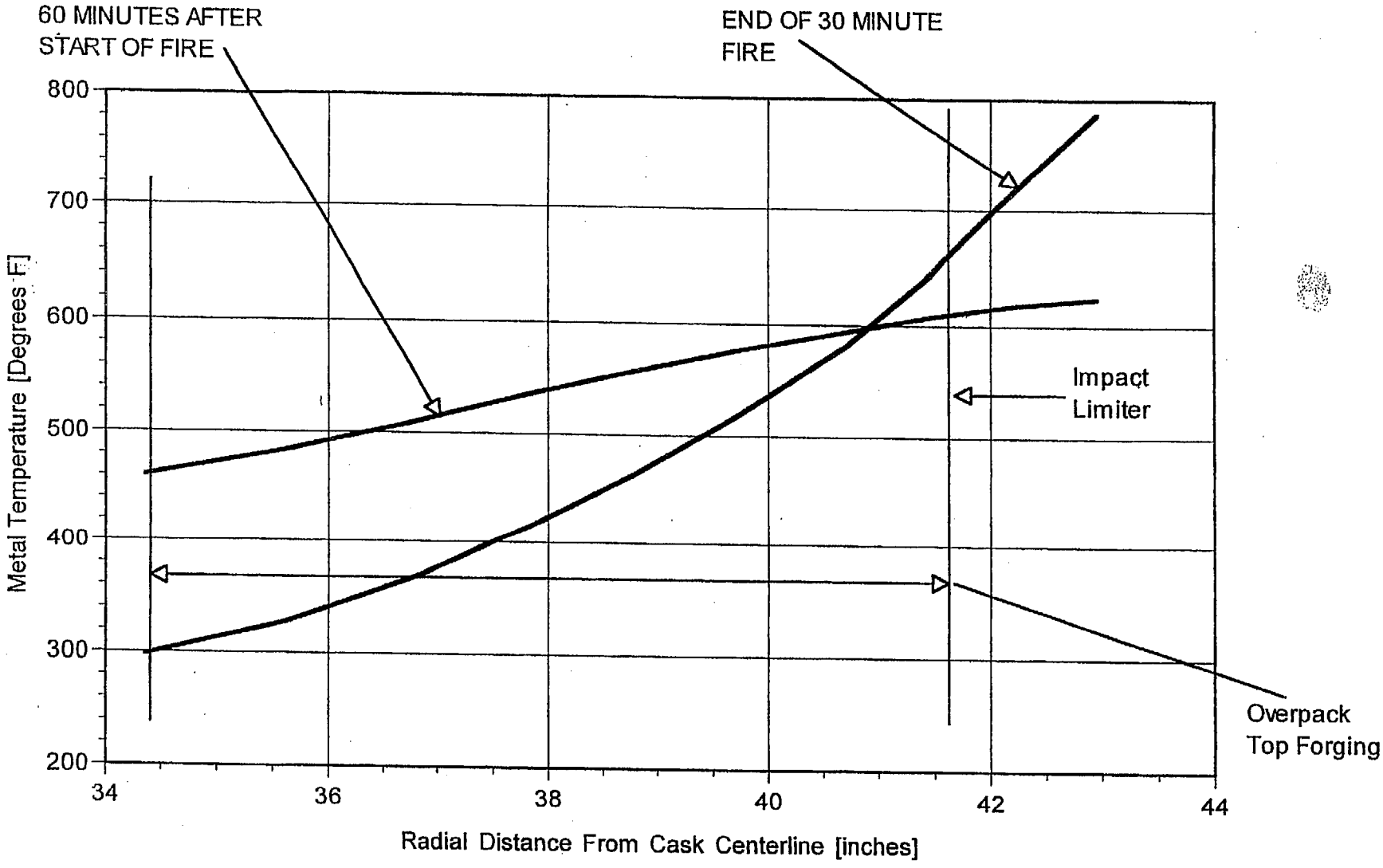

FIGURE 3.5.9: TRANSPORT FIRE CONDITION OVERPACK TOP FORGING TEMPERATURE DISTRIBUTIONS (SECTION C-C)

3.6 REGULATORY COMPLIANCE

10CFR71 defines the requirements and acceptance criteria, that must be fulfilled by the cask thermal design, which are addressed in Sections 3.1 through 3.5. These requirements and acceptance criteria, listed in Section 3.1, and the conclusion of the evaluations are summarized below.

1. The applicant must include a description of the proposed package in sufficient detail to identify the package accurately and provide a sufficient basis for the evaluation of the package. The description must include, with respect to the packaging: specific materials of construction, weights, dimensions, and fabrication methods of materials specifically used as non-fissile neutron absorbers or moderators; and structural and mechanical means for the transfer and dissipation of heat. The description must include, with respect to the contents of the package: chemical and physical form; maximum normal operating pressure; maximum amount of decay heat; and identification and volumes of any coolants.

   A general description of the HI-STAR System is included in Chapter 1. Descriptions of cask materials are presented in Subsection 1.2.1, Section 1.4 and Appendices 1.A, 1.B and 1.C. Shielding materials are specifically addressed in Subsection 1.2.1.4. Cask component weights are presented in Subsections 1.2.1.1 and 2.2. Cask component dimensions are presented in Subsection 1.2.1.2 and in engineering drawings included in Section 1.4. The transfer and dissipation of heat are discussed generally in Subsection 1.2.1.6, and in detail in this chapter.

   General descriptions of and requirements for fuel assemblies for transport are presented in Subsection 1.2.3, including design basis maximum decay heat load specifications in Subsection 1.2.3.5. Maximum normal operating pressures are reported in Subsection 3.4.4. As stated in Subsection 1.2.1.7, there are no coolant volumes (reservoirs) in the HI-STAR System.

2. A package must be designed, constructed, and prepared for shipment so that under normal conditions of transport there would be no substantial reduction in the effectiveness of the packaging.

   The results of thermal evaluations presented in Section 3.4 demonstrate that the HI-STAR System performs as designed under all normal conditions of transport.

3. A package must be designed, constructed, and prepared for shipment so that in still air at 100°F and in the shade, no accessible surface of the package would have a temperature exceeding 185°F in an exclusive use shipment.

   Maximum exposed surface temperatures for the HI-STAR System are reported in Subsection 3.4.2. All impact limiter surface temperatures are shown to be below 185°F. The personnel barrier, described in Chapter 7, renders the hot overpack enclosure shell surfaces inaccessible.

4. Compliance with the permitted activity release limits for a Type B package may not depend on filters or on a mechanical cooling system.

   As stated in Section 3.1, all cooling mechanisms in the HI-STAR System are completely passive.

5. With respect to the initial conditions for the events of normal conditions of transport and hypothetical accident conditions, the demonstration of compliance with the requirements of 10CFR71 must be based on the ambient temperature preceding and following the event remaining constant at that value between -20°F and 100°F which is most unfavorable for the feature under consideration. The initial internal pressure within the containment system must be considered to be the maximum normal operating pressure (MNOP), unless a lower internal pressure consistent with the ambient temperature considered to precede and follow the event is more unfavorable.

   Hypothetical fire accident transient calculations for the HI-STAR System are described in Section 3.5. The initial condition for this event corresponds to the most severe steady-state solution for normal conditions of transport, which correspond to a 100°F ambient temperature with full insolation. These same environmental conditions are applied during the post-accident phase of the evaluation as well. All calculated temperatures for this event are below the specified design temperature limits.

   Maximum calculated normal condition internal pressures (MNOPs) are reported in Subsection 3.4.4. Maximum calculated hypothetical accident condition internal pressures are reported in Subsection 3.5.4. All calculated MNOPs are below the design pressure limits for the MPC helium retention boundary and the overpack containment boundary.

6. For normal conditions of transport, a heat event consisting of an ambient temperature of 100°F in still air and prescribed insolation must be evaluated.

   The maximum temperatures in the HI-STAR System reported in Subsection 3.4.2 correspond to the heat event. All calculated temperatures for this event are below the appropriate design temperature limits. As stated in Subsection 3.4.5, thermal stresses are determined and reported in Chapter 2.

7. For normal conditions of transport, a cold event consisting of an ambient temperature of –40°F in still air and shade must be evaluated.

The minimum temperatures in the HI-STAR System reported in Subsection 3.4.3 correspond to the cold event. All calculated temperatures for this event are below the appropriate design temperature limits. As stated in Subsection 3.4.5, thermal stresses are determined and reported in Chapter 2.

8. Evaluation for hypothetical accident conditions is to be based on sequential application of the specified events, in the prescribed order, to determine their cumulative effect on a package.

   As described in Section 3.5, the HI-STAR System hypothetical accident thermal condition (hydrocarbon fuel/air fire) evaluation incorporates bounding representations of the results of the preceding accident conditions. Specifically, the impact limiters are assumed to be completely crushed (drop event) and the heat transfer effectiveness of the radial channels region is reduced (puncture event). All calculated temperatures for this event are below the appropriate design temperature limits.

9. For hypothetical accident conditions, a thermal event consisting of a fully engulfing hydrocarbon fuel/air fire with an average emissivity coefficient of at least 0.9, with an average flame temperature of at least 1475°F for a period of 30 minutes.

   The description of the HI-STAR System hypothetical accident thermal event model (Subsection 3.5.1.1) specifies the fire condition input parameters. All input parameters are in accordance with the requirements of 10CFR71.73(c)(4). All calculated temperatures for this event are below the appropriate design temperature limits.

The thermal evaluations provided in this SAR demonstrate that the HI-STAR System description and evaluation satisfy the thermal requirements of 10 CFR Part 71. Specifically:

- The material properties and component specifications used in the thermal evaluation are sufficient to provide a basis for evaluation of the HI-STAR System against the thermal requirements of 10 CFR Part 71.

- The methods used in the thermal evaluation are described in sufficient detail to permit an independent review, with confirmatory calculations, of the HI-STAR System thermal design.

- The accessible surface temperatures of the HI-STAR System as it will be prepared for shipment satisfy 10 CFR 71.43(g) for exclusive use shipments.

- The HI-STAR System design, construction, and preparations for shipment ensure that the material and component temperatures will not extend beyond the specified allowable limits during normal conditions of transport consistent with 10 CFR 71.71.

- The HI-STAR System design, construction, and preparations for shipment ensure that the material and component temperatures will not exceed the specified allowable temperature limits during hypothetical accident conditions consistent with 10 CFR 71.73.

It is therefore concluded that the thermal design of the HI-STAR System is in compliance with 10 CFR Part 71, and that the applicable design and acceptance criteria have been satisfied. The evaluation of the thermal design provides reasonable assurance that the HI-STAR System will allow safe transport of spent fuel. This conclusion is based on the technical data and analyses presented in this chapter in conjunction with provisions of 10 CFR Part 71, appropriate regulatory guides, applicable codes and standards, and accepted engineering practices.

3.7 REFERENCES

[3.1.1] ANSYS Finite Element Modeling Package, Swanson Analysis Systems, Inc., Houston, PA, 1993.

[3.1.2] FLUENT Computational Fluid Dynamics Software (Fluent, Inc., Centerra Resource Park, 10 Cavendish Court, Lebanon, NH 03766).

[3.1.3] "The TN-24P PWR Spent-Fuel Storage Cask: Testing and Analyses," EPRI NP-5128, (April 1987).

[3.1.4] Deleted.

[3.2.1] Baumeister, T., Avallone, E.A. and Baumeister III, T., "Marks' Standard Handbook for Mechanical Engineers", 8th Edition, McGraw Hill Book Company, 1978.

[3.2.2] Rohsenow, W.M. and Hartnett, J.P., "Handbook of Heat Transfer," McGraw Hill Book Company, New York, 1973.

[3.2.3] Greer et al., "The TN-24P Spent Fuel Storage Cask: Testing and Analyses," EPRI NP-5128, PNL-6054, UC-85, (April 1987).

[3.2.4] Rust, J.H., "Nuclear Power Plant Engineering," Haralson Publishing Company, (1979).

[3.2.5] Kern, D.Q., "Process Heat Transfer," McGraw Hill Kogakusha, (1950).

[3.2.6] "A Handbook of Materials Properties for Use in the Analysis of Light Water Reactor Fuel Rod Behavior", NUREG/CR-0497, (August 1981).

[3.2.7] "Safety Analysis Report for the NAC Storable Transport Cask," Docket No. 71-9235.

[3.2.8] ASME Boiler and Pressure Vessel Code, Section II, Part D, (1995).

[3.2.9] Jakob, M. and Hawkins, G.A., "Elements of Heat Transfer," John Wiley & Sons, New York, 1957.

[3.3.1] "Handbook of Aluminum," Alcan Aluminum Corporation, 3rd Edition, page 170, (1970).

[3.3.2] Levy, I.S. et al., "Recommended Temperature Limits for Dry Storage of Spent Light Water Reactor Zircaloy Clad Fuel Rods in Inert Gas," PNL-6189, (May 1987).

[3.3.3] Deleted.

[3.3.4] "Characteristics of Spent Fuel, High-Level Waste, and Other Radioactive Wastes Which May Require Long-Term Isolation," DOE/RW-0184, (December 1987).

[3.3.5] Johnson, Jr., A.B. and Gilbert, E.R., "Technical Basis for Storage of Zircaloy-Clad Spent Fuel in Inert Gases," PNL-4835, (September 1983).

[3.3.6] Cunningham et. al., "Evaluation of Expected Behavior of LWR Stainless Steel-Clad Fuel in Long-Term Dry Storage," EPRI TR-106440, (April 1996).

[3.3.7] "Temperature Limit Determination for the Inert Dry Storage of Spent Nuclear Fuel," EPRI TR-103949, (May 1994).

[3.4.1] Wooton, R.O. and Epstein, H.M., "Heat Transfer from a Parallel Rod Fuel Element in a Shipping Container," Battelle Memorial Institute, 1963.

[3.4.2] Rapp, D., "Solar Energy," Prentice-Hall, Inc., Englewood Cliffs, NJ, 1981.

[3.4.3] Sanders et al., "A Method for Determining the Spent-Fuel Contribution to Transport Cask Containment Requirements," Sandia Report SAND90-2406-TTC-1019UC-820, page II-127, (November 1992).

[3.4.4] Holman, J.P., "Heat Transfer," 6th ed., McGraw Hill Book Company, 1986.

[3.4.5] Hewitt, G.F., Shires, G.L., and Bott, T.R., "Process Heat Transfe (1994).

[3.4.6] Chandrasekhar, S., "Hydrodynamic and Hydromagnetic Stability," Dover, (1961).

[3.4.7] Gradshteyn, I.S. and Ryzhik, I.M., "Table of Integrals Series and Products," Academic Press, Fourth Edition, page 366, (1965).

[3.4.8] Deleted.

[3.4.9] Deleted.

[3.4.10] Cormack, D.E., L.G. Leal and J. Imberger, "Natural Convection in a Shallow Cavity With Differentially Heated End Walls. Part 1 Asymptotic Theory," J. Fluid Mechanics, 65, 209-229, (1974).

[3.4.11] Cormack, D.E., L.G. Leal and J.H. Seinfeld, "Natural Convection in a Shallow Cavity With Differentially Heated End Walls. Part 2 Numerical Solutions," J. Fluid Mechanics, 65, 231-246, (1974).

[3.4.12] Imberger, J., "Natural Convection in a Shallow Cavity with Differentially Heated End Walls. Part 3 Experimental Results," J. Fluid Mechanics, 65, 247-260, (1974).

[3.4.13] Hagrman, Reymann and Mason, "MATPRO-Version 11 (Revision 2) A Handbook of Materials Properties for Use in the Analysis of Light Water Reactor Fuel Rod Behavior," NUREG/CR-0497, Tree 1280, Rev. 2, EG&G Idaho, August 1981.

[3.4.14] Deleted.

[3.4.15] Deleted.

[3.4.16] Deleted.

[3.4.17] Deleted.

[3.5.1] 10CFR Part 71, Paragraph 71.73, (January 1, 1998).

[3.5.2] Jakob, M., "Heat Transfer," John Wiley & Sons, Inc., page 555, (1967).

CHAPTER 4: CONTAINMENT

4.0 INTRODUCTION

This chapter demonstrates the HI-STAR 100 containment boundary compliance with the permitted activity release limits specified in 10CFR71, 71.51(a)(1) and 71.51(a)(2) for both normal and hypothetical accident conditions of transport [4.0.1]. Satisfaction of the containment criteria, expressed as the leakage rate acceptance criterion (atm-cm^3/sec, Helium), ensures that the HI-STAR 100 package will not exceed the specified allowable radionuclide release rates. Leakage rates are determined in accordance with the recommendations of ANSI N14.5 [4.0.2], and utilizing NUREG/CR-6487, *Containment Analysis for Type B Packages Used to Transport Various Contents* [4.0.3], Regulatory Guide 7.4, *Leakage Tests on Packages for Shipment of Radioactive Materials* [4.0.4] as content guides, and Draft NUREG-1617, *Standard Review Plan for Transportation Packages for Spent Nuclear Fuel* [4.0.5].

The HI-STAR 100 packaging allowable leakage rates established herein ensures that the requirements of 10CFR71.51 and 10CFR71.63(b) are met. The primary containment system boundary for the HI-STAR 100 packaging consists of the overpack inner shell, the bottom plate, the top flange, the top closure plate, closure bolts, the overpack vent and drain port plugs, and their respective mechanical seals. The secondary containment system boundary for a HI-STAR 100 packaging containing ~~Dresden Unit 1 or Humboldt Bay~~ *BWR* fuel debris *in the MPC-68F or Trojan PWR fuel debris in the MPC-24EF* consists of the MPC~~-68F~~ enclosure vessel including the MPC shell, the MPC bottom plate, the MPC lid, closure ring, and vent and drain port cover plates. The *MPC-24EF and* MPC-68F *each* provides the separate inner container per 10CFR71.63(b) for the HI-STAR 100 System transporting fuel classified as fuel debris. The other MPC designs (MPC-24, *MPC-24E, MPC-32* and MPC-68) are not currently evaluated for secondary containment requirements.

Chapter 2 of this SAR shows that all primary and secondary containment boundary components are maintained within their code-allowable stress limits during all normal and hypothetical accident conditions of transport as defined in 10CFR71.71 and 10CFR71.73. Chapter 3 of this SAR shows that the peak containment component temperatures and pressures are within the design basis limits for all normal and hypothetical accident conditions of transport as defined in 10CFR71.71 and 10CFR71.73. Since both the primary and secondary containment boundaries are shown to remain intact, and the temperature and pressure design bases are not exceeded, the design basis leakage rates are not exceeded during normal or hypothetical accident conditions of transport.

The HI-STAR overpack is subjected to a containment system fabrication verification test before the first use as described in Chapter 8. The containment system fabrication verification test is performed at the factory as part of the HI-STAR 100 acceptance testing. The welds of the primary containment boundary, the closure plate inner seal, and the vent and drain port plug seals are helium leakage tested in accordance with ANSI N14.5. A containment system periodic verification test as described in Chapter 8, will be performed prior to each loaded transport. The mechanical seals of the

HI-STAR 100 overpack will be replaced and retested each time the HI-STAR 100 is loaded. The secondary containment boundary system (*MPC-24EF or* MPC-68F) will be subjected to the fabrication verification leakage testing at the fabrication facility as described in Chapter 8 of this SAR. Prior to transport of ~~the~~ *an* MPC-~~68F~~ containing fuel debris, a secondary containment boundary periodic verification leakage test will be performed as described in Chapter 8 to ensure that the measured leakage rates are below the limit specified in this chapter.

As the containment system periodic verification leakage test shall be performed on each containment boundary separately prior to each loaded transport, this test takes the place of and is performed in lieu of the assembly verification.

4.1 CONTAINMENT BOUNDARIES

The primary containment system boundary for the HI-STAR 100 packaging consists of the overpack inner shell, the bottom plate, the top flange, the top closure plate, closure bolts, the overpa ck vent and drain port plugs, and their respective mechanical seals. The primary containment boundary system components for the HI-STAR 100 system are designed and fabricated in accordance with the requirements of ASME Code, Section III, Subsection NB [4.1.1], to the maximum extent practicable. Chapter 1 provides design criteria for the containment design. Section 1.3 provides applicable Code requirements. Exceptions to specific Code requirements with complete justifications are presented in Table 1.3.2. The primary containment boundary components are shown on Figure 4.1.1 with additional details provided in Figures 4.1.2 and 4.1.3.

The secondary containment system boundary for a HI-STAR 100 packaging containing fuel debris *in the MPC-24EF or the MPC-68F* consists of the ~~MPC-68F~~ enclosure vessel including the MPC shell, the MPC bottom plate, the MPC lid, vent and drain port cover plates and MPC closure ring. The secondary containment boundary system components for the HI-STAR 100 system are designed and fabricated in accordance with the requirements of ASME Code, Section III, Subsection NB, to the maximum extent practicable. Chapter 2 provides design criteria for the containment design. Section ~~2.2.4~~*1.3* provides applicable Code requirements. ~~Exceptions~~ *Alternatives* to specific Code requirements with complete justifications are presented in Table ~~2.2.15~~*1.3.2*. The secondary containment boundary components are shown in Figure 4.1.4. The use of two independent and testable containment boundaries provides the capability to load and transport the specified fuel debris in accordance with the requirements of 10CFR71.63(b) [4.0.1]. The *MPC-24EF or* MPC-68F *each* provides the separate inner container per 10CFR71.63(b) for the HI-STAR 100 System transporting fuel classified as fuel debris. The other MPC designs (MPC-24, *MPC-24E, MPC-32* and MPC-68) are not currently evaluated for secondary containment requirements.

4.1.1 Containment Vessel

The primary containment vessel for the HI-STAR 100 packaging consists of the overpack components which form the inner cavity volume used to house any of the MPC designs which contain spent nuclear fuel. The primary containment vessel is represented by *the* overpack inner shell, bottom plate, the top flange, and the closure plate. These components create an enclosed cylindrical cavity sufficient for insertion and enclosure of an MPC. The materials of construction for the packaging primary containment vessel are specified in the ~~Bills of Material~~ *drawings* in Section 1.4.

The secondary containment vessel for the HI-STAR 100 packaging consists of *either* the *MPC-24EF or the* MPC-68F enclosure vessel complete with field-installed MPC lid, closure ring, vent and drain port cover plates. The ~~MPC-68F~~ enclosure vessel components create an enclosed cylindrical cavity sufficient for insertion and enclosure of fuel debris. The materials of construction for the secondary containment vessel ~~for the MPC-68F~~ are specified in the ~~Bills of Material~~*drawings* in Section 1.4.

Table 4.1.1 provides a summary of the containment boundary design specifications.

4.1.2 Containment Penetrations

The primary containment system boundary penetrations for the HI-STAR 100 package include the closure plate test port plug, the vent port plug, the drain port plug, and their respective mechanical seals. Each penetration has redundant mechanical seals. The vent port is located in the closure plate and the drain port is located in the bottom plate. The closure configuration of the vent and drain ports is essentially identical (See Figure 4.1.3). The primary containment penetrations are designed and tested to ensure that the radionuclide release rates specified in 10CFR71.51 will not be exceeded.

The secondary containment boundary for the HI-STAR 100 packaging is the *either the MPC-24EF or the* MPC-68F. The penetrations on the MPC ~~-68F-~~include the MPC vent and drain port cover plates. The MPC penetrations are designed to prevent the release of radi onuclides. Two penetrations (the MPC vent and drain ports) are provided in the MPC lid for MPC draining, vacuum drying and backfilling during MPC loading operations, and for fuel cool-down and MPC flooding during unloading operations. No other confinement penetrations exist in the MPC. The MPC vent and drain ports are equipped with metal-to-metal seals to minimize leakage and withstand the long-term effects of temperature and radiation. No containment credit is taken for the vent and drain mechanical seals. The vent and drain connectors allow the vent and drain ports to be operated like valves and prevent the need to hot tap into the penetrations during unloading operations. The vent and drain port covers are sealed with the fully welded vent and drain port cover plates. The MPC closure ring covers the vent and drain port cover plate welds, and the MPC lid-to-shell weld providing redundant closure of the MPC vessel. *Both* ~~T~~*the MPC-24EF and* MPC-68F ~~is~~ *are* designed and tested to ensure that the radionuclide release rates specified in 10CFR71.63(b) will not be exceeded.

4.1.3 Seals and Welds

The HI-STAR 100 primary containment vessel uses a combination of seals and welds designed and tested during normal transport conditions, and during and after the hypothetical transport accident conditions. The ~~MPC-68F-~~ secondary containment boundary utilizes a fully welded vessel to prevent the release of radioactive materials. Seals and welds are individually discussed below.

The seals and welds discussed below provide containment systems which are securely closed, cannot be opened unintentionally or by an internal pressure within the package as required in 10CFR71.43(c).

4.1.3.1 Containment Seals

The HI-STAR 100 closure plate uses two concentric metallic seals to form the closure between the top flange surface and the closure plate. To protect the sealing surfaces against corrosion, a stainless steel weld inlay is provided during manufacturing on both the closure plate and mating overpack surfaces. The closure plate inner seal is tested for leakage through a small test port in the overpack closure plate (See Figure 4.1.2). The test port provides access to the volume between the two mechanical lid seals for leakage testing of the closure plate inner seal. Following leakage testing, a threaded plug with a metallic seal is installed in the test port hole to provide redundant closure.

Primary closure of the vent and drain ports is achieved via a threaded plug with a single metallic seal. The metallic seal is compressed between the underside of the threaded plug head and the overpack body to form the seal. The sealing surfaces are not subject to corrosion due to the presence of the cover plates and their seals preventing exposure of the seal surfaces to the elements. Each port plug seal is independently tested for leakage to verify containment performance. A bolted cover plate, with a machined seal groove, is installed over the vent and drain ports. A metallic seal, installed in the cover plate groove, is compressed between the cover plate and the overpack body during cover plate bolt torquing. These cover plates provide redundant closure of the drain and vent port penetrations.

Details on the seals are provided in the ~~Design Drawings and Bills of Material~~ *drawings* in Section 1.4 and in Appendix 4.B. Table 4.1.1 contains reference information for the seals from the selected supplier. Note that the seals selected are designed and fabricated to meet the design requirements of the HI-STAR 100 System. The Chapter 7 procedures require replacement of any used seal after closure opening except for transportation of an empty overpack.

There are no seals on the secondary containment boundary.

4.1.3.2 Containment Welds

The primary containment boundary welds of the HI-STAR 100 overpack body include the welds forming the inner closure shell, the weld connecting the inner shell to the top flange, and the weld connecting the bottom plate to the inner shell. All primary containment boundary welds are fabricated and inspected in accordance with ASME Code Section III, Subsection NB (no stamp required). Full-penetration welds are specified for the plates that form the overpack inner shell. Full-penetration welds are also specified for the inner shell to the top flange and bottom plate welds. The weld details are shown in the ~~Design Drawings~~ *drawings* in Section 1.4. The containment boundary welds are volumetrically examined by radiography (RT) as described in Chapter 8.

The secondary containment boundary welds of the ~~HI-STAR 100~~ *MPC-24EF and* MPC-68F include the welds forming the MPC shell, the weld connecting the shell to the MPC baseplate, and the final field closure welds described in Section 4.1.4.2. All secondary containment welds are fabricated and inspected in accordance with ASME Code Section III, Subsection NB, except for the field installed closure welds. The ~~exceptions~~ *alternatives* to the ASME Code for the secondary containment are detailed in Table 1.3.2. The weld details are shown on the *MPC-24EF and* MPC-68F ~~Design Drawings~~ *drawings* in Section 1.4. The secondary containment boundary welds are volumetrically examined by radiography (RT) or ultrasonic (UT) inspection methods as described in Chapter 8.

4.1.4 Closure

4.1.4.1 Primary Closure

The HI-STAR 100 packaging closure plate is secured using multiple closure bolts around the perimeter. Torquing of the closure plate bolts compresses the closure plate concentric mechanical seals between the closure plate and the overpack flange forming the closure plate seal.

Closure of the overpack vent and drain ports is provided by a single threaded plug installed in each penetration (see Figure 4.1.3). The mechanical seal is compressed between the underside of the port plug head and the overpack body forming the primary port closure. A cover plate, containing a single metallic seal, is installed over each of the ports forming the redundant closure of the vent and drain port penetrations. The cover plate is secured by bolts. The closure plate test port is sealed using a port plug and mechanical seal in the same manner as the vent and drain port penetrations (see Figure 4.1.2).

The installation procedures, bolt torquing patterns, required lubrication, and torque values are provided in Table 7.1.~~3~~2. The torque values are established to maintain containment during normal and accident conditions of transport. Appendix 2.A contains the calculations used to determine the torque values for the closure plate bolts. Appendix 4.A contains the calculations for the test, vent and drain port plugs and the vent and drain port cover plates bolt torques.

Table 4.1.2 provides a summary of the containment closure bolting for the HI-STAR 100 overpack penetrations.

4.1.4.2 Secondary Closure

The secondary closure of the HI-STAR 100 packaging is provided by the MPC lid which is welded to the MPC shell. Following fuel loading and MPC lid welding, the MPC lid to shell weld may be examined by either volumetric or multi-layer liquid penetrant examination. If volumetric examination is used, it shall be the ultrasonic method and shall include a PT of the root and final weld layers. If PT alone is used, at a minimum, it must include the root and final weld layers and sufficient intermediate layers to detect critical weld flaws. The lid to shell weld is also volumetrically examined, helium leakage tested, and hydrostatic tested. If the MPC lid weld is acceptable, the vent and drain port cover plates are welded in place, examined by the liquid penetrant method (root and final), and a leakage rate test is performed. Finally, the MPC closure ring is installed, welded and inspected by the liquid penetrant method (root and final).

4.1.5 Damaged Fuel Container

Fuel assemblies classified as damaged fuel or fuel debris (assembly array/class 6x6A, 6x6B, 6x6C, 7x7A, and 8x8A *for BWR fuel* as specified in Table 1.2.11 *and Trojan damaged fuel and fuel debris for PWR fuel*) have been evaluated.

The MPC-~~68~~ is designed to ~~store~~ *transport* damaged fuel, fuel debris, or intact fuel. The sole additional requirement imposed on an MPC-~~68~~ to load fuel debris is an additional leakage rate criteria test just prior to shipment. Therefore, an MPC ~~-68-~~which is to transport fuel debris will be designated to ensure the proper leakage rate test criteria is applied. To distinguish an MPC-~~68~~ which is fabricated to transport fuel debris, the MPC will be designated ~~as an "MPC-68F". -~~*with an "F" after the MPC designation (i.e. MPC-68F or MPC-24EF)*

To aid in loading and unloading, damaged fuel assemblies and fuel debris will be loaded into

stainless steel DFCs prior to placement in the HI-STAR 100 System. The damaged fuel container (DFC) is shown in the ~~Design Drawings~~ *drawings* in Section 1.4. The DFC is designed to provide SNF loose component retention and handling capabilities. The DFC consists of a smooth-walled, welded stainless steel square canister with a removable lid. The canister lid provides the means of DFC closure and handling. The DFC is provided with stainless steel wire mesh screens in the top and bottom for draining, vacuum drying and helium backfill operations. The screens are specified as a 250-by-250-mesh with an effective opening of 0.0024 inches. There are no other openings in the DFC. Chapter 1 specifies the fuel assembly characteristics for damaged fuel acceptable for loading in the MPC-68, ~~or~~ MPC-68F, *or MPC-24EF* and for fuel debris acceptable for loading in the MPC-68F *or MPC-24EF.*

Up to four (4) DFCs containing specified fuel debris may be placed in a*n MPC-24EF (PWR fuel debris) or an* MPC-68F *(BWR fuel debris).* Up to *4 PWR* ~~68~~-damaged fuel assemblies in DFCs may be ~~stored~~ *transported* in *an MPC-24EF or up to 68 BWR damaged fuel assemblies in DFCs may be transported in* an MPC-68 or MPC-68F, *respectively.* The quantity of fuel debris is limited to meet the off-site transportation requirements of 10CFR71, specifically, 10CFR71.63(b). Analyses provided in this chapter conservatively assume 100% of the rods of the fuel debris are breached under normal conditions of transport. Therefore, 100% of the contents of the DFCs are available for release.

Table 4.1.1

SUMMARY OF CONTAINMENT BOUNDARY DESIGN SPECIFICATIONS

Design Attribute	Design Rating	
	Primary (Overpack) 10CFR71.51	Secondary (MPC) 10CFR71.63(b)
Closure Plate Mechanical Seals:†† Design Temperature Pressure Rating Design Leakage Rate	1200°F 1,000 psig $1X10^{-6}$ cm^3/s, Helium	N/A
Overpack Vent and Drain Port Cover Plate Mechanical Seals: †,†† Design Temperature Pressure Rating Design Leakage Rate	1300°F 1,000 psig 1×10^{-6} cm^3/sec, Helium	N/A
Overpack Vent and Drain Port Plug Mechanical Seals:†† Design Temperature Pressure Rating Design Leakage Rate	1300°F 1,000 psig 1×10^{-6} cm^3/sec, Helium	N/A
Leakage Rate Acceptance Criterion	4.3×10^{-6} atm cm^3/s, He	5.0×10^{-6} atm cm^3/s, He
Leakage Rate Test Sensitivity	2.15×10^{-6} atm cm^3/s, He	--

† No credit is taken for the overpack vent and drain port cover plate seals as part of the containment boundary. Specifications are provided for information.

†† Per manufacturer's recommended operating limits.

Table 4.1.2

CONTAINMENT CLOSURE BOLTING SUMMARY

Item	Qty	Type	Material
Closure Plate Bolt (Long)	52	1-5/8"-8 UNC x 7-3/8" LG Cap Screw	SB-637-N07718
Closure Plate Bolt (Short)	2	1-5/8"-8 UNC x 7-1/8" LG Cap Screw	SB-637-N07718
Vent/Drain Port Cover Plate Bolt	4 ea	3/8 -16 UNC x 1-1/4" LG Cap Screw	SA-193 GRADE B7
Vent/Drain/Closure Plate Test Port Plugs	1 ea	7/8" diameter Fabricated Plug	SA-193 GRADE B8

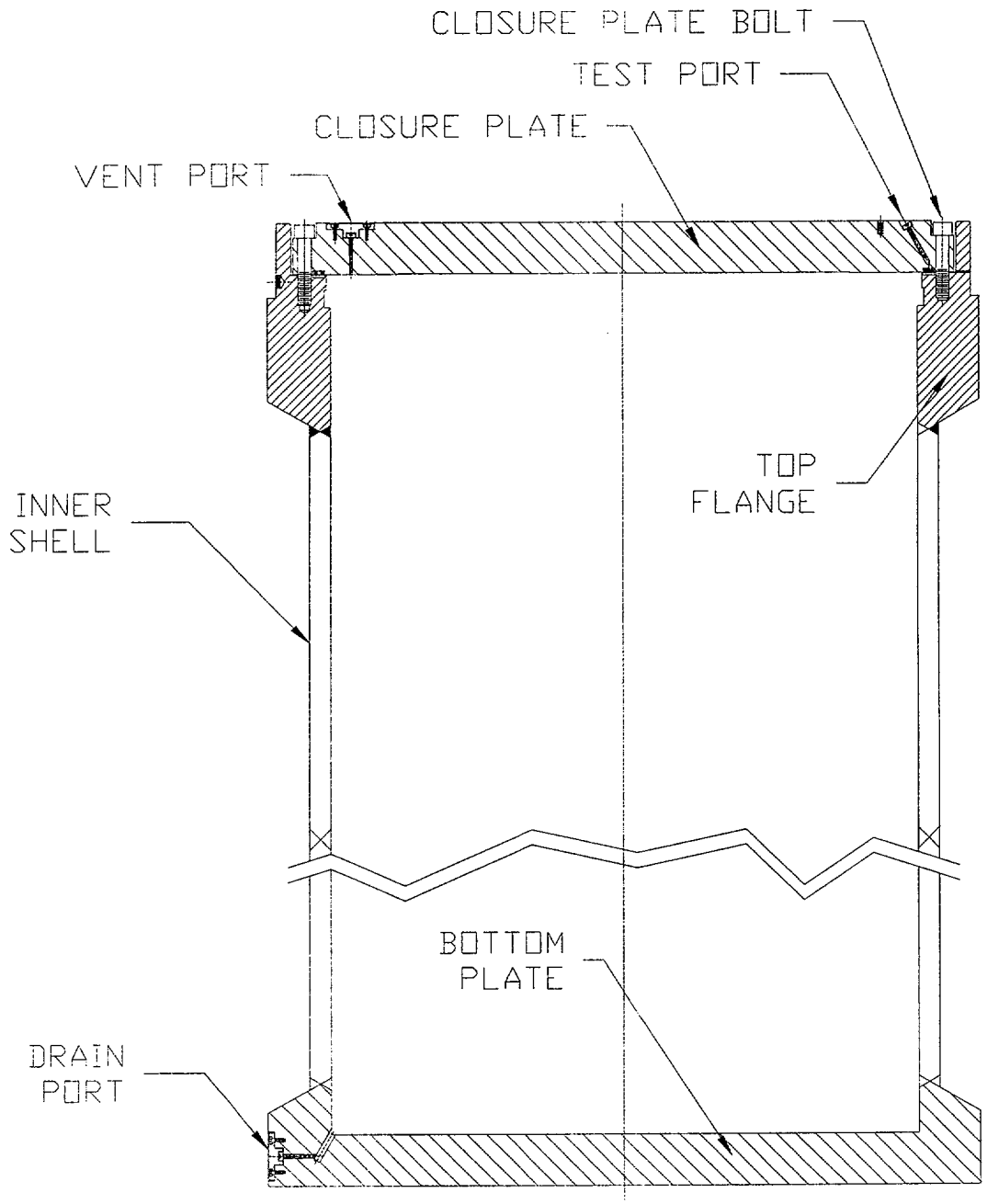

FIGURE 4.1.1; HI-STAR 100 OVERPACK PRIMARY CONTAINMENT BOUNDARY COMPONENTS

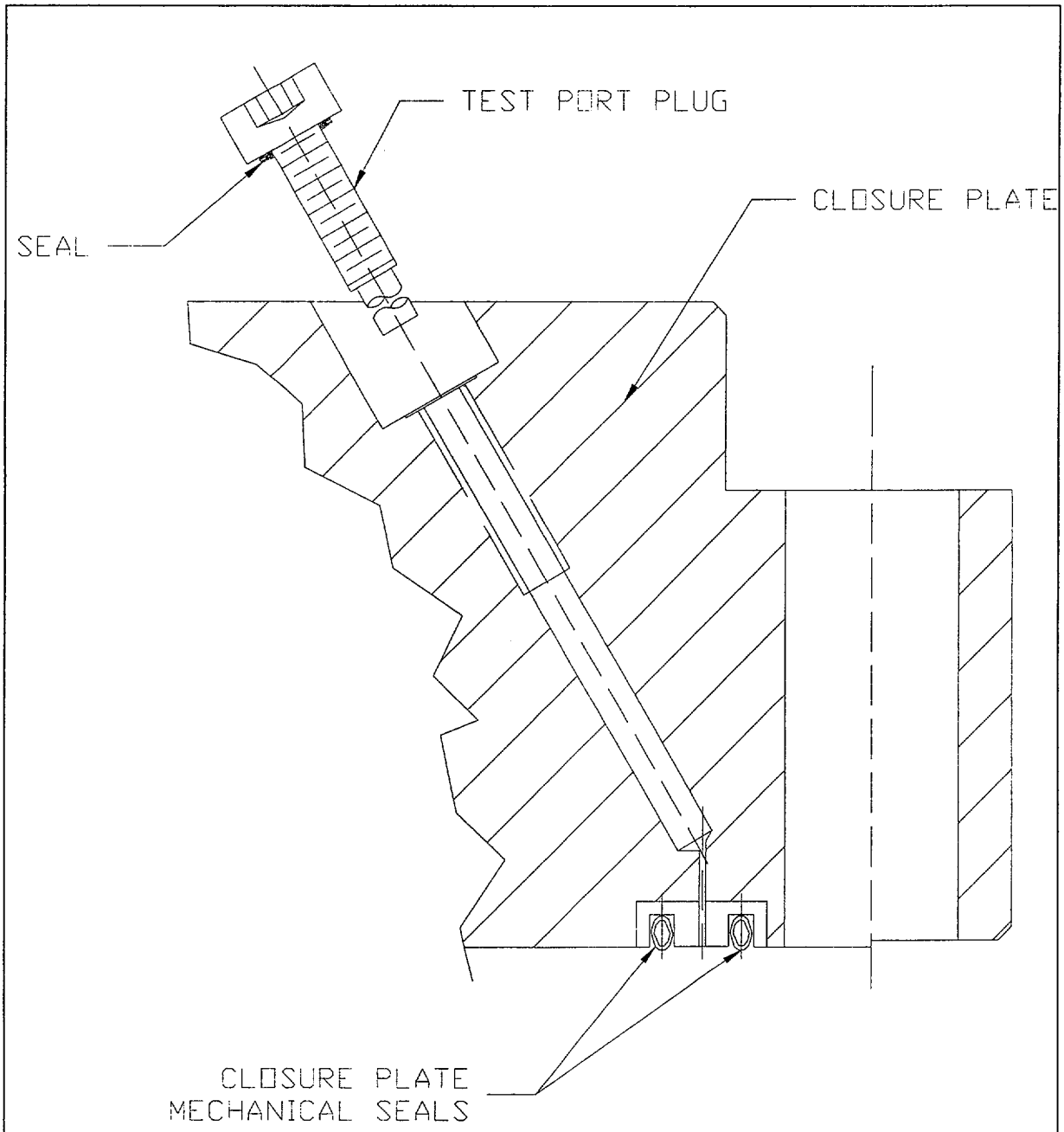

FIGURE 4.1.2; HI-STAR 100 CLOSURE PLATE CONTAINMENT DETAILS

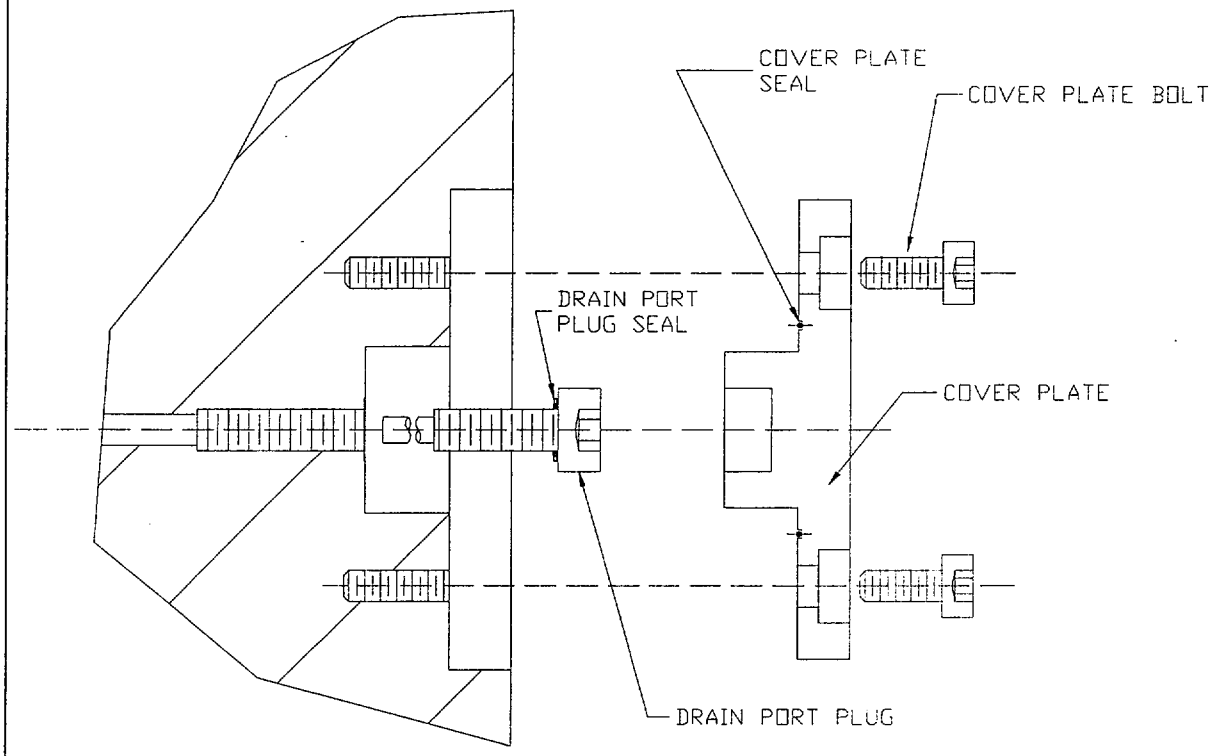

FIGURE 4.1.3; HI-STAR 100 OVERPACK VENT AND DRAIN PORT DETAILS

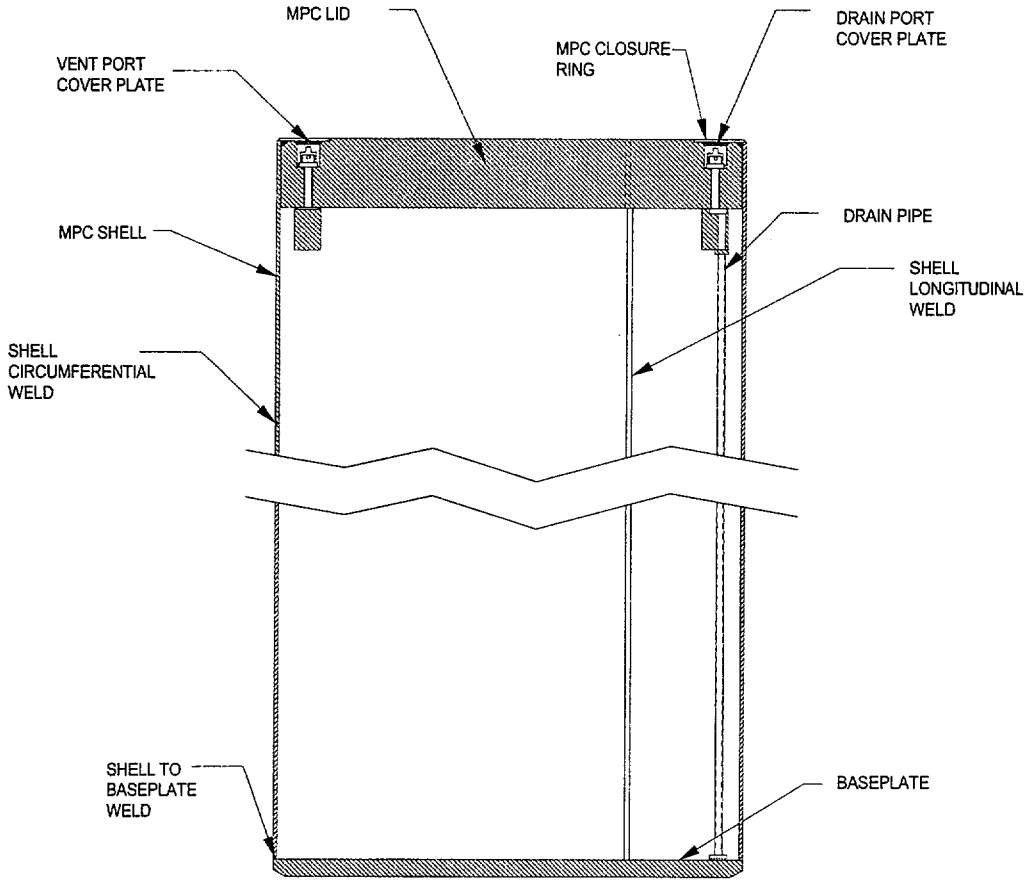

FIGURE 4.1.4; MPC-~~68F~~ SECONDARY CONTAINMENT BOUNDARY

4.2 REQUIREMENTS FOR NORMAL AND HYPOTHETICAL ACCIDENT CONDITIONS OF TRANSPORT

Chapter 2 shows that all primary and secondary containment components are maintained within their code-allowable stress limits during all normal and hypothetical accident conditions of transport as defined in 10CFR71.71 and 10CFR71.73 [4.0.1]. Chapter 3 shows that the peak containment component temperatures and pressure are within the design basis limits for all normal and hypothetical accident conditions of transport as defined in 10CFR71.71 and 10CFR71.73. Since the primary and secondary containment vessels remain intact, and the temperature and pressure design bases are not exceeded, the design basis leakage rate (see Table 4.1.1) will not be exceeded during normal or hypothetical accident conditions of transport.

4.2.1 Containment Criteria

The standard leakage rates presented in this chapter were determined in accordance with ANSI N14.5-*1997* [4.0.2] and shall be used for containment system fabrication verification and containment system periodic verification tests of the HI-STAR 100 containment boundaries. Measured leakage rates shall not exceed the values presented in Table 4.1.1. Compliance with these leakage rates ensures that the radionuclide release rates specified in 10CFR71.51 and 10CFR71.63(b) will not be exceeded during normal or hypothetical accident conditions of transport.

4.2.2 Containment of Radioactive Material

The HI-STAR 100 packaging standard leakage rate (See Table 4.1.1) ensures that the requirements of 10CFR71.51 and 10CFR71.63(b) are met. Section 4.2.5 determines the maximum leakage rate for normal and hypothetical accident conditions of transport and the standard leakage rate criterion for the HI-STAR 100 packaging containing each of the MPC types. The maximum calculated leakage rates for normal transport conditions assume a full complement of design fuel assembly types with bounding radiological source terms. The calculations also assume 3% fuel rod rupture for normal conditions. This bounds all possible MPC fuel loading configurations. For calculating the maximum leakage rates for normal conditions of transport, the internal design pressure is conservatively assumed to be equal to the MPC internal design pressure. Following testing, no credit is taken for the MPC as a containment boundary for the transport of intact fuel. The MPC ~~68F~~ enclosure vessel is identified as the secondary containment boundary for the transport of the specified fuel debris in accordance with the 10CFR71.63(b) requirements for a separate inner container. However, in calculating the overpack leakage rate for the transport of fuel debris, the overpack internal pressure is conservatively assumed to be equal to the MPC internal pressure.

The standard leakage rate is then conservatively chosen to be less than the calculated maximum leakage rates for normal conditions of transport. This ensures that the 10CFR71.51(a)(1) and 71.63(b) limits for radionuclide release are not exceeded.

4.2.3 Pressurization of Containment Vessel

The HI-STAR 100 overpack contains a sealed MPC during normal conditions of transport. Except for the small space between the MPC and overpack, the overpack internal cavity is essentially filled. This space (annulus) is drained, dried, evacuated and backfilled with helium gas prior to final closure of the overpack; therefore, no vapors or gases are present which could cause a reaction or explosion inside the overpack. Procedural steps (Chapter 7) prevent overpack over-pressurization during closure operations. The enclosed MPC is also drained, dried, and backfilled with helium gas prior to final closure; therefore, any MPC leak would not introduce any explosive gases into the overpack cavity. Since the exterior of the MPC is entirely composed of stainless steel, there is no possibility of chemical reaction that would produce gas or vapor. The overpack accident condition design basis internal pressure analysis assumes a non-mechanistic event resulting in the loss of MPC closure welds, a full-complement of design basis fuel with 100% fill gas and 30% of significant fission gas release, and the hypothetical 10CFR71.73(c)(4) fire condition. Even in this event, structural integrity and containment of the HI-STAR 100 packaging are maintained.

As the MPC is drained, dried, evacuated and backfilled with helium gas, no vapors or gases are present which could cause a reaction or explosion inside the MPC. Procedural steps (Chapter 7) prevent MPC over-pressurization during closure operations. The interior of the MPC contains stainless steel, Boral, and *optional* ~~A~~aluminum heat conductive inserts. There is no possibility of chemical reaction that would produce gas or vapor.

4.2.4 Assumptions

The HI-STAR 100 System is designed to meet the radioactive release limit requirements of 10CFR71.51 and 10CFR71.63(b). Allowable standard leakage rates are determined in accordance with the requirements of ANSI N14.5, and utilizing NUREG/CR-6487, *Containment Analysis for Type B Packages Used to Transport Various Contents* [4.0.3] and Regulatory Guide 7.4, *Leakage Tests on Packages for Shipment of Radioactive Materials* [4.0.4] as guides.

The following assumptions have been used in determining the allowable leakage rates:

1. For MPCs other than the *MPC-24EF and* MPC-68F, three percent of the fuel rods are assumed to have failed during normal conditions of transportation. One-hundred percent of the fuel rods are assumed to have failed during hypothetical accident conditions.

2. Thirty percent of the ~~iodine, tritium and ^{85}Kr is~~ *radioactive gases are* assumed to escape each failed fuel rod.

3. Fifteen percent of the ^{60}Co from the crud on the surface of the fuel rods is released as an aerosol in normal conditions of transport. One-hundred percent of the ^{60}Co is released as an aerosol from the surfaces of the fuel assemblies during accident conditions.

4. Since the overpack internals are never exposed to contaminants, the residual activity on the overpack interior surface and the MPC exterior surface is negligible compared to crud

deposits on the fuel and is neglected as a source term.

5. Up to four (4) DFCs containing specified fuel debris may be placed in a*n MPC-24EF or an* MPC-68F.

6. Crud spallation and cladding breaches occur instantaneously after fuel loading and container closure operations.

7. The calculation for normal transport conditions of an MPC-~~68F~~ containing fuel debris assumes 100% of the rods of the fuel debris are breached.

8. For containment analysis purposes, the MPC-24, *MPC-24E or MPC-24EF* contains *up to* 24 PWR assemblies, *of which 4 of these in the MPC-24EF may be DFCs with fuel debris, the MPC-32 contains up to 32 PWR assemblies, the* MPC-68 contains *up to* 68 BWR assemblies, and the MPC-68F contains ~~4 DFCs of fuel debris and~~ *up to* 6~~8~~4 intact BWR fuel assemblies, *of which 4 of those may be fuel debris in damaged fuel containers.*

9. 0.003% of the total fuel mass contained in a rod is assumed to be released as fines if the cladding on the rod ruptures (i.e., $f_f=3x10^{-5}$).

10. Bounding values for the crud surface activity for PWR rods is $140x10^{-6}$ Ci/cm^2 and for BWR rods is $1254x10^{-6}$ Ci/cm^2.

11. The rod surface area per assembly is $3x10^5$ cm^2 for PWR and $1x10^5$ cm^2 for BWR fuel assemblies. Th~~is~~*ese* ~~BWR~~ surface area*s* ~~is~~*are* also conservatively used for the surface area of ~~the~~ damaged fuel *or fuel debris*~~which is currently limited to Dresden 1 and Humboldt Bay fuel assemblies which have much smaller surface areas~~.

12. The release fractions for volatiles (^{89}Sr, ^{90}Sr, ^{103}Ru, ^{106}Ru, ^{134}Cs, ^{135}Cs, and ^{137}Cs) are all assumed to be $2x10^{-4}$ ($f_V=2x10^{-4}$).

13. In the analysis of the primary containment boundary, the MPC is assumed to rupture. In the analysis of the ~~MPC-68F~~ secondary containment boundary, the primary containment is assumed to fail.

14. In calculating the leakage rates of the primary containment for normal conditions of transport, the internal design pressure of the overpack is conservatively assumed to be equal to the MPC internal design pressure.

15. The average cavity temperature for all analyses is conservatively assumed to be the design basis peak cladding temperature.

16. All of the activity associated with crud is assumed to be Cobalt-60.

17. It is assumed that the flow is unchoked for all leakage analyses.

18. In the evaluation to demonstrate compliance with 10CFR71.63(b), the source activity due to Plutonium was determined by conservatively assuming that all of the rods develop cladding breaches during normal transportation and hypothetical accident conditions (i.e., f_B=1.0).

19. In the evaluation to demonstrate compliance with 10CFR71.63(b), the assumption was also made that roughly 0.003% of the plutonium is released from a fuel rod (i.e., $f_{Pu}=3x10^{-5}$).

20. Only 10% of the fines released to the MPC cavity are assumed to remain in aerosol form and available for release during normal transport conditions.

4.2.5 Analysis and Results

The leakage rates for the primary and secondary containment boundaries under normal and hypothetical accident conditions of transport at operating conditions and the standard leakage rates for the HI-STAR 100 packaging containing each of the MPC types were determined and are presented in this chapter. To calculate the leakage rates for a particular contents type and transportation condition, the following were determined: the source term concentration for the releasable material; the effective A_2 of the individual contributors; the releasable activity; the effective A_2 for the total source term; the allowable radionuclide release rates; and the allowable leakage rates at transport (operating) conditions. Using the equations for continuum and molecular flow, the corresponding leakage hole diameters were calculated. Then, using these leak hole diameters, the corresponding standard leakage rates at test conditions were calculated. Parameters were utilized in a way that ensured conservatism in the final leakage rates for the conditions, contents, and package arrangements considered.

The methodology and analysis results are summarized below.

4.2.5.1 Volume in the Containment Vessel

As discussed above, the primary containment system boundary for the HI-STAR 100 packaging consists of the overpack inner shell and associated components and the secondary containment system boundary consists of the MPC ~~-68F-~~enclosure vessel and associated components. The MPC-~~68F~~ provides the separate inner container per 10CFR71.63(b) for the HI-STAR 100 System transporting fuel classified as fuel debris.

Except for a small volume between the MPC and the overpack (the annulus), the overpack internal cavity is essentially filled. Therefore, the free gas volume for the primary containment boundary includes the free gas volume for the MPC plus the overpack annulus volume. The free gas volume in each of the MPC types is presented in Chapter 3. The free gas volumes of the primary and secondary containment are repeated in Table 4.2.1 for completeness. *The MPC-24E and MPC-24EF basket designed for Trojan are shorter to allow for storage in their overpacks. These shorter baskets are designated as the Trojan MPC-24E and Trojan MPC-24EF, respectively, where necessary. For calculating the free volume in the primary containment (overpack) with either of the Trojan MPCs, it is assumed that the annulus space is the same as that for the larger generic MPCs (i.e. the larger*

annulus space between the Trojan MPC and HI-STAR overpack is neglected). This will conservatively underestimate the free volume inside the primary containment.

4.2.5.2 Source Terms For Spent Nuclear Fuel Assemblies

In accordance with NUREG/CR-6487 [4.0.3], the following contributions are considered in determining the releasable source term for packages designed to transport irradiated fuel rods: (1) the radionuclides comprising the fuel rods, (2) the radionuclides on the surface of the fuel rods, and (3) the residual contamination on the inside surfaces of the vessel. NUREG/CR-6487 goes on to state that a radioactive aerosol can be generated inside a vessel when radioactive material from the fuel rods or from the inside surfaces of the container become airborne. The sources for the airborne material are (1) residual activity on the cask interior, (2) fission and activation-product activity associated with corrosion-deposited material (crud) on the fuel assembly surface, and (3) the radionuclides within the individual fuel rods. In accordance with NUREG/CR-6487, contamination due to residual activity on the cask interior surfaces is negligible as compared to crud deposits on the fuel rods themselves and therefore may be neglected. The source term considered for this calculation results from the spallation of crud from the fuel rods and from the fines, gases and volatiles which result from cladding breaches.

The inventory for isotopes other than ^{60}Co is calculated with the SAS2H and ORIGEN-S modules of the SCALE 4.3 system as described in Chapter 5. The inventory for the ~~MPC-24~~*all PWR MPCs* was conservatively based on the B&W 15x15 fuel assembly with a burnup of 4~~5~~0,000 MWD/MTU, 5 years of cooling time, and an enrichment of 3.*6*4%. The inventory for the MPC-68 was based the GE 7x7 fuel assembly with a burnup of 4~~0~~5,000 MWD/MTU, 5 years of cooling time, and 3.~~0~~2% enrichment. The inventory for the MPC-68F was based on the GE 6x6 fuel assembly with a burnup of 30,000 MWD/MTU, 18 years of cooling time, and 1.8% enrichment. Additionally, an MPC-68F was analyzed containing 67 GE 6x6 assemblies and a DFC containing 18 thorium rods. Finally, an Sb-Be source stored in one fuel rod in one assembly with 67 GE 6x6 assemblies was analyzed. The isotopes which contribute greater than 0.01% to the total curie inventory for the fuel assembly are considered in the evaluation as fines. Additionally, isotopes with A_2 values less than 1.0 in Table A-1, Appendix A, 10CFR71 are included as fines. Isotopes which contribute greater than 0.01% but which do not have an assigned A_2 value in Table A-1 are assigned an A_2 value based on the guidance in Table A-2, Appendix A, 10CFR71. Isotopes which contribute greater than 0.01% but have a radiological half life less than 10 days are neglected. Table 4.2.2 presents the isotope inventory used in the calculation.

A. Source Activity Due to Crud Spallation from Fuel Rods

The majority of the activity associated with crud is due to ^{60}Co [4.0.3]. The inventory for ^{60}Co was determined by using the crud surface activity for PWR rods (140×10^{-6} Ci/cm^2) and for BWR rods (1254×10^{-6} Ci/cm^2) provided in NUREG/CR-6487 [4.0.3] multiplied by the surface area per assembly (3×10^5 cm^2 and 1×10^5 cm^2 for PWR and BWR, respectively, also provided in NUREG/CR-6487).

The source terms were then decay corrected (5 years for ~~the MPC-24~~ *all PWR MPCs* and *the* MPC-

68; 18 years for the MPC-68F) using the basic radioactive decay equation:

$$A(t) = A_0 e^{-\lambda t} \quad \textbf{(4-1)}$$

where:

A(t) is activity at time t [Ci]
A_o is the initial activity [Ci]
λ is the $\ln 2/t_{1/2}$ (where $t_{1/2}$ = 5.272 years for ^{60}Co)
t is the time in years (5 years for ~~the MPC-24~~ *all PWR MPCs* and *the* MPC-68; 18 years for the MPC-68F)

The inventory for ^{60}Co was determined using the methodology described above with the following results:

PWR
Surface area per Assy = 3.0E+05 cm^2
140 $\mu Ci/cm^2$ x 3.0E+05 cm^2 = 42.0 Ci/*assy*

BWR
Surface area per Assy = 1.0E+05 cm^2
1254 $\mu Ci/cm^2$ x 1.0E+05 cm^2 = 125.4 Ci/*assy*

$^{60}Co(t) = {}^{60}Co_0\, e^{-(\lambda t)}$, where $\lambda = \ln 2/t_{1/2}$, t = 5 years (for ~~the MPC-24~~ *all PWR MPCs* and *the* MPC-68), t = 18 years (MPC-68F), $t_{1/2}$ = 5.272 years for ^{60}Co [4.2.4]

~~MPC-24~~*All PWR MPCs*
$^{60}Co(5) = 42.0\ Ci\ e^{-(\ln 2/5.272)(5)}$
$^{60}Co(5) = 21.77$ Ci/*assy*

MPC-68
$^{60}Co(5) = 125.4\ Ci\ e^{-(\ln 2/5.272)(5)}$
$^{60}Co(5) = 64.98$ Ci/*assy*

MPC-68F
$^{60}Co(18) = 125.4\ Ci\ e^{-(\ln 2/5.272)(18)}$
$^{60}Co(18) = 11.76$ Ci/*assy*

A summary of the ^{60}Co inventory available for release is provided in Table 4.2.2.

The activity density that results inside the containment vessel as a result of crud spallation from spent fuel rods can be formulated as:

$$C_{crud} = \frac{f_C M_A N_A}{V} \quad \textbf{(4-2)}$$

where:

C_{crud} is the activity density inside the containment vessel as a result of crud spallation [Ci/cm^3],
M_A is the total crud activity inventory per assembly [Ci/assy],
f_C is the crud spallation fraction,
N_A is the number of assemblies, and
V is the free volume inside the containment vessel [cm^3].

NUREG/CR-6487 states that measurements have shown 15% to be a reasonable value for the percent of crud spallation for both PWR and BWR fuel rods under normal transportation conditions. For hypothetical accident conditions, it is assumed that there is 100% crud spallation [4.0.3].

B. Source Activity Due to Releases of Fines from Cladding Breaches

A breach in the cladding of a fuel rod may allow radionuclides to be released from the resulting cladding defect into the interior of the MPC. If there is a leak in the primary or secondary containment vessels, then the radioisotopes emitted from a cladding breach that were aerosolized may be entrained in the gases escaping from the package and result in a radioactive release to the environment.

NUREG/CR-6487 suggests that a bounding value of 3% of the rods develop cladding breaches during normal transportation (i.e., f_B=0.03). For hypothetical accident conditions, it is assumed that all of the rods develop a cladding breach (i.e., f_B=1.0). These values were used for both PWR and BWR fuel rods. As described in NUREG/CR-6487, roughly 0.003% of the fuel mass contained in a rod is released as fines if the cladding on the rod ruptures (i.e., $f_f=3x10^{-5}$).

In addition to the small number of fines that are released from the cladding in the event of a cladding breach, only about 10% of the ejected fines remain airborne sufficiently long to be available for release from the MPC cavity [4.2.5] (f_a = 0.10).

The calculation for normal transport conditions of *either a Trojan MPC-24EF or* an MPC-68F containing four (4) DFCs containing fuel debris assumes that for the four DFCs, 100% of the rods of the fuel debris are breached. The remaining *20 or* 64 assemblies in *either the Trojan MPC-24EF or* the MPC-68F, *respectively,* were assumed to have a 3% cladding rupture. Therefore, f_B for *a Trojan MPC-24EF or* an MPC-68F containing fuel debris is:

$$f_B = (0.03)\frac{20}{24} + (1.0)\frac{4}{20}$$
$$f_B = 0.192 \qquad \textbf{(4-3a)}$$

$$f_B = (0.03)\frac{64}{68} + (1.0)\frac{4}{68}$$
$$f_B = 0.087 \qquad \textbf{(4-3b)}$$

The activity concentration inside the containment vessel due to fines being released from cladding breaches is given by:

$$C_{fines} = \frac{f_f f_a I_{fines} N_A f_B}{V} \qquad \textbf{(4-4)}$$

where:

C_{fines} is the activity concentration inside the containment vessel as a result of fines released from cladding breaches [Ci/cm^3],
f_f is the fraction of a fuel rod's mass released as fines as a result of a cladding breach (f_f=3x10^{-5}),
I_{fines} is the total activity inventory [Ci/assy],
N_A is the number of assemblies,
f_a *is the fraction of fines that remain in an aerosol form (f_a = 0.10 for normal conditions, f_a = 1.00 for accident conditions),*
f_B is the fraction of rods that develop cladding breaches, and
V is the free volume inside the containment vessel [cm^3].

C. Source Activity from Gases due to Cladding Breaches

If a cladding failure occurs in a fuel rod, a large fraction of the gap fission gases will be introduced into the free volume of the system. Tritium and Krypton-85 are typically the major sources of radioactivity among the gases present [4.0.3]. NUREG/CR-6487 suggests that a bounding value of 30% of the fission product gases escape from a fuel rod as a result of a cladding breach (i.e., f_g=0.3).

The activity concentration due to the release of gases form a cladding breach is given by:

$$C_{gases} = \frac{f_g I_{gases} N_A f_B}{V} \quad \textbf{(4-5)}$$

where:

C_{gases} is the releasable activity concentration inside the containment vessel due to gases released from cladding breaches [Ci/cm^3],
f_g is the fraction of gas that would escape from a fuel rod that developed a cladding breach,
I_{gases} is the gas activity inventory [^{3}H, ^{129}I, ^{85}Kr] [Ci/assy],
N_A is the number of assemblies,
f_B is the fraction of rods that develop cladding breaches, and
V is the free volume inside the containment vessel [cm^3].

D. Source Activity from Volatiles due to Cladding Breaches

Volatiles such as cesium, strontium, and ruthenium, can also be released from a fuel rod as a result of a cladding breach. NUREG/CR-6487 estimates that 2x10^{-4} is a conservative bounding value for the fraction of the volatiles released from a fuel rod (i.e., f_V=2x10^{-4}).

The activity concentration due to the release of volatiles is given by:

$$C_{vol} = \frac{f_v I_{vol} N_A f_B}{V} \quad \textbf{(4-6)}$$

where:

C_{vol} is the releasable activity concentration inside the containment vessel due to volatiles released from cladding breaches [Ci/cm^3],
f_V is the fraction of volatiles that would escape from a fuel rod that developed a cladding breach,
I_{vol} is the volatile activity inventory [^{90}Sr, ^{137}Cs, ^{134}Cs, ^{106}Ru] [Ci/assy],
N_A is the number of assemblies,
f_B is the fraction of rods that develop cladding breaches, and
V is the free volume inside the containment vessel [cm^3].

E. Total Source Term for the HI-STAR 100 System

The total source term was determined by combining Equations 4-2, 4-4, 4-5, and 4-6:

$$C_{total} = C_{crud} + C_{fines} + C_{gases} + C_{vol} \quad \textbf{(4-7)}$$

where C_{total} has units of Ci/cm^3.

Table 4.2.3 presents the total source term determined using the above methodology. Table 4.2.4 summarizes the parameters from NUREG/CR-6487 used in this analysis.

4.2.5.3 Effective A_2 of Individual Contributors (Crud, Fines, Gases, and Volatiles)

The A_2 of the individual contributions (i.e., crud, fines, gases, and volatiles) were determined in accordance with NUREG/CR-6487. As previously described, the majority of the activity due to crud is from Cobalt-60. Therefore, the A_2 value of 10.8 Ci used for crud for both PWR and BWR fuel is the same as that for Cobalt-60 found in 10CFR71, Appendix A.

In accordance with 10CFR71.51(b) the methodology presented in 10CFR71, Appendix A for mixtures of different radionuclides was used to determine the A_2 values for the gases, fines and volatiles.

$$A_2 \text{ for a mixture} = \frac{1}{\sum_{i=1}^{I} \frac{f(i)}{A_2(i)}} \quad \textbf{(4-8)}$$

Where f(i) is the fraction of activity of nuclide I in the mixture and $A_2(i)$ is the appropriate A_2 value for the nuclide I.

10CFR71.51(b) also states that for Krypton-85, an effective A_2 value equal to 10 A_2 may be used. Table 4.2.5 summarizes the effective A_2 for all individual contributors.

4.2.5.4 Releasable Activity

The releasable activity is the product of the respective activity concentrations (C_{fines}, C_{gas}, C_{crud}, and C_{vol}) and the respective MPC volume. The releasable activity of fines, volatiles, gases, and crud were determined using this methodology.

$$\text{Releasable Activity [Ci]} = \text{Activity Concentration } [\frac{\text{Ci}}{\text{cm}^3}] \text{ x Volume } [\text{cm}^3] \qquad \textbf{(4-9)}$$

4.2.5.5 Effective A_2 for the Total Source Term

Using the releasable activity and the effective A_2 values from the individual contributors (i.e., crud, fines, gases, and volatiles), the effective A_2 for the total source term was calculated for each MPC type, for normal transportation and hypothetical accident conditions. The methodology used to determine the effective A_2 is the same as that used for a mixture, which is provided in Equation 4-8.

The results are summarized in Table 4.2.6. As stated in 4.2.5.3, the effective A_2 used for Krypton-85 is 10 A_2 (2700 Ci).

4.2.5.6 Allowable Radionuclide Release Rates

The containment criterion for the HI-STAR 100 System under normal conditions of transport is given in 10CFR71.51(a)(1). This criterion requires that a package have a radioactive release rate less than $A_2 \times 10^{-6}$ in one hour, where A_2 is the effective A_2 for the total source term in the packaging determined in 4.2.5.5. Additionally, 10CFR71.51(b)(2) specifies that for hypothetical accident conditions, the quantity that may be released in one week is A_2 (effective A_2 for the total source term determined in 4.2.5.5).

NUREG/CR-6487 and ANSI N14.5 provides the following equations for the allowable release rates.

Release rate for normal conditions of transport:

$$R_N = L_N C_N \leq A_2 \times 2.78 \times 10^{-10}/\text{second} \qquad \textbf{(4-10)}$$

where:

R_N is the release rate for normal transport [Ci/s]
L_N is the volumetric gas leakage rate [cm^3/s]
C_N is the total source term activity concentration [Ci/cm^3]
A_2 is the appropriate effective A_2 value [Ci].

Release rate for hypothetical accident conditions:

$$R_A = L_A C_A \leq A_2 \times 1.65 \times 10^{-6}/\text{second} \qquad \textbf{(4-11)}$$

where:

R_A is the release rate for hypothetical accident conditions [Ci/s]
L_A is the volumetric gas leakage rate [cm^3/s]
C_A is the total source term activity concentration [Ci/cm^3]
A_2 is the appropriate effective A_2 value [Ci].

Equations 4-10 and 4-11 were used to determine the allowable radionuclide release rates for each MPC type and transport condition. The release rates are summarized in Table 4.2.7.

4.2.5.7 Allowable Leakage Rates

The allowable leakage rates at operating conditions were determined by dividing the allowable release rates by the appropriate source term activity concentration (modifying Equations 4-10 and 4-11).

$$L_N = \frac{R_N}{C_N} \text{ or } L_A = \frac{R_A}{C_A} \quad \textbf{(4-12)}$$

where,

L_N or L_A is the allowable leakage rate at the upstream pressure for normal (N) or accident (A) conditions [cm^3/s],
R_N or R_A is the allowable release rate for normal (N) or accident (A) conditions [Ci/s], and
C_N or C_A is the allowable release rate for normal (N) or accident (A) conditions [Ci/cm^3].

The allowable leakage rates determined using Equation 4-12 are the allowable leakage rates at the upstream pressure. Table 4.2.9 summarizes the allowable leakage rates at the upstream pressures. The most limiting allowable leakage rate presented in Table 4.2.9 (~~1~~*2.1193*x10^{-5} cm^3/s under normal conditions of transport) was conservatively selected and used to determine the leakage rate acceptance criterion ~~at average pressure using the ratio presented in Equation 4-13.~~.

Equation deleted **(4-13)**

~~where:~~

~~$L_{@P_a}$ is the allowable leakage rate at the average pressure [cm^3/s]~~
~~$L_{@P_u}$ is the allowable leakage rate at the upstream pressure [cm^3/s]~~
~~P_u is the upstream pressure [ATM],~~
~~P_a is the average pressure; $P_a = (P_u + P_d)/2$ [ATM], and~~
~~P_d is the downstream pressure [ATM].~~

~~Substituting $1.93x10^{-5}$ cm^3/s for $L_{@P_u}$, 7.8 ATM (the upstream pressure reported in Table 4.2.12) for P_u, and 4.4 ATM ($(P_u + P_d)/2$ where P_u and P_d are presented in Table 4.2.12) the allowable leakage~~

~~rate at the average pressure is determined. The corresponding allowable leakage rate at the average pressure was 3.41×10^{-5} cm^3/s.~~

4.2.5.8 Leakage Rate Acceptance Criteria

The leakage rate*s* discussed thus far w*ere*~~as~~ determined at operating conditions (see normal *and accident* conditions in Table 4.2.12). The following provides details of the methodology used to convert the allowable leakage rate *at operating conditions* ~~(3.41×10^{-5} cm^3/s)~~ to a leakage rate acceptance criterion at test conditions.

For conservatism, unchoked flow correlations were used as the unchoked flow correlations better approximate the true measured flow rate for the leakage rates associated with transportation packages. Using the equations for molecular and continuum flow provided in NUREG/CR-6487, the corresponding leak hole diameter was calculated by solving Equation 4-14*a* for D, the leak hole diameter. The capillary length required for Equation 4-14*a* for the primary containment was conservatively chosen as the closure plate inner seal seating width which is 0.25 cm; for the secondary containment ~~(MPC-68F)~~, the capillary length was conservatively chosen to be the MPC lid closure weld thickness which is 1.25 inches thick (3.175 cm).

$$L_{@P_u} = \left[\frac{2.49 \times 10^6 \, D^4}{a \, u} + \frac{3.81 \times 10^3 \, D^3 \sqrt{\frac{T}{M}}}{a \, P_a} \right] [P_u - P_d] \frac{P_a}{P_u} \qquad \textit{(4-14a)}$$

where:

$L_{@P_{au}}$ is the allowable leakage rate at the ~~average~~ *upstream* pressure for normal and accident conditions [cm^3/s],
a is the capillary length [cm],
T is the temperature for normal and accident conditions [K],
M is the gas molecular weight [g/mole] = 4.0 from ANSI N14.5, Table B1 [4.0.2],
u is the fluid viscosity for helium [cP] from Rosenhow and Hartnett [4.2.3]
P_u is the upstream pressure [ATM],
D leak hole diameter [cm],
P_d is the downstream pressure for normal and accident conditions [ATM], and
P_a is the average pressure; $P_a = (P_u + P_d)/2$ for normal and accident conditions [ATM].

The leak hole diameter was determined by solving Equation 4-14*a* for 'D' where $L_{@Pu}$ is equal to ~~3.41~~*2.11* $\times 10^{-5}$ cm^3/s and using the parameters for normal conditions of transport presented in Table 4.2.12. The corresponding leak hole diameter was determined to be 3.*37*~~29~~ $\times 10^{-4}$ cm.

Using this leak hole diameter ~~(3.29×10^{-4} cm),~~ and the temperature and pressures for test conditions provided in Table 4.1.12, Equation 4-14*a* was solved for the *volumetric* leakage rate ~~acceptance criterion~~ (*85.3120* $\times 10^{-6}$ ~~atm~~ cm^3/s, helium) at test conditions. ~~For additional conservatism to ensure~~

~~compliance with 10CFR71.51, this leakage rate acceptance criterion (8.20×10^{-6} atm cm^3/s, helium) was then conservatively reduced and is presented in Table 4.1.1.~~

Equation B-1 of ANSI N14.5-1997 [4.0.2] is used to express this volumetric leakage rate into a mass-like helium flow rate (Q_u) as follows:

$$Q_u = L_u * P_u \ (atm\text{-}cm^3/sec) \qquad \textbf{(4-14b)}$$

where:

L_u *is the upstream volumetric leakage rate [cm^3/sec],*
Q_u *is the mass-like helium leak rate [atm-cm^3/sec], and*
P_u *is the upstream pressure [atm].*

Using Equation 4-14b to convert the volumetric flow rate into a mass-like flow, the leakage rate acceptance criteria is calculated to be 8.92×10^{-6} atm-cm^3/sec, which has been conservatively reduced and is presented in Table 4.1.1.

Table 4.2.12 provides additional parameters used in the analysis.

4.2.5.9 10CFR71.63(b) Plutonium Leakage Verification

The HI-STAR 100 System configured to transport fuel debris must meet the criteria of 10CFR71.63(b) for plutonium shipments. This criteria specifies that for normal conditions of transport, the separate inner container must not release plutonium as demonstrated to a sensitivity of $A_2 \times 10^{-6}$ in one hour, where A_2 is the effective A_2 for the plutonium inventory in the damaged fuel (up to four DFCs containing specified fuel debris). Additionally, 10CFR71.63(b) specifies that for hypothetical accident conditions, the separate inner container must restrict the loss of plutonium to not more than A_2 in one week (effective A_2 for the plutonium inventory determined using the methodology described in Section 4.2.5.3).

To demonstrate compliance with this requirement, the leakage rate acceptance criterion was determined following the basic methodology described above. To determine this leakage rate, ~~only~~ the plutonium inventory for the GE 6x6 MOX fuel assembly *and the plutonium inventories for the assemblies described in Section 4.2.5.2 was analyzed.* ~~was used as this inventory bounds the standard GE 6x6 fuel assembly Plutonium inventory~~. Table 4.2.11 contains the plutonium inventory for the MOX fuel used in this evaluation.

As discussed in 4.2.5.2, Equation 4-3*a and Equation 4-3b* presents the methodology to determine f_B for an *MPC-24EF and an* MPC-68F containing fuel debris, *respectively*. This f_B was applied in determining the source activity due to Plutonium. The calculation for normal transport conditions of an MPC-~~68F~~ containing four (4) DFCs containing fuel debris assumes that for the four DFCs, 100% of the rods of the fuel debris are breached. The remaining ~~64~~ assemblies in the MPC-~~68F~~ were assumed to have a 3% cladding rupture. ~~Therefore, f_B for an MPC-68F containing fuel debris under normal conditions of transport is 0.087.~~ The source activity due to Plutonium was determined by

conservatively assuming that all of the rods develop cladding breaches during hypothetical accident conditions (i.e., f_B=1.0). The assumption was also made that roughly 0.003% of the plutonium is released from a fuel rod (i.e., $f_{Pu}=3x10^{-5}$). Therefore, the activity concentration inside the containment vessel due to plutonium is given by:

$$C_{Pu} = \frac{f_{Pu} I_{Pu} N_A f_B}{V} \quad \textbf{(4-15)}$$

where:

C_{Pu} is the activity concentration inside the containment vessel from Plutonium [Ci/cm^3],
f_{Pu} is the fraction of a fuel rod's mass released as Plutonium ($f_f = 3x10^{-5}$),
I_{Pu} is the total Plutonium inventory of one ~~GE 6x6 MOX~~ assembly [Ci/assy],
N_A is the number of ~~GE 6x6 MOX~~ assemblies ~~(68)~~,
f_B is the fraction of rods that develop cladding breaches (f_B=0.087 for normal conditions of transport and f_B=1.0 for accident conditions), and
V is the free volume inside the containment vessel [cm^3] from Table 4.2.1.

The methodology described in 4.2.5.3 for mixtures was used to calculate the effective A_2 for Plutonium ~~(0.0297 Ci)~~. The methodology in 4.2.5.4 was used to determine the releasable activity. The allowable radionuclide release rates were determined using the methodology presented in 4.2.5.6 and are summarized in Table 4.2.13. The allowable leakage rates at the upstream pressure were determined as discussed in 4.2.5.7 (using Equation 4-12). The allowable leakage rates are presented in Table 4.2.14. As in 4.2.5.7, the most limiting allowable leakage rate presented in Table 4.2.14 (~~3.77~~*1.41*x10^{-5} cm^3/s under normal conditions of transport) was conservatively selected and used to determine the ~~allowable~~ leakage rate *acceptance criterion for the MPC* ~~at average pressure using the ratio presented in Equation 4-13. The corresponding allowable leakage rate at average pressure was 6.68x10^{-5} cm^3/s.~~

As discussed in 4.2.5.8, the allowable leakage rate ~~at average pressure (6.68x10^{-5} cm^3/s)~~ was then converted to a leakage rate acceptance criterion at test conditions using the equations for molecular and continuum flow provided in NUREG/CR-6487 (Equation 4-14*a*). The capillary length required for Equation 4-14*a* for the secondary containment ~~(MPC-68F)~~ was conservatively chosen to be the MPC lid closure weld thickness which is assumed to be 1.25 inches thick (3.175 cm). Equation 4-14*a* was solved for D, the leak hole diameter (D=~~7.73~~*5.97*x10^{-4} cm) and then using this leak hole diameter, and the temperature and pressures for test conditions (Table 4.1.12), Equation 4-14*a* was solved for the *volumetric* leakage rate acceptance criterion at test conditions (~~1.88~~*4.47*x10^{-6}~~5~~ ~~std~~ cm^3/s, helium). *Equation 4-14b is used to convert the volumetric flow rate into the mass-like flow rate, resulting in an acceptance criterion leakage rate of 8.94x10^{-6} atm-cm^3/sec.* For additional conservatism to ensure compliance with 10CFR71.63(b), this leakage rate acceptance criterion (1.88x10^{-5} std cm^3/s, helium) was conservatively reduced and is presented in Table 4.1.1.

4.2.5.10 Leak Test Sensitivity

The sensitivity for the overpack leakage test procedures is equal to one-half of the allowable leakage

rate. The HI-STAR 100 containment packaging tests in Chapter 8 incorporate the appropriate leakage test procedure sensitivity. The leakage rates for the HI-STAR 100 containment packaging with its corresponding sensitivity are presented in Table 4.1.1.

Table 4.2.1

FREE GAS VOLUME OF THE PRIMARY
AND SECONDARY CONTAINMENT

MPC Type	Primary Containment Volume (overpack) (cm^3)	Secondary Containment Volume (MPC~~-68F~~) (cm^3)
MPC-24	6.7~~069~~ $\times 10^6$	N/A
MPC-24E *MPC-24EF*	*6.67×10^6*	*N/A*
Trojan MPC-24E *Trojan MPC-24EF*	*6.12×10^6*	*5.96×10^6*
MPC-32	*6.35×10^6*	*N/A*
MPC-68	6.15×10^6	N/A
MPC-68F	6.15×10^6	5.99×10^6

Table 4.2.2

ISOTOPE INVENTORY
Ci/Assembly

Nuclide	~~MPC-24~~*All PWR MPCs* Ci/Assembly	MPC-68 Ci/Assembly	MPC-68F Ci/Assembly
Gases			
^{3}H	2.76~~21~~E+02	~~8.72~~*1.09*E+0*2*~~1~~	1.78E+01
^{129}I	*2.17*~~1.93~~E-02	*8.66*~~7.72~~E-03	3.49E-03
^{85}Kr	*4.69*~~3.75~~E+03	1.79~~43~~E+03	2.37E+02
^{81}Kr	*7.97E-08*	*3.50E-08*	*1.19E-08*
^{127}Xe	*5.95E-11*	*2.05E-11*	*1.62E-17*
Crud			
^{60}Co	2.18E+01	6.50E+01	1.18E+01
Volatiles			
^{90}Sr	~~3.91~~*4.53*E+04	1.76~~52~~E+04	4.29E+03
^{106}Ru	*4.97*~~1.18~~E+04	*1.74*~~4.16~~E+0*43*~~3~~	2.30E-01
^{134}Cs	*4.43*~~1.90~~E+04	*1.66*~~7.20~~E+0*43*~~3~~	3.16E+01
^{137}Cs	*6.76*~~5.77~~E+04	2.68~~29~~E+04	7.21E+03
^{89}Sr	*1.25E-01*	*3.47E-02*	*2.41E-35*
^{103}Ru	*3.65E-03*	*1.13E-03*	*0.00E+00*
^{135}Cs	*2.79E-01*	*1.11E-01*	*4.54E-02*
Fines			

^{225}Ac*	*3.052.26*E-08	*2.141.42*E-08	9.69E-09
^{227}Ac*	2.*3677*E-06	1.*1832*E-06	1.45E-06
^{110m}*Ag*	*1.73E+02*	*6.58E+01*	*4.97E-06*
^{241} Am	*4.766.46*E+02	*1.612.20*E+02	2.52E+02

Table 4.2.2 (continued)

ISOTOPE INVENTORY

Ci/Assembly

	MPC-24 Ci/Assembly	MPC-68 Ci/Assembly	MPC-68F Ci/Assembly
^{242M}Am*	*5.600.00*E+00	*0.001.94*E+00	*9.35E-010.00E+00*
^{243}Am*	*2.231.73*E+01	*9.427.39*E+00	3.30E+00
^{137m}*Ba*	*6.39E+04*	*2.53E+04*	*6.81E+03*
^{210M} Bi*	0.00E+00	0.00E+00	0.00E+00
^{247}Bk*	*2.82E-080.00E+00*	*1.32E-080.00E+00*	*5.94E-080.00E+00*
^{144}Ce	*7.974.77*E+0*43*	*2.461.45*E+0*43*	7.33E-03
^{248}Cf*	0.00E+00	0.00E+00	0.00E+00
^{249}Cf*	*3.428.01*E-05	*1.94.47*E-05	3.62E-06
^{250}Cf*	*1.032.92*E-04	*6.751.86*E-04*5*	6.69E-06
^{251}Cf*	*3.401.27*E-06	*7.952.06*E-06*7*	1.36E-07
^{252}Cf*	*84*.11E-0*54*	*6.373.14*E-04*5*	3.64E-07
^{254}Cf*	*8.461.19*E-13	*7.671.05*E-13	0.00E+00

	~~8~~	~~8~~	
^{240}Cm*	0.00E+00	0.00E+00	0.00E+00
^{242}Cm*	~~1.54~~*3.21*E+0~~2~~*1*	~~6.10~~*1.26*E+0~~2~~*0*	7.71E-01
^{243}Cm*	1.~~14~~*61*E+01	~~4.8~~*6.5*1E+00	1.54E+00
^{244}Cm	~~2.06~~*3.26*E+03	~~9.30~~*1.43*E+0~~3~~*2*	2.17E+02
^{245}Cm*	~~2.07~~*3.25*E-01	~~8.10~~*1.23*E-0*1*~~2~~	2.48E-02
^{246}Cm*	~~5.96~~*1.06*E-0*1*~~2~~	~~3.09~~*5.40*E-02	1.01E-02
^{247}Cm*	~~3.5~~*7.07*E-07	~~1.92~~*3.72*E-07	5.26E-08
^{248}Cm*	~~1.85~~*4.20*E-06	~~1.09~~*2.43*E-06	2.53E-07

Table 4.2.2 (continued)

ISOTOPE INVENTORY

Ci/Assembly

	MPC-24 Ci/Assembly	MPC-68 Ci/Assembly	MPC-68F Ci/Assembly
^{253}Es*	~~0.00~~*6.35*E~~+0 0~~*-20*	~~2.78~~*4.62*E-*20*~~3~~*1*	0.00E+00
^{254}Es*	~~8.69~~*1.93*E-*08*~~1~~*0*	~~9.12~~*1.96*E-*08*~~1~~*0*	8.05E-16
^{154}Eu	~~2.89~~*4.03*E+03	~~1.07~~*1.47*E+03	1.44E+02
^{155}Eu	~~8.5~~*1.3*~~3~~*4*E+0~~3~~*2*	~~3.51~~*5.46*E+02	2.23E+01
^{55}Fe	~~3~~*6.98*~~6~~E+01	~~1.83~~*3.23*E+01	2.94E-01
^{257}Fm*	*4.26E-07*~~0.00E+00~~	*1.69E-07*~~0.00E+00~~	0.00E+00

^{148}Gd*	0.00E+00	0.00E+00	0.00E+00
^{182}Hf*	0.00E+00	0.00E+00	0.00E+00
^{236}Np*	~~7.28~~*9.77*E-06	~~2.47~~*3.29*E-06	7.30E-07
^{237}Np*	~~2.02~~*2.33*E-01	~~7.05~~*8.07*E-02	2.55E-02
^{239}Np	~~1.7~~*2.23*E+01	~~7.39~~*9.42*E+00	3.30E+00
^{231}Pa*	~~1.59~~*1.82*E-05	~~7.04~~*8.17*E-06	3.16E-06
^{210}Pb*	~~5.18~~*4.30*E-09	~~2.45~~*2.17*E-09	1.17E-08
^{147}Pm	~~2.48~~*4.28*E+04	~~8.88~~*1.52*E+0*43*	1.18E+02
^{208}Po*	0.00E+00	0.00E+00	0.00E+00
^{209}Po*	0.00E+00	0.00E+00	0.00E+00
^{210}Po*	~~4.50~~*3.92*E-09	~~2.16~~*1.98*E-09	1.08E-08
^{144}Pr	*4.77E+04*	*1.45E+04*	*7.33E-03*
^{144m}Pr	*6.68E+02*	*2.04E+02*	*1.03E-04*
^{236}Pu*	~~9.65~~*2.04*E-0*1*~~2~~	~~3.04~~*6.32*E-02	3.66E-04

Table 4.2.2 (continued)

ISOTOPE INVENTORY

Ci/Assembly

	MPC-24 Ci/Assembly	MPC-68 Ci/Assembly	MPC-68F Ci/Assembly
^{238}Pu	~~1.98~~*2.56*E+03	~~7.49~~*9.55*E+02	2.50E+02
^{239}Pu	1.~~86~~*91*E+02	6.~~16~~*24*E+01	2.95E+01
^{240}Pu	3.~~06~~*27*E+02	1.~~26~~*34*E+02	6.81E+01
^{241}Pu	~~6.33~~*7.55*E+0	2.~~10~~*47*E+04	5.16E+03

	4		
^{242}Pu*	1.~~38~~65E+00	~~5.95~~7.05E-01	3.06E-01
^{244}Pu*	~~7.75~~1.11E-13 4	~~4.65~~6.58E-14	3.73E-14
^{223}Ra*	2.~~78~~37E-06	1.~~32~~18E-06	1.45E-06
^{225}Ra*	~~2.26~~3.05E-08	~~1.4~~2.14~~2~~E-08	9.69E-09
^{226}Ra*	~~4.86~~2.82E-08	~~2.03~~1.32E-08	5.94~~2.03~~E-08
^{106}Rh	*4.97E+04*	*1.74E+04*	*2.30E-01*
^{222}Rn*	~~4.86~~2.82E-08	~~2.03~~1.32E-08	5.94E-08
^{125}Sb	~~1.57~~2.87E+0 3	~~6.40~~1.15E+0 ~~32~~	8.02~~9.46~~E+0 0
^{151}Sm	~~2.37~~2.60E+0 2	~~7.29~~7.92E+0 1	2.53E+01
^{119m}Sn	~~9.27~~5.46E+0 ~~21~~	~~5.27~~3.08E+0 ~~21~~	1.07E-06~~0.00E+00~~
^{125m}Te	~~3.84~~6.99E+0 2	~~1.56~~2.82E+0 2	1.96~~2.31~~E+0 0
^{227}Th*	~~2.74~~2.33E-06	~~1.31~~1.16E-06	1.43E-06
^{228}Th*	~~9.63~~8.56E-03	~~3.63~~3.40E-03	1.71E-03
^{229}Th*	~~2.26~~3.05E-08	~~1.42~~2.14E-08	9.69E-09
^{230}Th*	~~3.07~~2.16E-05	~~1.13~~8.26E-06 ~~5~~	1.29E-05
^{230}U*	~~2.55~~1.33E-23 ~~34~~	~~9.17~~4.74E-24 ~~35~~	0.00E+00

Table 4.2.2 (continued)

ISOTOPE INVENTORY

Ci/Assembly

	MPC-24 Ci/Assembly	MPC-68 Ci/Assembly	MPC-68F Ci/Assembly

^{232}U*	~~1.36~~*1.51*E-02	~~4.92~~*5.58*E-03	1.69E-03
^{233}U*	1.48*1*E-05	4.~~52~~*20*E-06	3.03E-06
^{234}U*	~~5.10~~*4.97*E-01	1.74*0*E-01	7.26E-02
^{236}U*	1.~~47~~*60*E-01	5.~~39~~*85*E-02	1.84E-02
^{90}Y	*4.53*~~*3.91*~~E+04	1.~~52~~*76*E+04	4.29E+03

Note: The isotopes which contribute greater than 0.01% to the total curie inventory for the fuel assembly are considered in the evaluation as fines. Additionally, isotopes with A_2 values less than 1.0 in Table A-1, Appendix A, 10CFR71 are included as fines and are designated in the table by an "*".

Table 4.2.3

TOTAL SOURCE TERM FOR THE HI-STAR 100 SYSTEM (Ci/cm^3)

	C_{crud} (Ci/cm^3)	C_{fines} (Ci/cm^3)	C_{vol} (Ci/cm^3)	C_{gas} (Ci/cm^3)	Total (Ci/cm^3)
Normal Transport Conditions					
MPC-24	1.17E-05	*1.26~~4.73~~E-0~~7~~7*	*4.45~~2.75~~E-06*	1.60~~28~~E-04	1.78~~43~~E-04
MPC-24E MPC-24EF	*1.17E-05*	*1.26E-07*	*4.47E-06*	*1.61E-04*	*1.78E-04*
Trojan MPC-24E	*1.28E-05*	*1.38E-07*	*4.87E-06*	*1.75E-04*	*1.94E-04*
Trojan MPC-24EF Primary	*1.28E-05*	*8.82E-07*	*3.12E-05*	*1.12E-03*	*1.17E-03*
MPC-32	*1.65E-05*	*1.77E-07*	*6.26E-06*	*2.25E-04*	*2.50E-04*
MPC-68	1.08E-04	*1.36~~5.18~~E-0~~7~~7*	*5.20~~3.28~~E-06*	1.89~~51~~E-04	*3.03~~2.63~~E-04*
MPC-68F Primary Containment	1.95E-05	*5.02~~3.06~~E-08~~7~~*	2.22E-06	7.35E-05	9.58~~6~~E-05
Accident Conditions					
MPC-24	7.80~~1~~E-05	*4.20~~1.58~~E-05*	*1.48~~9.16~~E-04~~5~~*	*5.34~~4.27~~E-03*	*5.60~~4.46~~E-03*
MPC-24E MPC-24EF	*7.83E-05*	*4.21E-05*	*1.49E-04*	*5.36E-03*	*5.63E-03*
Trojan MPC-24E	*8.54E-05*	*4.59E-05*	*1.62E-04*	*5.84E-03*	*6.14E-03*
Trojan MPC-24EF Primary	*8.54E-05*	*4.59E-05*	*1.62E-04*	*5.84E-03*	*6.14E-03*
MPC-32	*1.10E-04*	*5.90E-05*	*2.09E-04*	*7.51E-03*	*7.88E-03*
MPC-68	7.18E-04	*4.52~~1.73~~E-05*	1.73~~09~~E-04	*6.30~~5.03~~E-03*	*7.23~~5.88~~E-03*
MPC-68F Primary Containment	1.30E-04	*5.77~~3.52~~E-06*	2.55E-05	8.45E-04	1.0~~1~~0E-03

Table 4.2.4

VARIABLES FOUND IN NUREG/CR-6487 USED IN THE LEAKAGE RATE ANALYSIS

Variable	PWR		BWR	
	Normal	Accident	Normal	Accident
Fraction of crud that spalls, f_C	0.15	1.0	0.15	1.0
Crud surface activity (Ci/cm^2)	$140x10^{-06}$	$140x10^{-06}$	$1254x10^{-06}$	$1254x10^{-06}$
Surface area per assembly, cm^2	$3x10^5$	$3x10^5$	$1x10^5$	$1x10^5$
Fraction of rods that develop cladding breach, f_B†	0.03	1.0	0.03	1.0
Fraction of fines that are released, f_f	$3x10^{-5}$	$3x10^{-5}$	$3x10^{-5}$	$3x10^{-5}$
Fraction of gases that are released, f_G	0.3	0.3	0.3	0.3
Fraction of volatiles that are released, f_V	$2x10^{-04}$	$2x10^{-04}$	$2x10^{-04}$	$2x10^{-04}$

† The calculation for normal transport conditions of *the Trojan MPC-24EF and* ~~an~~ MPC-68F *each* containing four (4) DFCs ~~containing~~ *with* fuel debris ~~damaged fuel~~ assumes that for the four DFCs, 100% of the rods of the fuel debris are breached. The remaining *20 or* 64 assemblies in the *Trojan MPC-24EF and* MPC-68F, *respectively,* were assumed to have a 3% cladding rupture. Therefore, f_B for ~~an~~ *the Trojan MPC-24EF and the* MPC-68F containing fuel debris is *0.192 and* 0.087, *respectively.*

Table 4.2.5

INDIVIDUAL CONTRIBUTOR EFFECTIVE A_2
FOR GASES, CRUD, FINES, AND VOLATILES

MPC Type	A_2 (Ci)
Gases	
~~MPC-24~~*All PWR MPCs*	*2822*~~490~~
MPC-68	*2822*~~490~~
MPC-68F	~~2440~~*285*
Crud	
All MPC-~~24~~*s*	10.8
Fines	
All PWR MPC-~~24~~*s*	0.*308*~~144~~
MPC-68	0.*284*~~135~~
MPC-68F	0.0*57*~~470~~
Volatiles	
All PWR MPC-~~24~~*s*	*6.04*~~5.71~~
MPC-68	*6.05*~~5.73~~
MPC-68F	5.43

Table 4.2.6

TOTAL SOURCE TERM EFFECTIVE A_2 FOR
NORMAL AND HYPOTHETICAL
ACCIDENT CONDITIONS

Normal Transport Conditions	
	Effective A_2 (Ci)
MPC-24	*63.1~~27.4~~*
MPC-24E	*63.1*
Trojan MPC-24E	*63.1*
Trojan MPC-24EF	*88.4*
MPC-32	*63.1*
MPC-68	*25.2~~18.6~~*
MPC-68F	*28.5~~8.54~~*
Accident Conditions	
MPC-24	*30.0~~3.2~~*
MPC-24E	*30.0*
Trojan MPC-24E	*30.0*
Trojan MPC-24EF	*30.0*
MPC-32	*30.0*
MPC-68	*26~~7.23~~*
MPC-68F	*~~1~~48.37~~.9~~*

Table 4.2.7

RADIONUCLIDE RELEASE RATES

	Effective A_2 (Ci)	Allowable Release Rate (R_N or R_A) (Ci/s)
Normal Transport Conditions		
MPC-24	*63.1*~~28.6~~	*1.75*~~8.12~~E-0*8*~~9~~
MPC-24E	*63.1*	*1.75E-08*
Trojan MPC-24E	*63.1*	*1.75E-08*
Trojan MPC-24EF	*88.4*	*2.46E-08*
MPC-32	*63.1*	*1.75E-08*
MPC-68	*25.2*~~17.9~~	~~5.06~~*7.01*E-09
MPC-68F Primary Containment	*28.5* ~~14.5~~	*7.92*~~4.02~~E-09
Accident Conditions		
MPC-24	*30.0*~~32.5~~	*4.94*~~5.47~~E-05
MPC-24E	*30.0*	*4.94E-05*
Trojan MPC-24E	*30.0*	*4.94E-05*
Trojan MPC-24EF	*30.0*	*4.94E-05*
MPC-32	*30.0*	*4.94E-05*
MPC-68	*26.2*~~26.8~~	4.~~51~~*32*E-05
MPC-68F Primary Containment	*8.37*~~14.9~~	*1.38*~~2.46~~E-05

Table 4.2.8

Table Deleted

Table 4.2.9

ALLOWABLE LEAKAGE RATES AT UPSTREAM PRESSURE

	C_{total} (Ci/cm^3)	Allowable Leakage Rate at P_u L_N or L_A (cm^3/s)
Normal Transport Conditions		
MPC-24	1.*7643*E-04	*9.945.67*E-05
MPC-24E	*1.77E-04*	*9.90E-05*
Trojan MPC-24E	*1.93E-04*	*9.08E-05*
Trojan MPC-24EF	*1.17E-03*	*2.11E-05*
MPC-32	*2.48E-04*	*7.07E-05*
MPC-68	*3.022.63*E-04	*2.321.93*E-05
MPC-68F Primary Containment	9.536E-05	*8.314.20*E-055
Accident Conditions		
MPC-24	*5.604.46*E-03	*8.821.23*E-032
MPC-24E	*5.63E-03*	*8.78E-03*
Trojan MPC-24E	*6.14E-03*	*8.06E-03*
Trojan MPC-24EF	*6.14E-03*	*8.06E-03*
MPC-32	*7.88E-03*	*6.27E-03*
MPC-68	*7.235.88*E-03	*5.967.67*E-03
MPC-68F Primary Containment	1.010E-03	*1.372.45*E-02

Table 4.2.10

Table Deleted

Table 4.2.11

~~GE 6X6 MOX FUEL~~
PLUTONIUM INVENTORY
(Ci/assembly)

Nuclide	*MPC-68F MOX fuel* Ci/Assy	*MPC-68F UO_2 fuel Ci/Assy*	*Trojan MPC-24EF UO_2 fuel Ci/Assy*
Pu-236	4.92E-04	*3.66E-04*	*2.04E-01*
Pu-237	0.00*E+00*	*0.00E+00*	*3.04E-07*
Pu-238	1.1*1*E+03	*2.50E+02*	*2.56E+03*
Pu-239	3.29E+01	*2.95E+01*	*1.91E+02*
Pu-240	7.83E+01	*6.81E+01*	*3.27E+02*
Pu-241	6.15E+03	*5.16E+03*	*7.55E+04*
Pu-242	3.44E-01	*3.06E-01*	*1.65E+00*
Pu-244	0.0	*3.73E-14*	*1.11E-13*
Total	**7.37E+03**	***5.51E+03***	***7.86E+04***

Table 4.2.12

PARAMETERS FOR NORMAL, HYPOTHETICAL ACCIDENT AND STANDARD CONDITIONS

Parameter	Normal (helium)	Hypothetical Accident (helium)	Standard (Test Conditions, helium)
P_u	114.7 psia (7.8 ATM)	*214.7*~~139.7~~ psia (*~~9~~14.61~~5~~* ATM)	Primary: 1.68 ATM
			Secondary: 2.0 ATM
P_d	14.7 psia (1 ATM)	14.7 psia (1 ATM)	14.7 psia (1 ATM)
T	400°C (673 K)	1058°F (843 K)	373 K
M	4 g/mol	4 g/mol	4 g/mol
u	0.0341 cP	0.0397 cP	0.0231 cP
a	Primary: 0.25 cm	Primary: 0.25 cm	Primary: 0.25 cm
	Secondary: 3.175 cm	Secondary: 3.175 cm	Secondary: 3.175 cm

Table 4.2.13

RADIONUCLIDE RELEASE RATES
FOR SECONDARY CONTAINMENT

	Effective A_2 (Ci)	Allowable Release Rate (R_N or R_A) (Ci/s)
Normal Transport Conditions		
MPC-68F *MOX Fuel* ~~Secondary Containment~~	0.0297	8.24E-12
MPC-68F UO_2 Fuel	*0.0660*	*1.84E-11*
Trojan MPC-24EF UO_2 Fuel	*0.0926*	*2.57E-11*
Accident Conditions		
MPC-68F ~~Secondary Containment~~	0.0297	4.89E-08
MPC-68F UO_2 Fuel	*0.0660*	*1.09E-07*
Trojan MPC-24EF UO_2 Fuel	*0.0926*	*1.53E-07*

Table 4.2.14

ALLOWABLE LEAKAGE RATES AT UPSTREAM PRESSURE
FOR SECONDARY CONTAINMENT

	C_{Pu} (Ci/cm^3)	Allowable Leakage Rate at P_u L_N or L_A (cm^3/s)
Normal Transport Conditions		
MPC-68F *MOX Fuel* ~~Secondary Containment~~	2.18E-07	3.77E-05
MPC-68F UO_2 Fuel	*1.63E-07*	*1.12E-04*
Trojan MPC-24EF UO_2 Fuel	*1.82E-06*	*1.41E-05*
Accident Conditions		
MPC-68F ~~Secondary Containment~~	2.51E-06	1.95E-02
MPC-68F UO_2 Fuel	*1.88E-06*	*5.81E-02*
Trojan MPC-24EF UO_2 Fuel	*9.49E-06*	*1.61E-02*

4.3 REGULATORY COMPLIANCE

Chapter 4 of this SAR has been prepared to summarize the containment features and capabilities of the HI-STAR 100 packaging. The containment boundaries of the HI-STAR 100 packaging are designed and tested to ensure that the radionuclide release rates specified in 10CFR71.51 and 10CFR71.63(b) [4.0.1] will not be exceeded.

Leakage rates presented in Chapter 4 are determined in accordance with the requirements of ANSI N14.5 [4.0.2], and utilizing NUREG/CR-6487, *Containment Analysis for Type B Packages Used to Transport Various Contents* [4.0.3], Regulatory Guide 7.4, *Leakage Tests on Packages for Shipment of Radioactive Materials* [4.0.4] as content guides, and NUREG-1617, Standard Review Plan for Transportation Packages for Spent Nuclear Fuel [4.0.5].

The containment features and capabilities of the HI-STAR 100 packaging can be summarized in the following evaluation statements:

1. The HI-STAR 100 packaging, as presented in Chapter 4, complies with all applicable codes and standards for the containment system as identified in the chapter.

2. The primary containment boundary is securely closed by using multiple bolts and plugs. The secondary containment boundary is closed using multi-pass welds. The closure of both containment boundaries is sufficient to prevent unintentional opening or opening by pressure that may arise in the package as required by 10CFR71.43(c).

3. The materials of construction for the packaging primary and secondary containment are specified in the Bills-of-Material in Section 1.4. All materials and construction assure that there will be no significant chemical, galvanic, or other reaction as required by 10CFR71.43(d).

4. The overpack and MPC penetrations are designed to prevent leakage and protect against unauthorized operation by using cover plates to provide redundant closure as required by 10CFR71.43(e).

5. The primary containment system boundary for the HI-STAR 100 packaging consists of the overpack inner shell, the bottom plate, the top flange, the top closure plate, closure bolts, the overpack vent and drain port plugs, and their respective mechanical seals. The secondary containment system boundary for a HI-STAR 100 packaging containing ~~damaged~~ fuel *debris* ~~assemblies~~ consists of the MPC-~~68F~~ enclosure vessel including the MPC shell, the MPC bottom plate, the MPC lid, closure ring, and vent and drain port cover plates. The use of two independent containment boundaries provides the capability to load and transport specified fuel debris in accordance with the requirements of 10CFR71.63(b).

6. The HI-STAR 100 packaging is design, constructed, and prepared for shipment so that under the tests specified in 10CFR71.71 (normal conditions of transport), the package satisfies the containment requirement of 10CFR71.43(f) and 10CFR71.51(a)(1) for normal conditions of transport and 10CFR71.51(a)(2) for hypothetical accident conditions with no dependence on filters or a mechanical cooling system as required by 10CFR71.51(c).

7. The HI-STAR 100 packaging satisfies the requirements of 10CFR71.63(b) for transport related to fuel debris with plutonium in excess of 20 Ci per package.

8. The HI-STAR 100 packaging satisfies the containment requirements of 10CFR71, and the packaging meets the containment criteria of ANSI N14.5.

4.4 REFERENCES

[4.0.1] 10CFR71. "Packaging and Transportation of Radioactive Material."

[4.0.2] ANSI N14.5-1997. "American National Standard for Radioactive Materials-Leakage Tests on Packages for Shipment."

[4.0.3] B.L. Anderson et al. *Containment Analysis for Type B Packages Used to Transport Various Contents.* NUREG/CR-6487, UCRL-ID-124822. Lawrence Livermore National Laboratory, November 1996.

[4.0.4] U.S. Nuclear Regulatory Commission, Regulatory Guide 7.4, *Leakage Tests on Packages for Shipment of Radioactive Materials*, June 1975.

[4.0.5] NUREG-1617, "Standard Review Plan for Transportation Packages for Spent Nuclear Fuel", Draft Report for Comment, March 1998.

[4.1.1] American Society of Mechanical Engineers (ASME), Boiler and Pressure Vessel Code, Section III, Division 1, Subsection NB, Class 1 Components, 1995 Edition.

[4.2.1] Deleted.

[4.2.2] Deleted.

[4.2.3] Rosenhow, W.M. and Hartnett, J.P., *Handbook of Heat Transfer*, Hemisphere Publishing Corporation, New York, 1973.

[4.2.4] Shleien, B., *The Health Physics and Radiological Health Handbook*, Scinta, Inc. Silver Spring, MD, 1992.

[4.2.5] Rashid, Y.R., et. al, "An Estimate of the Contribution of Spent Fuel Products to the Releasable Source Term in Spent Fuel Transport Casks," SAND88-2778C, Sandia National Laboratories, 1988.

APPENDIX 4.A: BOLT AND PLUG TORQUES

This appendix provides the calculations used to determine the torque values for the vent and drain port plugs and cover plate bolts.

4.A.1 HI-STAR 100 Vent and Drain Port Plug Torques†

The HI-STAR 100 vent and drain port are sealed with plugs under which a mechanical seal is compressed. The objective of this calculation is to determine the torque required on the plug and to provide the required compressive load.

Given:

O-Ring (Mechanical Seal) Diameter: D_{OR} =0.683 in

O-Ring Compression: q_{OR} =800 lbf/in (pound force per linear inch)

Internal Pressure: p_i =100 psi

Plug Diameter: D_B =0.5 inch

Load due to internal overpack pressure: $q_i = p_i \ \pi D_B^2/4 =$ 19.6 lbf

Determine the required seating load:

The circumference of the O-Ring is: $C_{OR}=\pi D_{OR}$ C_{OR}= 2.14 in

The required seating load is: $F_i = q_i + P_{OR}$

$p_{OR}=C_{OR}q_{OR}$ p_{OR}= 1712 lbf

F_i=1732 lbf

The procedure presented here is taken from Shingley, Joseph Edward and Mischke, Charles R., Mechanical Engineering Design, Fifth Edition, McGraw Hill, p. 344-346.

† Since the closure plate test port plug is the same material, diameter and uses the same seal, this calculation also applies to the closure plate test port plug.

Given a torque factor K= 0.30 (for non-plated, non-lubricated plug).

Determine the required torque:

$T= KFiD_B$

T=0.30 (1732 lbf)0.5 in T=259 in-lbf T=22 ft-lbf

4.A.2 HI-STAR 100 Vent and Drain Port Cover Plate Bolt Torques

The HI-STAR 100 vent and drain port cover plates are sealed with a mechanical seal that is compressed under a bolted cover plate. The objective of this calculation is to determine the torque required on the bolts and to provide the required compressive load.

Given:

O-Ring (Mechanical Seal) Diameter: D_{OR} =2.5 in

Required O-Ring Compression: q_{OR} =1150 lbf/in (pound force per linear inch)

Internal Pressure: p_i =100 psi (assumed)

Bolt Diameter: D_B =0.375 inch

Number of Bolts: n= 4 bolts

Determine the required seating load:

The circumference of the O-Ring is: $C_{OR}=\pi D_{OR}$ C_{OR}= 7.85 in

The required seating load per bolt is: $F_i = q_i + P_{OR}/n$

$qi= p_i \pi D_{OR}^2/4$ qi= 491 lbf
$P_{OR}=C_{OR}q_{OR}$ P_{OR}= 9028 lbf

F_i=9516 lbf/4 F_i=2380 ft-lbf

The procedure presented here is taken from Shingley, Joseph Edward and Mischke, Charles R., Mechanical Engineering Design, Fifth Edition, McGraw Hill, p. 344-346.

Given a torque factor K= 0.15 (See technical Bulletin for FELPRO N-5000 in Appendix 1.C).

For conservatism, the torque factor is increased by an additional 5 percent in the following calculation.

Determine the required torque:

$T = KFiD_B$

T=0.1575 (2380 lbf)0.375 in T=141 in-lbf T=11.8 ft-lbf

APPENDIX 4.B: Manufacturer Seal Information
(Total of 5 Pages Including This Page)

The information provided in this appendix provides additional details on the mechanical seals specified to ensure containment. The following is a listing of the drawings provided in this appendix.

- ASE Drawing No. 050038, ".375 C-Ring, Spring Ener., Internal Pressure"
  (Detail of Closure Plate Mechanical Seals, Holtec Dwg. 1397 and Bill-of-Material 1476, Items 26 and 27)

- ASE Drawing No. 050033, "C-Ring, .062 Spring Energized"
  (Detail of Port Plug Mechanical Seal, Holtec Dwg. 1397 and Bill-of-Material 1476, Item 19)

- ASE Drawing No. 050118, ".062 C-Ring, Spring Ener., Internal Pressure"
  (Detail of Port Cover Mechanical Seal, Holtec Dwg. 1398 and Bill-of-Material 1476, Item 30)

The detailed dimensions, materials, and groove requirements are provided below for each mechanical seal.

Closure Plate Outer Seal:

Holtec Item No.	27
ASE Part No.	ASE050038-1
Seal Type	Spring energized C-ring, internal pressure
Seal Size	72.50 OD x 3/8 free height
Material	Jacket Alloy X750
	Spring Alloy X750
Plating	Silver
Groove OD	72.54/72.55 inches
Groove ID	71.68/71.69 inches
Groove Depth	.300/.305 inches

Closure Plate Inner Seal:

Holtec Item No.	26
ASE Part No.	ASE050038-2
Seal Type	Spring energized C-ring, internal pressure
Seal Size	71.00 OD x 3/8 free height
Material	Jacket Alloy X750
	Spring Alloy X750
Plating	Silver
Groove OD	71.04/71.05 inches
Groove ID	70.18/70.17 inches
Groove Depth	.300/.305 inches

Port Plug Seal:

Holtec Item No.	19
ASE Part No.	ASE050033
Seal Type	Spring energized C-ring, internal pressure
Seal Size	0.75 OD x 0.062 free height
Material	Jacket Alloy X750
	Spring Alloy X750
Plating	Nickel
Groove OD	0.760 +1/6, -0 inches
Groove Depth	.020 +/- 0.005 inches

Port Cover Seal:

Holtec Item No.	30
ASE Part No.	ASE050118
Seal Type	Spring energized C-ring, internal pressure
Seal Size	2.50 OD x 0.062 free height
Material	Jacket Alloy X750
	Spring Alloy X750
Plating	Nickel
Groove OD	2.52/2.515 inches
Groove ID	2.314/2.309 inches
Groove Depth	.045 +0, - 0.003 inches

FIGURE WITHHELD AS SENSITIVE UNCLASSIFIED INFORMATION

FIGURE WITHHELD AS SENSITIVE UNCLASSIFIED INFORMATION

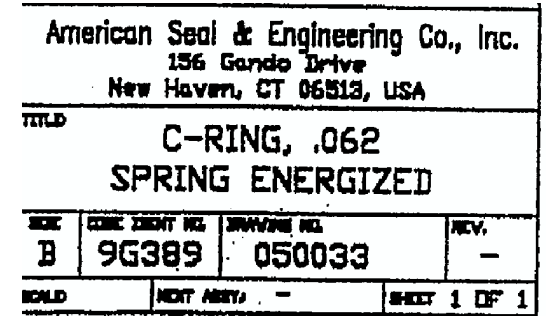

FIGURE WITHHELD AS SENSITIVE UNCLASSIFIED INFORMATION